Graduate School ETD Form 9
(Revised 12/07)

PURDUE UNIVERSITY
GRADUATE SCHOOL
Thesis/Dissertation Acceptance

This is to certify that the thesis/dissertation prepared

By Amardeep Singh Sidhu

Entitled
FAULT DIAGNOSIS OF LITHIUM ION BATTERY USING MULTIPLE MODEL ADAPTIVE ESTIMATION

For the degree of Master of Science in Mechanical Engineering

Is approved by the final examining committee:

Sohel Anwar (Co-chair)
Chair

Afshin Izadian (Co-chair)

Jian Xie

To the best of my knowledge and as understood by the student in the *Research Integrity and Copyright Disclaimer (Graduate School Form 20)*, this thesis/dissertation adheres to the provisions of Purdue University's "Policy on Integrity in Research" and the use of copyrighted material.

Approved by Major Professor(s): Sohel Anwar

Approved by: Sohel Anwar 12/02/2013
Head of the Graduate Program Date

FAULT DIAGNOSIS OF LITHIUM ION BATTERY USING MULTIPLE MODEL ADAPTIVE ESTIMATION

A Thesis
Submitted to the Faculty
of
Purdue University
by
Amardeep Singh Sidhu

In Partial Fulfillment of the
Requirements for the Degree
of
Master of Science in Mechanical Engineering

December 2013
Purdue University
Indianapolis, Indiana

To my Parents

ACKNOWLEDGEMENTS

I would like to gratefully acknowledge my thesis advisors, Dr. Sohel Anwar and Dr. Afshin Izadian, for their assistance, guidance, and supervision during the entire course of this research and thesis work. Dr. Anwar and Dr. Izadian generously shared with me their research experience and directed me towards perfection in every detail, for which I am always thankful.

I would like to thank my advisory committee member Dr. Jian Xie for his time and insight during the completion of this thesis.

I would also like to thank my fellow students and staff at the Energy Systems and Power Electronics Laboratory (ESPEL); Mr. Henry Smith, Mr. Masoud Vaezi and Mr. Craig Stephens for their help and support during this phase of my life.

TABLE OF CONTENTS

Page

LIST OF TABLES

LIST OF FIGURES

Figure Page

Figure Page

Appendix Figure

Appendix Figure Page

Appendix Figure Page

NOMENCLATURE

SYMBOL	UNITS	DESCRIPTION
R_b	Ohm	Bulk electrolyte resistance
C	Farad	Constant phase element
R	Ohm	Resistive member for constant phase element
R_{ct}	Ohm	Charge transfer resistance
C_{dl}	Farad	Double layer capacitance
V_{OCV}	Volts	Open circuit voltage
Z_{CPE}	Ohm	Impedance with C and R in parallel
α	-	Depression factor
k	-	Slope
SOC	-	State of charge
d	Volts	Open circuit voltage at zero state of charge
$C_{b.}$	Farad	Bulk capacitance
I_L	Amp	Load/charge current
V_C	Volts	Voltage across capacitor C
$V_{C_{dl}}$	Volts	Voltage across capacitor C_{dl}
V_{C_b}	Volts	Voltage across the bulk capacitor $C_{b.}$
V_t	Volts	Terminal voltage
Δt, T	Sec	Sample time
η	-	Coulomb efficiency
C_n	Ah	Battery nominal capacity
V	Volts	IS frequency sweep amplitude

ω	rad/sec	Angular frequency of sweep
ω_0	rad/sec	Start angular frequency
ω_n	rad/sec	Stop angular frequency
I	Amp	IS current response amplitude
θ	rad	Phase shift
C'	Farad	Capacitance
V'	Volts	Voltage across capacitor C'
I'	Amps	Current through the capacitor C'
s	-	Complex argument
Z_C	Ohm	Capacitive impedance
R'	Ohm	Resistor
Z_R	Ohm	Resistive Impedance
e	-	Error
K	-	Kalman gain
r	-	Residual
$\hat{x}$	-	Estimated state
$\hat{y}$	-	Estimated output
y	-	Measurement
u	-	Input
p	-	Conditional probability
${I_L}'$	Amp	Excited load current
${V'}_t$	Volts	Excited terminal voltage

ABSTRACT

Sidhu, Amardeep Singh. M.S.M.E., Purdue University, December 2013. Fault Diagnosis of Lithium Ion Battery Using Multiple Model Adaptive Estimation. Major Professors: Sohel Anwar and Afshin Izadian.

Lithium ion batteries have become integral parts of our lives; they are widely used in applications like handheld consumer products, automotive systems, and power tools among others. To extract maximum output from a Li-ion battery under optimal conditions it is imperative to have access to the state of the battery under every operating condition. Faults occurring in the battery when left unchecked can lead to irreversible, and under extreme conditions, catastrophic damage.

In this thesis, an adaptive fault diagnosis technique is developed for Li-ion batteries. For the purpose of fault diagnosis the battery is modeled by using lumped electrical elements under the equivalent circuit paradigm. The model takes into account much of the electro-chemical phenomenon while keeping the computational effort at the minimum. The diagnosis process consists of multiple models representing the various conditions of the battery. A bank of observers is used to estimate the output of each model; the estimated output is compared with the measurement for generating residual signals. These residuals are then used in the multiple model adaptive estimation (MMAE) technique for generating probabilities and for detecting the signature faults.

The effectiveness of the fault detection and identification process is also dependent on the model uncertainties caused by the battery modeling process. The diagnosis performance is compared for both the linear and nonlinear battery models. The non-linear

battery model better captures the actual system dynamics and results in considerable improvement and hence robust battery fault diagnosis in real time. Furthermore, it is shown that the non-linear battery model enables precise battery condition monitoring in different degrees of overdischarge.

1. INTRODUCTION

1.1. Problem Statement

Since its discovery more than two centuries ago, battery technology has come a long way. Today's battery is smaller in size, has higher energy density, is safe and has a longer life [1] when compared to its earlier incarnations. Due to these benefits and more, the usage of Li-ion batteries has shown a tremendous increase in the last decade. The annual lithium consumption for battery production has gone from negligible in 1993 to 6500 metric tons per year in 2008 [2]. The rechargeable Li-ion battery available in various form factors has made its way into a wide variety of applications. These applications range from consumer products like mobile phones, cameras to critical application in hybrid electric vehicles (HEV) , electric vehicles (EV) and medical implants [3]. With these growing applications in mind the health of the Li-ion battery becomes a critical factor in the combined system functionality of the device.

Like any physical system, the battery is susceptible to failure due to manufacturing defects and/or human abuse. Out of the various fault scenarios, over charge and over discharge causes appreciable change in battery performance. Both these conditions are destructive in nature and hence adversely affect the health of the battery. over charge in Li-ion batteries has been linked to nominal capacity loss during cycling [4], and in extreme conditions overheating and thus vaporization of active material and hence explosion. Meanwhile over discharge can short the internal circuit of the battery cell [5]. These failure modes develop with time and it is only when these faults are left unchecked that they lead to irreversible, and in extreme conditions, catastrophic failure [6, 7].

A testing procedure must be developed to evaluate the Li-ion battery parameters in real-time. This diagnostic tool should be insensitive to system and measurement noise yet it should be sensitive enough to capture any variation in the battery performance. In addition to detecting non-optimal Li-ion battery performance the diagnostic tool should be able to diagnose the particular type of fault leading to non-optimal behavior using fault detection and diagnosis (FDD).

1.2. Objectives

The objectives of this research are to develop a fault detection and isolation technique. Suitable models to represent the Li-ion battery are to be identified; these models should be able to closely represent the various operating and fault conditions of the battery cell without excessive computational load. System identification techniques should also be explored for parameter extraction. This research must also be conducted towards extending MMAE to electro-chemical systems for fault detection and diagnosis. MMAE is an established fault detection technique based on Bayesian framework.

1.3. About This Thesis

The need for effective fault detection in li-ion battery is a basic requirement which has attracted considerable attention from academia and industry. Some of the earlier used methods along with their benefits and shortcomings are shown in Chapter 2.

Two equivalent circuit models, both linear and non-linear, were explored in this research. Through simulation it was seen that some of the models result in better FDD. The modeling approach and the models are explained in Chapter 3.

For system identification, impedance spectroscopy (IS) and least square techniques were explored for Li-ion battery parameter extraction. These methods are explained in Chapter 4.

The FDD process has a two pronged approach, the first part deals with the implementation of a state estimator, while the second part implements a residual evaluation process. The FDD technique is examined in Chapter 5.

In Chapter 6, experiments are designed for Li-ion battery over charge and over discharge fault detection using MMAE. The results verify the effectiveness of the battery fault detection technique.

The FDD performance has a strong relationship with the process model. The resulting FDD for the linear and non-linear models is evaluated and compared in Chapter 7. Finally the conclusion and recommendations for future work are given in Chapter 8.

2. LITERATURE SURVEY

The application of FDD on Li-ion batteries is not new, extensive work in this area has been done by researchers with focus on different faults and related techniques. The work on Li-ion battery FD is based primarily on the state estimation, empirical techniques, parameter identification, data driven methods and others.

Sate estimation involves the evaluation of the state of the battery, while the choice of technique can differ based on the requirements, the aim is to access the information related to the Li-ion battery that is not readily available through measurement [8]. The choice of state variable depends on the model of the system, but for Li-ion batteries, SOC among others is a natural candidate. Application of Luenberger observers (LO) for FDD can be found in [9], here the authors implement FDD on a string of Li-ion batteries using a bank of reduced order observers. LO is a good candidate for FDD in systems with little or no measurement noise, but with presence of noise, this setup will face inherent difficulties especially under subtle but important performance variation. The use of Kalman filters under the paradigm of observer based fault diagnosis for FDD in Li-ion batteries is given in [10], where the optimal filter shows strong robustness to noise and the adaptive nature of the MMAE algorithm ensures accurate fault detection. MMAE is a robust fault detection and identification technique with extensive applications in the aerospace industry [11, 12] and recently in the fault detection of micro electro mechanical systems [13, 14].

Substantial work in the field of FDD and prognosis in Li-ion battery using data driven methods has been carried out by Saha et al. [15-17]. Related research by using support vector machine algorithm for state of health (SOH) and remaining useful life (RUL) was

recently carried out by Nuhic et al. [18] and Wang et al. [19]. These methods involve the application of classification and regression algorithms found under the paradigm of machine learning. In [20], the author uses impedance spectroscopy (IS) along with auto regressive moving average (ARMA), neural network, and fuzzy logic techniques for parameter identification, estimation and eventually battery prognosis. Data driven techniques do not require in depth knowledge of the battery and its underlying mechanisms, hence their implementation does not involve expert knowledge of the process under study. The biggest hurdle in using data driven methods can be attributed to the computational expensiveness and requirement of extensive data for training, and the time involved in learning.

A combination of rule based signal monitoring and probability based Li-ion battery FDD was explored by Xiong et al. [21], these methods rely heavily on the thermal signatures of the battery which in turn depend on the rate of charge/discharge applied on the cell. Further, there is little information regarding the initial state of the cell under test; as it is difficult to achieve an over discharge cell failure in LiFePO4 cell chemistries after two cycles. In [22], the open circuit voltage (OCV) is analyzed along with model based approach to detect the cell nominal capacity fade due to cycling. This technique gives good results for offline applications where the load can be disconnected and there is enough time to accurately access the OCV of a given cell [23].

3. BATTERY MODELING

Li-ion batteries can be modeled using different techniques namely electro chemical, neural networks, empirical, experimental and equivalent circuit [24, 25]. The choice of modeling technique is a tradeoff between capturing cell dynamics and computational demand. For real time application the equivalent circuit model approach is adopted because it gives good representation of cell dynamics while maintaining low computational resource usage.

The Li-ion battery can be modeled as a third order system using lumped electrical elements like resistors and capacitors. The equivalent circuit model is shown in Figure 3.1.

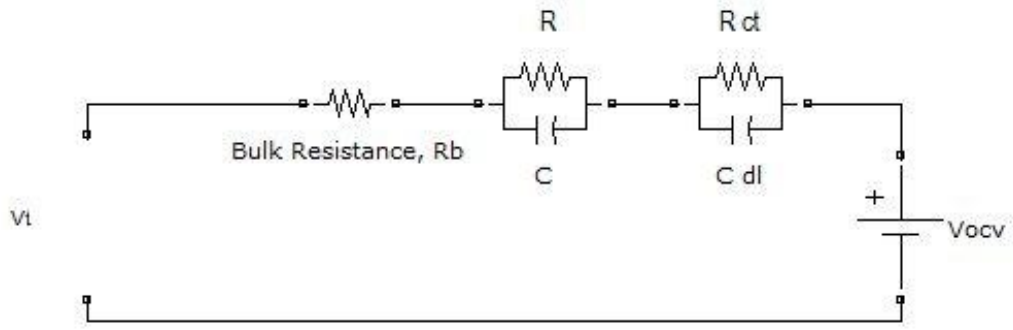

Figure 3.1 Li-ion battery equivalent circuit model

where, R_b is the ohmic resistance, which accounts for the limited conductance of the metallic contacts, inter cell connections, electrode material and the bulk electrolytic resistance to electron and ion migration [26, 27], constant phase

element (CPE) C and resistance R are used to model the distribution of reactivity depicting the local property of the electrode., charge transfer resistance R_{ct} and double layer capacitance C_{dl} represent the interfacial impedance of the cell [28, 29] and V_{OCV} represents the battery cell OCV. The CPE captures the distribution of reactivity at the electrodes which can be attributed to variation in surface properties. The impedance function of the combined RC pair is given by [28, 29].

$$Z_{CPE}(\omega) = \frac{R}{1 + (j\omega)^{\alpha} QR}$$

where, α is the depression factor associated with the CPE and is assumed to be unity. As a result $Q = C$ and CPE behaves like a normal capacitor [26, 28].

The circuit parameters depend on the SOC, temperature and capacity fade effects [30]. For this study, parameter dependency on these factors is assumed to be small. The effect of non-linear element in the equivalent circuit namely Warburg impedance representing the diffusion phenomenon is considered to be negligible [31].

3.1. Linear Li-Ion Battery Model

The OCV is represented by a voltage source and is given by

$$OCV = f(SOC) \qquad (1)$$

where *f* represents a non-linear function mapping the relationship between OCV and SOC. The non-linear relationship between OCV and SOC for a Li-ion battery is given by the classical OCV-SOC curve (solid line) [32, 33] shown in Figure 3.2. This data was recorded from a sample $LiFePO_4$ battery cell tested at room temperature at the Energy Systems and Power Electronics Laboratory (ESPEL) at IUPUI. Unlike the almost linear trend shown by lead acid batteries [27], the OCV-SOC profile for Li-ion battery shows non-linear behavior with a relatively flat trend between 20 and 80 % SOC. In cases where the OCV is used as an indicator of battery SOC, a small error in OCV evaluation can

result in appreciable error in the resulting SOC. In addition, temperature along with age also has an effect on the OCV-SOC trend, and can cause it to shift.

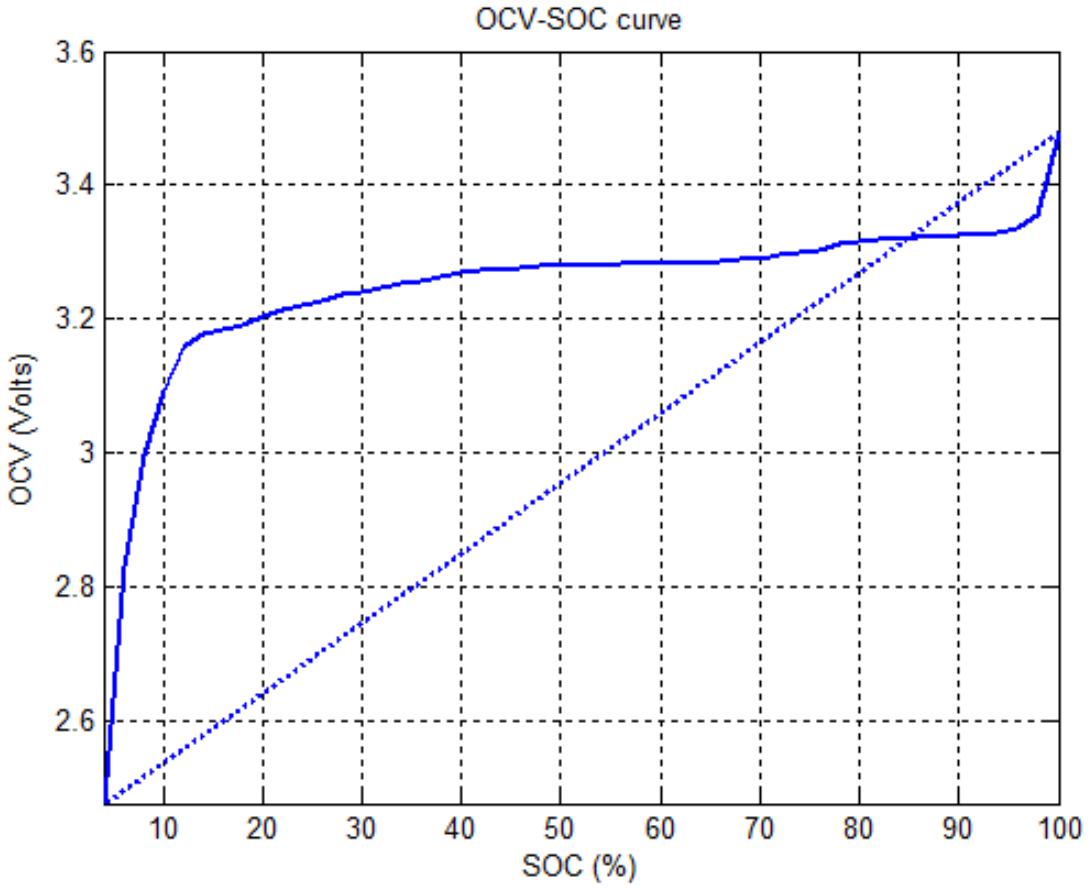

Figure 3.2 Experimental OCV-SOC curve for LiFePO4 battery cell

For the linear system model the OCV-SOC characteristic curve can be replaced by a straight line (Figure 3.2) and hence the function f can now be represented as

$$f = k\,SOC + d \qquad (2)$$

where k represents the slope of the line while d represents the OCV when SOC is zero. The linear approximation is shown by the dotted line in Figure 3.2. Also, the voltage source V_{OCV} can be considered as a large capacitor [26, 34] namely bulk capacitor given by $C_{b.}$. The modified equivalent circuit model is shown in Figure 3.3.

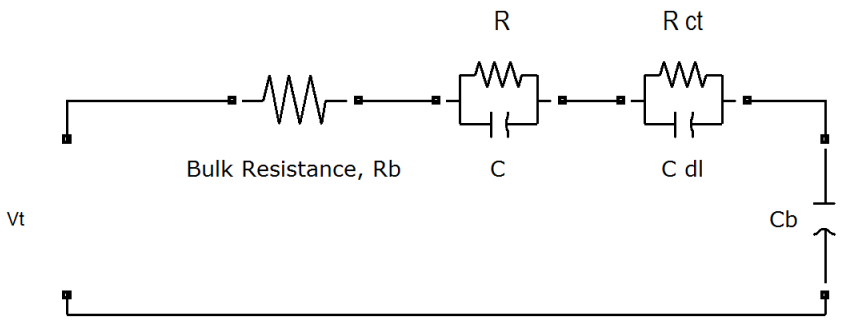

Figure 3.3 Li-ion battery equivalent circuit model with bulk capacitance

Let I_L be the load/charging current through the circuit. The sign convention used in this study considers negative sign of I_L as discharging while positive sign as charging.
Using Kirchhoff's voltage law, the voltage across capacitor C is given by

$$\dot{V}_C = -\frac{V_C}{R\,C} + \frac{I_L}{C} \tag{3}$$

The voltage across the double layer capacitor is given by

$$\dot{V}_{C_{dl}} = -\frac{V_{C_{dl}}}{R_{ct}C_{dl}} + \frac{I_L}{C_{dl}} \tag{4}$$

The voltage across the bulk capacitor is given by

$$\dot{V}_{C_b} = \frac{I_L}{C_b} \tag{5}$$

The voltage across the bulk capacitor V_{C_b} is the same as the OCV and hence equal to f given by (2). Differentiating (2) with respect to time, we get

$$\dot{V}_{C_b} = k\,\dot{SOC} \tag{6}$$

Substituting (5) in (6) and rearranging, the variation in SOC can be obtained as

$$\dot{SOC} = \frac{I_L}{k\,C_b} \tag{7}$$

The terminal voltage V_t can be obtained from

$$V_t = I_L R_b + V_C + V_{C_{dl}} + V_{C_b} \tag{8}$$

where, $I_L R_b$ represents the voltage drop across the bulk resistance.

The state space representation of continuous time system is given by

$$\begin{aligned} \dot{x}(t) &= A\,x(t) + B\,u(t) + Gw(t) \\ y(t) &= C\,x(t) + D\,u(t) + v(t) \end{aligned} \tag{9}$$

It is important to note here that the C in (9) comes from the state space representation of the system and should not be confused with the CPE.

Equations (3), (4), (7) and (8) can be rearranged into state space representation (9) as given below

$$\begin{bmatrix} \dot{\mathrm{SOC}} \\ \dot{\mathrm{V_C}} \\ \dot{\mathrm{V_{C_{dl}}}} \end{bmatrix} = \begin{bmatrix} 0 & 0 & 0 \\ 0 & -\frac{1}{\mathrm{R\,C}} & 0 \\ 0 & 0 & -\frac{1}{\mathrm{R_{ct}\,C_{dl}}} \end{bmatrix} \begin{bmatrix} \mathrm{SOC} \\ \mathrm{V_C} \\ \mathrm{V_{C_{dl}}} \end{bmatrix} + \begin{bmatrix} \frac{1}{\mathrm{k\,C_b}} \\ \frac{1}{\mathrm{C}} \\ \frac{1}{\mathrm{C_{dl}}} \end{bmatrix} [\,\mathrm{I_L}] \tag{10}$$

The terminal voltage can be obtained as

$$\mathrm{V}_t = [k \quad 1 \quad 1] \begin{bmatrix} SOC \\ V_C \\ V_{C_{dl}} \end{bmatrix} + [R_b][\,I_L] + d\,. \tag{11}$$

In (9) and (10), $A = \begin{bmatrix} 0 & 0 & 0 \\ 0 & -\frac{1}{\mathrm{R\,C}} & 0 \\ 0 & 0 & -\frac{1}{\mathrm{R_{ct}\,C_{dl}}} \end{bmatrix}$, $B = \begin{bmatrix} \frac{1}{\mathrm{k\,C_b}} \\ \frac{1}{\mathrm{C}} \\ \frac{1}{\mathrm{C_{dl}}} \end{bmatrix}$, $C = [k \quad 1 \quad 1]$, $D = [R_b]$ and d is considered as the disturbance. $x(t) = \begin{bmatrix} \mathrm{SOC} \\ \mathrm{V_C} \\ \mathrm{V_{C_{dl}}} \end{bmatrix}$ is the state vector of the system, $u(t) = [\,\mathrm{I_L}]$ is the input to the systems and $y(t) = \mathrm{V}_t$ is the system output.

The discrete time counterparts of (3), (4) and (7) can be obtained by using zero-order hold (ZOH) [35] as given below

$$V_C(k) = \left(e^{-\frac{\Delta t}{RC}}\right) V_C(k-1) + R\left[1 - \left(e^{-\frac{\Delta t}{RC}}\right)\right] I(k-1) \tag{12}$$

$$V_{C_{dl}}(k) = \left(e^{-\frac{\Delta t}{R_{ct}C_{dl}}}\right) V_{C_{dl}}(k-1) + R_{ct}\left[1 - \left(e^{-\frac{\Delta t}{R_{ct}C_{dl}}}\right)\right] I(k-1) \tag{13}$$

$$SOC(k) = SOC(k-1) + \frac{\Delta t}{k\, C_b} \tag{14}$$

The discrete time representation of (9) is given by

$$\begin{aligned} x[k] &= \Phi\, \mathrm{x}[\mathrm{k}-1] + \Gamma\, u[k-1] + G\, w[k-1] \\ z[k] &= Hx[k] + D\, u[k] + v[k] \end{aligned} \tag{15}$$

As with the continuous time case, equations (12), (13), (14) and (11) can be rearrange into discrete state space representation (15) where $x = \begin{bmatrix} \mathrm{SOC} \\ \mathrm{V_C} \\ \mathrm{V_{C_{dl}}} \end{bmatrix}$, $\Phi = \begin{bmatrix} 1 & 0 & 0 \\ 0 & e^{-\frac{\Delta t}{RC}} & 0 \\ 0 & 0 & e^{-\frac{\Delta t}{R_{ct}C_{dl}}} \end{bmatrix}$, $\Gamma = \begin{bmatrix} \frac{\Delta t}{k\, C_b} \\ R\left[1 - \left(e^{-\frac{\Delta t}{RC}}\right)\right] \\ R_{ct}\left[1 - \left(e^{-\frac{\Delta t}{R_{ct}C_{dl}}}\right)\right] \end{bmatrix}$, $H = C$, $D = D$, G is the system noise matrix, w is the input noise with zero mean and variance of

$$E\{w_n[l]{w_n}^T[m]\} = \begin{cases} Q, & l = m \\ 0, & l \neq m \end{cases} \tag{16}$$

and v is the measurement noise, independent from w, with zero mean value as

$$E\{v_n[l]{v_n}^T[m]\} = \begin{cases} R, & l = m \\ 0, & l \neq m \end{cases}. \tag{17}$$

Q and R are the process and measurement noise variances respectively. The process and measurement white Gaussian noise is generated using the polar method [36].

3.2. Non-Linear Li-Ion Battery Model

The non-linear Li-ion battery model considered in this study carries forward all the assumptions made for the linear model of section 2.1. The non-linearity in the system is introduced by the OCV-SOC relationship of (1) and the model representation is given by Figure 3.4.

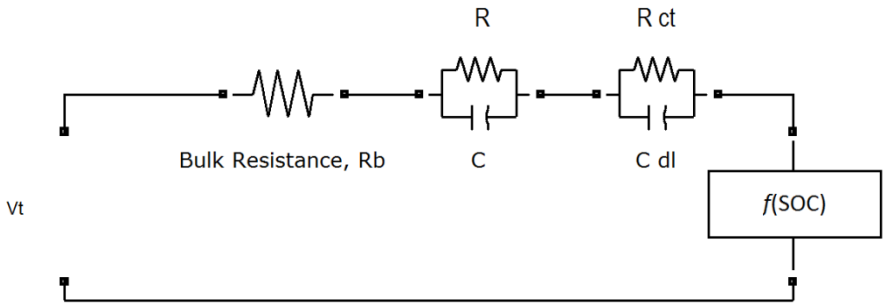

Figure 3.4 Nonlinear Li-ion battery equivalent circuit model

The non-linear function *f*(SOC) is extracted from the OCV-SOC curve in Figure 3.2. Polynomial with varying degree and coefficients are formulated and their fit to the experimental OCV-SOC curve is tested. Using the curve fitting toolbox in Matlab [37], a ninth degree polynomial is found to give the best fit with coefficient of determination R squared equal to 0.99. The function *f* is then given by

$$\begin{aligned} f(SOC) = {} & a_1(SOC)^9 + a_2(SOC)^9 + a_3(SOC)^9 + a_4(SOC)^9 \\ & + a_5(SOC)^9 + a_6(SOC)^9 + a_7(SOC)^9 \\ & + a_8(SOC)^9 + a_9(SOC) + a_{10} \end{aligned} \tag{18}$$

where $a_1 = 0.0385$, $a_2 = -0.01936$, $a_3 = -0.169$, $a_4 = 0.06142$, $a_5 = 0.2328$, $a_6 = -0.05715$, $a_7 = -0.08321$, $a_8 = 0.0005257$, $a_9 = 0.03205$, $a_{10} = 3.297$

Since the relationship between OCV and SOC is no longer assumed to be a straight line, we cannot employ (14) into the non-linear model framework.

The SOC is defined as the ratio of the remaining capacity to the fully charged nominal capacity of the battery [38] and is given by

$$SOC(t) = SOC(0) + \int_0^t \frac{\eta I_L(\tau)}{C_n} d\tau \tag{19}$$

where SOC(0) represents the initial state of charge, C_n represents the battery cell nominal capacity in Ampere hour, I_L is the charge/discharge current, and η represents the coulomb efficiency given by $\eta = \begin{cases} 1, charging \\ 0.98, discharging \end{cases}$. In discrete time, (19) can be given as

$$SOC(k) = SOC(k-1) + \frac{\eta I_L(k-1)\Delta t}{C_n} \tag{20}$$

The state vector for the non-linear model is given by $x = [SOC \quad V_C \quad V_{C_{dl}}]^T$ and is same as its linear counterpart. The battery model is given by the non-linear system model of the form

$$\begin{aligned} x(k) &= g(x_{k-1}, I_{k-1}) + w_{k-1} \\ z(k) &= h(x_k, I_k) + v_k \end{aligned} \tag{21}$$

where *g* and *h* are continuously differentiable non-linear functions while *w* and *v* are same as given in (16) and (17) respectively. From (12), (13), (20),(18) and (21) the functions *g* and *h* are given by

$$g(k-1) = \begin{bmatrix} SOC(k-1) + \frac{\eta\, \Delta \mathrm{t}\, \mathrm{I}_L(\mathrm{k}-1)}{C_n} \\ \left(e^{-\frac{\Delta t}{RC}}\right) V_C(k-1) + R\left[1 - \left(e^{-\frac{\Delta t}{RC}}\right)\right] I(k-1) \\ \left(e^{-\frac{\Delta t}{R_{ct}C_{dl}}}\right) V_{C_{dl}}(k-1) + R_{ct}\left[1 - \left(e^{-\frac{\Delta t}{R_{ct}C_{dl}}}\right)\right] I(k-1) \end{bmatrix} \tag{22}$$

$$h(k) = I(k)R_b + V_C + V_{C_{dl}} + f(SOC) \tag{23}$$

4. SYSTEM IDENTIFICATION

4.1. Impedance Spectroscopy

The equivalent circuit parameters for the Li-ion battery model depicting the various health condition of the battery can be extracted from offline impedance spectroscopy (IS) [26, 30]. IS when applied to electrochemical systems is a technique to identify and characterize the various underlying mechanisms that govern the behavior of the electrochemical system. The technique involves the perturbation of a system under test by a known electrical input and subsequent examination of the system response. The magnitude of the input or the stimulus is governed by the requirement of a linear system response and should be less than the thermal voltage of the system [28, 29].

Among the different types of electrical inputs that can be applied to the system, most commonly a frequency sweep of voltage given by

$$v(t) = V\sin(\omega t)\,, \omega_0 \leq \omega \leq \omega_n \tag{24}$$

is applied and the subsequent current response given by

$$i(t) = I\sin(\omega t + \theta) \tag{25}$$

is measured, where V is the small magnitude stimulus in Volts, I is the magnitude of current response in Amps, θ is the phase shift which depends on the system's characteristics, ω is the angular frequency in rad/s, ω_0 and ω_n are respectively the initial and final frequencies of the intended sweep [29, 39]. The evaluation of system properties based on the voltage and current data is usually carried out in the frequency domain because of the resulting simplicity.

When using lumped electrical elements in equivalent circuit representation along with periodic excitation it becomes advantageous to analyze the circuit in frequency domain. The time domain current-voltage relationship for a pure capacitor is given by

$$I'(t) = C' \frac{dV'(t)}{dt} \tag{26}$$

where C' is the capacitance in Farad.

Taking the Laplace transform of (26) and assuming zero initial condition yields

$$I'(s) = sC'V'(s) \tag{27}$$

Analogous to the resistance evaluation using Ohm's law in direct current (DC) circuits, the impedance of a capacitive element of (26) can be given as

$$Z_C(s) = \frac{V'(s)}{I'(s)} = \frac{1}{sC'} \tag{28}$$

where *s* is the complex argument and can be replaced by $j\omega$ ($j = \sqrt{-1}$).

The time and frequency domain current- voltage relationship and therefore impedance for an ideal resistor remain the same and is given by

$$Z_R(s) = R' = \frac{V'(s)}{I'(s)} \tag{29}$$

The impedance of an element in frequency domain is the quantity similar to resistance, inductance and capacitance in the time domain [40].

The combined impedance of the system consisting of lumped electrical elements will be a complex number of the type $Z = a + bj$ and which varies with angular frequency ω. The real and imaginary parts of the complex number Z are given by $Re(Z) = |Z|\cos(\theta)$ and $Im(Z) = |Z|\sin(\theta)$ respectively and phase angle is given by $\theta = \tan^{-1}\left(\frac{Im(Z)}{Re(Z)}\right)$.

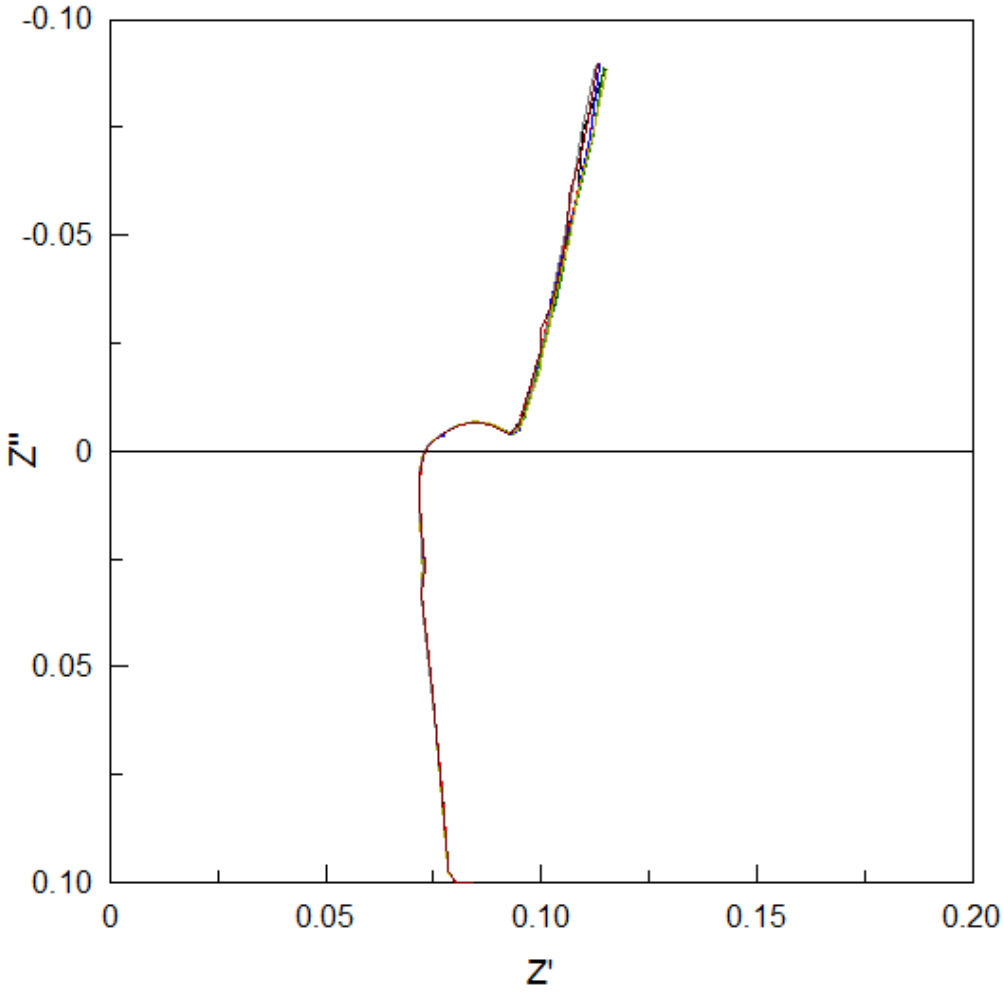

Figure 4.1 Impedance plane plot for healthy Li-ion battery

The complex number Z with its real and imaginary parts is plotted on the Cole-Cole plot with the $Re(Z)$ on the x axis and $Im(Z)$ on the y axis [29]. A typical impedance plot for a Li-ion battery is as shown in Figure 4.1.

The impedance spectroscopy and subsequent parameter extraction given in Tables 6.1 and 6.2 was carried out using an 8-channel Solartron 1470E Multistat (Solartron, England).at the advanced energy research laboratory (AERL) at IUPUI. The general overview of the testing and subsequent parameter identification is as shown in Figure 4.2.

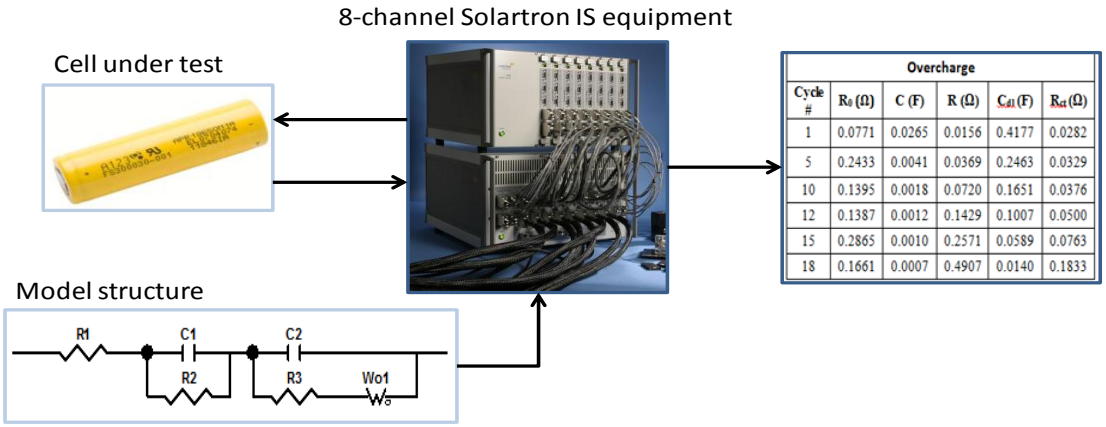

Overcharge					
Cycle #	R_0 (Ω)	C (F)	R (Ω)	C_{dl} (F)	R_{ct} (Ω)
1	0.0771	0.0265	0.0156	0.4177	0.0282
5	0.2433	0.0041	0.0369	0.2463	0.0329
10	0.1395	0.0018	0.0720	0.1651	0.0376
12	0.1387	0.0012	0.1429	0.1007	0.0500
15	0.2865	0.0010	0.2571	0.0589	0.0763
18	0.1661	0.0007	0.4907	0.0140	0.1833

Figure 4.2 Impedance spectroscopy setup

The frequency analysis of an electrochemical system like the Li-ion battery involves the use of a PC that runs application software, which controls the AC IS equipment, stores the data, and displays the graphical results using the data analysis programs like the LEVM/LEVMW complex nonlinear least squares (CNLS) fitting program [41]. After fixing the equivalent circuit model using the LEVM software interface, the program uses the measured cell impedance to minimize the sum of the squares function given by [29],

$$S = \sum_{i=1}^{k} \left\{ w_i{}^a [f_{ei}{}^a - f_t{}^a(\omega_i; P)]^2 + w_i{}^b [f_{ei}{}^b - f_t{}^b(\omega_i; P)]^2 \right\} \qquad (30)$$

where, $w_i{}^a$ and $w_i{}^b$ are the weights, $f_{ei}{}^a$ and $f_{ei}{}^b$ are the experimental impedance values with a and b referring to the real and imaginary parts of cell impedance respectively. $f_t{}^a$ and $f_t{}^b$ are functions of angular frequency ω and the set of model parameters P. Also, i is the number of data points associated with a particular angular frequency ω_i. The entire process of testing and parameter identification using Solartron 1470E Multistat testing platform is highly automated and the parameter values are reported at the end of the test.

4.2. Recursive Least Squares

The recursive least squares (RLS) is an effective time domain system identification technique which aims at fitting battery mathematical model to a sequence of observed current and voltage data by minimizing the sum of the squares of the difference between the observed and computed data recursively [42]. The recursive parameter identification requires the system to be represented in the discrete- time parametric form given by

$$z(k) = \theta^{*T}\varphi \tag{31}$$

where $z(k)$ is the system output as terminal voltage, θ^* is a linear vector of unknown parameters and is being identified by RLS, $\varphi(k)$ is the vector of earlier current inputs and voltage outputs. By taking the Kirchhoff's voltage law about the equivalent circuit in Figure 3.4and using (18), the terminal voltage is given by,

$$\begin{aligned} V_t(k) = {} & a_9(SOC^9)+a_8(SOC^8)+a_7(SOC^7)+a_6(SOC^6)+a_5(SOC^5) \\ & +a_4(SOC^4)+a_3(SOC^3)+a_2(SOC^2)+a_1(SOC)+a_0 - I_L(k)R_b - V_c(k) \\ & - V_{Cdl}(k) \end{aligned} \tag{32}$$

separating the unknown parameters from the known signals, the parametric form for the battery model is given by

$$\begin{aligned} V_t(k) = {} & \left[a_9 \quad \dots \quad a_0 \quad R_b \quad e^{-\frac{\Delta t}{RC}} \quad R\left(1-e^{-\frac{\Delta t}{RC}}\right) \quad e^{-\frac{\Delta t}{R_{ct}C_{dl}}} \quad R_{ct}\left(1-e^{-\frac{\Delta t}{R_{ct}C_{dl}}}\right)\right]^T \\ & \times [SOC(k)^9 \quad \dots \quad SOC(k)^0 \quad -I_L(k) \quad -V_c(k-1) \quad -I_L(k-1) \quad -V_{Cdl}(k-1) \quad -I_L(k-1)] \end{aligned} \tag{33}$$

For further simplification of (32), the combined parameters can be lumped together as

$$A_1 = e^{-\frac{\Delta t}{RC}}, B_1 = R\left(1-e^{-\frac{\Delta t}{RC}}\right), A_2 = e^{-\frac{\Delta t}{R_{ct}C_{dl}}}, B_2 = R_{ct}\left(1-e^{-\frac{\Delta t}{R_{ct}C_{dl}}}\right)$$

The estimation equation is given by

$$\theta(k) = \theta(k-1) + P(k)\varphi(k)\varepsilon(k) \tag{34}$$

where P is the covariance matrix, ε is the normalized estimation error, φ is from (30), and at $k = 1$, $\theta(0)$ is the best initial guess on the parameters to be identified.

The normalized estimation error ε is given by

$$\varepsilon(k) = \frac{V_t(k) - \theta(k)^T \varphi(k)}{m^2(k)} \tag{35}$$

where m^2 is the normalizing signal and given by

$$m^2(k) = cc + \varphi^T(k)\varphi(k) \tag{36}$$

where cc is positive scalar value.

The covariance matrix P is recursively updated by using the following equation

$$P(k) = P(k-1) - \frac{P(k-1)\varphi(k)\varphi(k)^T P(k-1)}{m^2(k) + \varphi(k)^T P(k-1)\varphi(k)} \tag{37}$$

with $P(0) = P_0 = {P_0}^T > 0$

5. FAULT DETECTION AND DIAGNOSIS

Like any physical system, Li-ion batteries are designed for increased performance and reliability by incorporating better chemistry, protection circuitry, fuses etc. Even with all these measures in place it is hard to guarantee failure free operation of the battery. Fault diagnosis when applied to batteries is more than just an on-off switch; it provides the type of the fault occurring and predicts the changes in the system well ahead of time.

Different techniques for FDD are available with each having its own advantages and limitations. The various fault diagnosis methods can be broadly classified into hardware redundancy schemes, plausibility tests, software/ analytical redundancy schemes, and signal processing. The choice of diagnosis method is based on a combination of factors like cost, range of operation and complexity of process [43]. Software/ analytical redundancy fault diagnosis is particularly important because it can be implemented at a lower cost, incorporate process complexity and encompass greater range of system operation.

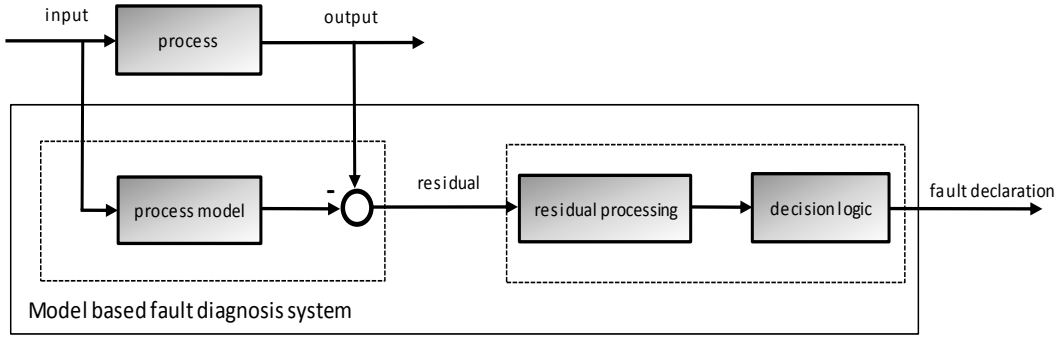

Figure 5.1 Model based fault diagnosis scheme [43]

Model based fault diagnosis is an integral part of software redundancy based fault diagnoses and is based on the process/ physical model of the system. The general model based fault diagnoses scheme is given in Figure 5.1.

In the model based fault diagnosis scheme, the process model is the mathematical representation of the system. While this model should be able to show good agreement with the system dynamics of the process it should more importantly conform to the fault carrying dynamics of the process. Also for real time applications, a computationally inexpensive system representation will be advantageous as computational resources are limited; this consideration takes all the more precedence in mobile application. The measured output from the process is compared with the model response to generate the residuals. While this residual carries valuable information pertaining to system health, most often they have to be processed to get rid of the unwanted information incorporated due to system noise, measurement noise and modeling inaccuracies before being used in decision logic.

The shortcomings of the pure model based fault diagnosis especially in the area of residual evaluation can be overcome by replacing the process model and the subsequent residual generation process by a state observer [43-45]. This fundamental shift in residual generation process enables the removal of errors in the residue signal due to faulty initial condition, and unknown disturbances. Different observer like Luenberger state observer, output observer and Kalman filter have been considered in the observer based fault diagnosis techniques [43]. In this study, we will focus on the Kalman filter based fault diagnosis framework.

5.1. Observer Based Fault Diagnosis- Kalman Filter

The Kalman filter based fault diagnosis uses Kalman filter in conjunction with the process under observation to generate the fault carrying residuals. The general

configuration of model based fault diagnosis with Kalman filter state observer used in this study is shown in Figure 5.2.

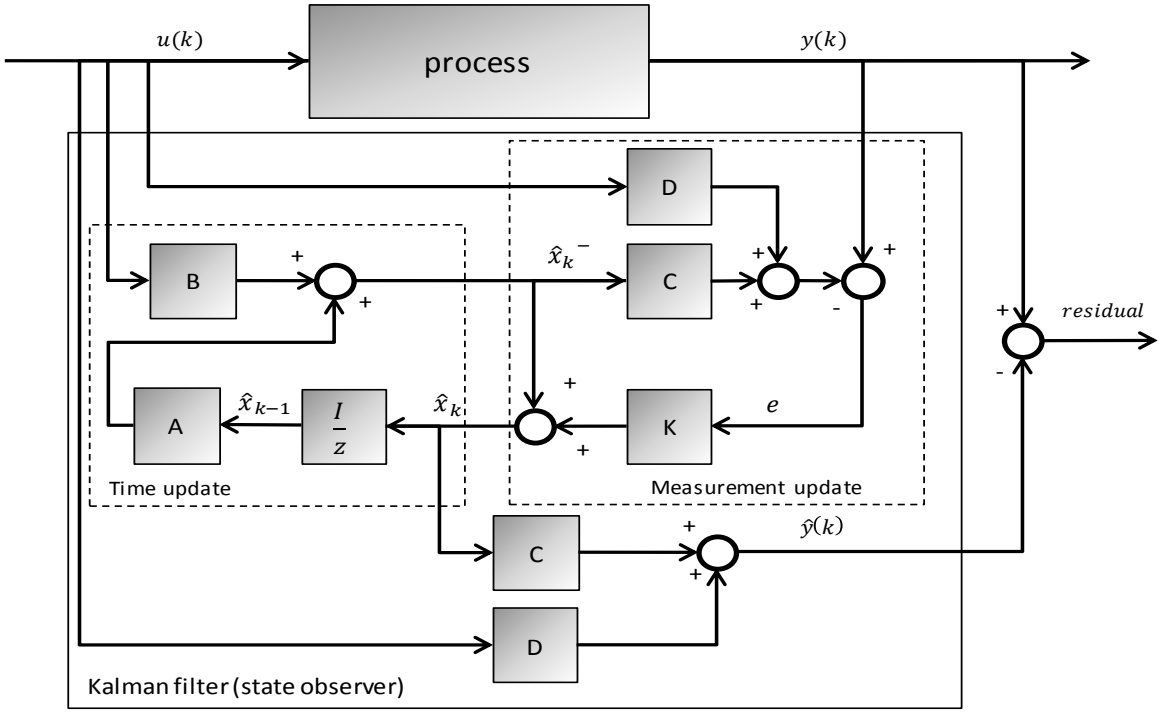

Figure 5.2 Observer based fault diagnosis with Kalman filter

In the Figure 5.2, $u(k)$ and $y(k)$ are the accessible process control and output vectors respectively, B is the input matrix, A is the system matrix, C is the output matrix, K is the Kalman gain vector and $\hat{y}(k)$ is the estimated output. Kalman filter and its non-linear counterpart- the extended Kalman filter are used for estimating the states of the linear and non-linear system by minimizing the mean of the squared error. In the following two sections both Kalman filter and its extended version will be introduced in sufficient detail with reference to application on battery systems.

5.1.1. Kalman Filter Design

For a discrete, linear time invariant state space model given by (9), (10) and (11), Kalman filter estimates the state of the system using two groups of equations namely time update and measurement update [46, 47]. The time update equations are given by

$$\begin{aligned} \hat{x}_k^- &= A\hat{x}_{k-1} + Bu_{k-1} \\ P_k^- &= AP_{k-1}A^T + Q \end{aligned} \tag{38}$$

where $\hat{x}_k^-$ represents the projection of current state estimate based on previous state estimate $\hat{x}_{k-1}$ and input u_{k-1}, P_k^- represents the *a priori* estimate error covariance based on previous covariance estimate P_{k-1}. A, B are from (10) while Q is from (16).

The measurement update equations are given by

$$\begin{aligned} K_k &= P_k^- C^T (CP_k^- C + R)^{-1} \\ \hat{x}_k &= \hat{x}_k^- + K_k[y_k - (C\hat{x}_k^- + Du_k)] \\ P_k &= (I - K_k C)P_k^- \end{aligned} \tag{39}$$

where K_k is the Kalman gain vector which minimizes the error covariance given by $E[e_k e_k^T]$ with $e_k = x_k - \hat{x}_k$, R is from (17), $\hat{x}_k$ is the current state estimate, y_k is measurement also represented as z_k, D is from (11), P_k is the *a posteriori* estimate error covariance. With an initial estimate of $\hat{x}_{k-1}$ and P_{k-1} the equations (30) and (31) are used recursively to obtain accurate estimation of the states for the battery system.

A more compact version of Kalman filter equations given by (30) and (31) can be obtained by substituting (30) into (31) and rearranging [48].

$$\begin{aligned} \hat{x}_k &= A\hat{x}_{k-1} + Bu_{k-1} + K_k\{y_k - [C(A\hat{x}_{k-1} + Bu_{k-1}) + Du_k]\} \\ K_k &= P_k^- C^T (CP_k^- C + R)^{-1} \\ P_k &= (I - K_k C)(AP_{k-1}A^T + Q) \end{aligned} \tag{40}$$

The residual signal is obtained by subtracting the estimated terminal voltage signal from the measured terminal voltage of the battery. This is obtained using the following equation,

$$r_k = y_k - \hat{y}_k \tag{41}$$

where, r_k is the residual, y_k is the measured terminal voltage and $\hat{y}_k = C\hat{x}_k + Du_k$ is the estimated terminal voltage of the battery at time step k.

5.1.2. Extended Kalman Filter Design

In the case where the process is modeled as a non-linear system, we cannot directly employ Kalman filters for state estimation. Extended Kalman filters are used for state estimation of non-linear systems by linearizing around the current mean and covariance. When applied to the non-linear system of (21), (22) and (23), the time update equations are given by [46, 49]:

$$\begin{aligned} \hat{x}_k^- &= g(\hat{x}_{k-1}, u_{k-1}) \\ P_k^- &= G_k P_{k-1} G_k^T + Q_{k-1} \end{aligned} \tag{42}$$

and the measurement update equations are given by:

$$\begin{aligned} K_k &= P_k^- H_k^T (H_k P_k^- H_k^T + R_k)^{-1} \\ \hat{x}_k &= \hat{x}_k^- + K_k[y_k - h(\hat{x}_k^-)] \\ P_k &= (I - K_k H_k)\, P_k^- \end{aligned} \tag{43}$$

where $\hat{x}_k^-$ represents predicted state based on the function g evaluated at the previously estimated state and available input, P_k^- is the *a priori* estimate error covariance, K_k is the Kalman gain, $\hat{x}_k$ is the updated state estimate and P_k is the updated covariance estimate. The state transition matrix G_k and observation matrix H_k are evaluated at each step and are given by,

$$\begin{aligned} G_k &= \left.\frac{\partial g}{\partial x}\right|_{\hat{x}_{k-1}, u_{k-1}} \\ H_k &= \left.\frac{\partial h}{\partial x}\right|_{\hat{x}_k^-, u_k} \end{aligned} \tag{44}$$

The estimated terminal voltage is given by,

$$\hat{y}_k = h(\hat{x}_k, u_k) \tag{45}$$

The residual signal is obtained by subtracting the estimated terminal voltage form the measured terminal voltage and is similar to the representation of (33)

5.2. Multiple Model Adaptive Estimation

MMAE is a special type of observer based fault diagnosis technique as it employs a Kalman filter bank (KFB) of n filters, where one observer represents the healthy condition of the process being monitored while the remaining $n-1$ observers represent the fault conditions of the process [10, 13, 14]. In addition to this apparent extension to the single observer case, MMAE also provides the added advantage of including a probabilistic approach to FDD.

FDD using MMAE can be divided into two major parts; the first part deals with the state estimation using KFB and generating the residuals for each of the n signature conditions while the second part, also called the conditional probability evaluation, processes the residuals and assign a fault weightage to each of the n operational cases of the process. The individual weights range between 0 and 1 and sum of all the n weights is equal to 1.

The earliest use of conditional probability density evaluation and weighting of coefficients can be found in [50-52], where the primary emphasis is the optimal state estimation and its applications. With respect to FDD based implementation of Kalman filter and conditional probability density evaluation, extensive work has been done by Maybeck et al. [11, 12, 53-55] and Athans et al. [56] on the FDD of aircraft systems.

The general layout of MMAE when applied to linear process model with $n-1$ distinct faults is shown in Figure 5.3.

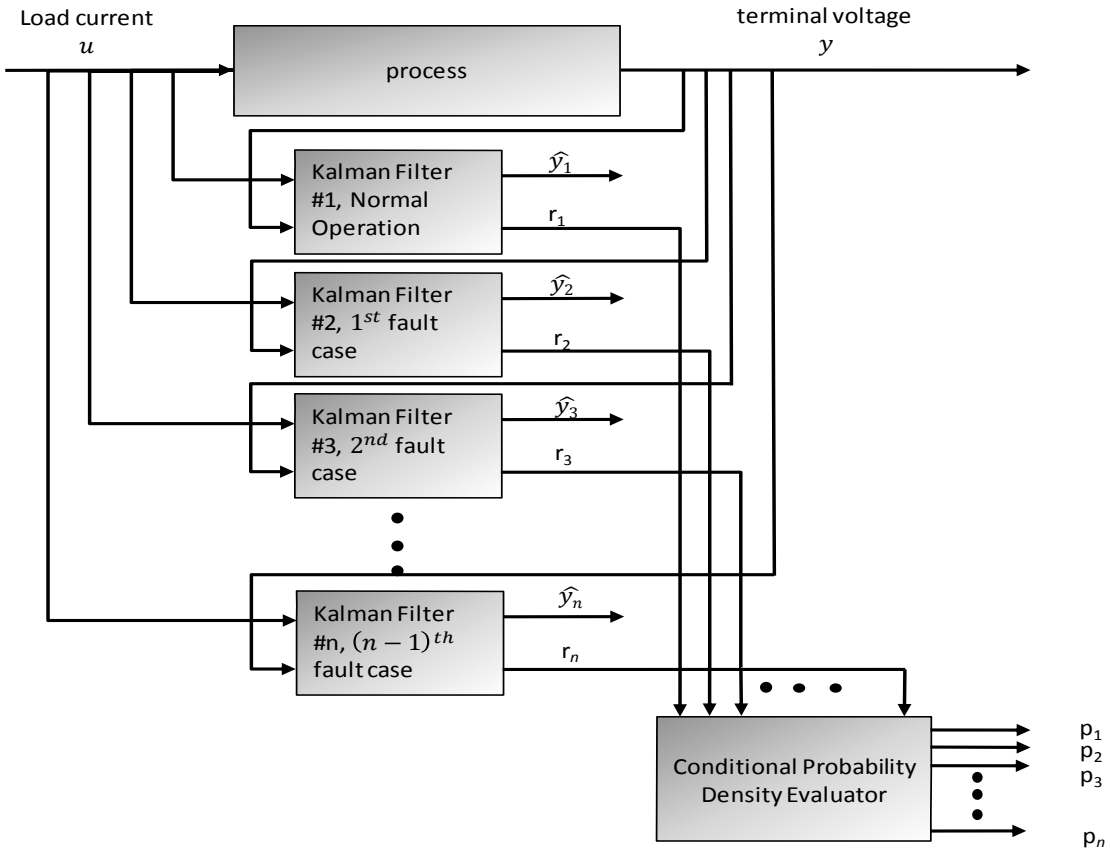

Figure 5.3 Residual generation and probability evaluation for linear process model

The Kalman filters in the MMAE run in a parallel fashion with all the n filters receiving the same input u and measurement y. For the linear battery model case given by (9), (10), (11), when the process response matches with the estimated output from the filter, the mean value of the residual signal goes to zero, the covariance ψ for the n^{th} operational case can then be computed by [12, 48, 57],

$$\psi_n = C_n P_n {C_n}^T + R \tag{46}$$

where P and R are from (32) and (17) respectively and C is the output matrix given by (11). The conditional probability density function considering the history of measurements $y(k-1) = [y(k-1), y(k-2), y(k-3) \ldots]$ is given by [12, 54, 57],

$$f_{y(k)|a,y(k-1)}(\boldsymbol{y}_k|\boldsymbol{a}_n, y_{k-1}) = \beta_n \exp(\circ) \tag{47}$$

where,

$$\beta_n = \frac{1}{(2\pi)^{l/2}\,|\psi_n(k)|^{1/2}} \tag{48}$$

l is the measurement dimension, equal to one as we are measuring the terminal voltage, and

$$(\circ) = -\frac{1}{2}\, r_n{}^T(k)\psi_n{}^{-1} r_n(k) \tag{49}$$

r_n is the residual of the n^{th} model.

For the n^{th} operational case, the probability p_n of being correct at any time t_i is given by [12, 14]:

$$p_n(k) = \frac{f_{y(k)|a,y(k-1)}(\boldsymbol{y}_k|\boldsymbol{a}_n, y_{k-1})p_n(k-1)}{\sum_{j=1}^{n} f_{y(k)|a,y(k-1)}(\boldsymbol{y}_k|\boldsymbol{a}_j, y_{k-1})p_j(k-1)} \tag{50}$$

where p_j is the conditional probability of the j^{th} model and $j = 1,2,\dots,n$.

The evaluation of probability at any given time requires *a priori* samples to compute the current values and is normalized over a complete sum of conditional probabilities of all the n systems [12, 48].The largest conditional probability amongst all is used as an indicator of fault in the process. In some cases where the probability changes rapidly and makes the FDD unpredictable, the probabilities can then be compared with a threshold [48].

In case of non-linear process model the Kalman filter in the MMAE scheme is replaced by extended Kalman filters. Non-linear dynamics can be used in the context of MMAE by using a bank of EKF's. These filters represent the normal and faulty operational conditions of the system [58, 59]. EKF's have been used extensively in Li-ion battery equivalent circuit models for state and parameter estimation [8, 33, 60-63]. The layout when MMAE is applied to non-linear process model is as shown in Figure 5.4.

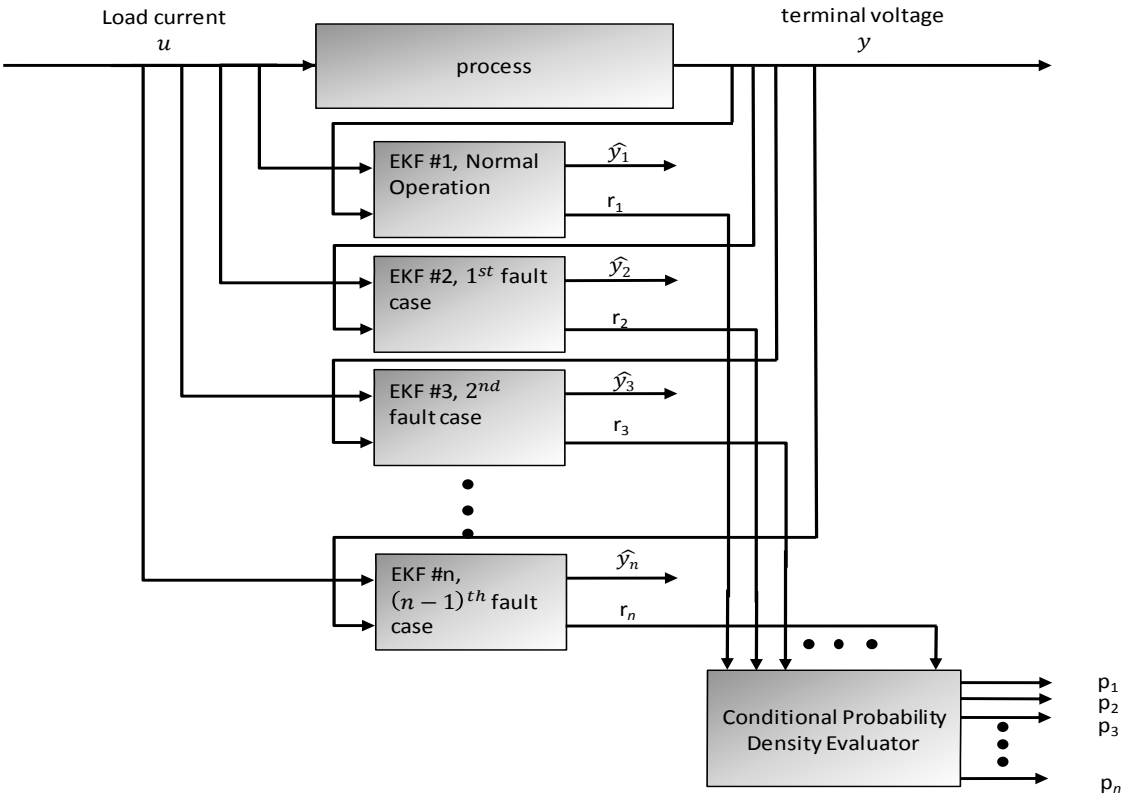

Figure 5.4 Residual generation and probability evaluation for non-linear process model

The conditional probability density evaluator equations in the non-linear process model case are given by:

$$\psi_{n,k} = C_{n,k} P_{n,k} {C_{n,k}}^T + R$$

$$f_{y(k)|a,y(k-1)}(\boldsymbol{y}_k|\boldsymbol{a}_n, y_{k-1}) = \beta_n \exp(\circ) \tag{51}$$

and,

$$p_n(k) = \frac{f_{z(k)|a,Z(k-1)}(\boldsymbol{z}_k|\boldsymbol{a}_n, Z_{k-1}) p_n(k-1)}{\sum_{j=1}^{n} f_{z(k)|a,Z(k-1)}(\boldsymbol{z}_k|\boldsymbol{a}_j, Z_{k-1}) p_j(k-1)}$$

where, $C_{n,k} = \left.\frac{\partial h}{\partial x}\right|_{\hat{x}_k}$ is the linearized output vector updated at every state estimate, $P_{n,k}$ and R are from (35) and (17) respectively, $f_{y(k)|a,y(k-1)}(\boldsymbol{y}_k|\boldsymbol{a}_n, y_{k-1})$ is the probability

density function of the current measurement, β_n and $(\circ)$ are the same as (40) and (41) respectively.

6. DESIGN OF EXPERIMENTS

As mentioned earlier, a Li-ion battery cell can be modeled using lumped circuit elements like resistors and capacitors where each one of them signifies a particular physical phenomenon in the battery. When a fault occurs in the Li-ion battery, these circuit parameters namely bulk resistance, constant phase elements including one each of a resistor and capacitor, charge transfer resistance and double layer capacitance show a marked variation from their healthy battery counterparts. The primary focus of this study is the FDD of over charge and over discharge condition of the Li-ion battery. When considering over charge and over discharge faults, the battery model parameters show a particular and distinct trend in parameter variation with increasing numbers of test cycles.

The test subject selected for this study was A123 18650 $LiFePO_4$ Battery (APR18650M 1A 3.3V 1000 mAh) from A123 Systems (Cambridge, MA) [64]. Cell parameters when under nominal discharge/ over charge and nominal charge/ over discharge were extracted using impedance spectroscopy technique; impedance spectroscopy involves applying a sinusoidal small amplitude frequency sweep to the battery and measuring the resulting battery impedance. Further the impedance response is fit to the selected circuit arrangement for accurate parameter extraction. The impedance spectroscopy results are a function of temperature, SOC and ageing. In this study the effects of temperature and ageing are neglected. Tables 6.1 and 6.2 give the impedance spectroscopy results for the 18650 $LiFePO_4$ battery cell under nominal discharge/ over charge and nominal charge/ over discharge conditions respectively.

Table 6. 1 AC Impedance spectroscopy data under nominal discharge/ over charge

NOMINAL DISCHARGE/ OVER CHARGE					
Cycle	$R_b(\Omega)$	$C(F)$	$R(\Omega)$	$C_{dl}(F)$	$R_{ct}(\Omega)$
1	0.0771	0.0265	0.0156	0.4177	0.0282
5	0.2433	0.0041	0.0369	0.2463	0.0329
10	0.1395	0.0018	0.0720	0.1651	0.0376
12	0.1387	0.0012	0.1429	0.1007	0.0500
15	0.2865	0.0010	0.2571	0.0589	0.0763
18	0.1661	0.0007	0.4907	0.0140	0.1833

Table 6. 2 AC Impedance spectroscopy data under nominal charge/ over discharge

NOMINAL CHARGE/ OVER DISCHARGE					
Cycle	$R_b(\Omega)$	$C(F)$	$R(\Omega)$	$C_{dl}(F)$	$R_{ct}(\Omega)$
1	0.0503	0.1922	0.0051	0.8213	0.0126
2	0.0566	0.2623	0.0045	2.6470	0.0098
3	0.0578	0.2669	0.0055	3.2500	0.0123
4	0.0594	0.4379	0.0053	4.2580	0.0126
5	0.0569	0.4067	0.0056	4.3360	0.0112
6	0.0623	0.2590	0.0054	2.9430	0.0081

In time domain analysis, the parameter values for over discharge are extracted using the recursive least squares technique. For this study, a brand new Li-ion battery under test was subjected to nominal charge/ over discharged in a cyclic fashion. The over discharge regime is based on Navy over discharge cycle [65] and a 24 hour over discharge cycle. In the Navy over discharge cycle, the Li-ion battery is discharged at maximum suitable discharge rate for 25 % over discharge. The charging of the battery is carried out using a standard non-abusive charge regime. The battery is cycled 25 times using this discharge-charge regime and the critical battery parameters are continuously monitored. In the 24 hour over discharge test regime, the battery is discharged at a suitable discharge rate until

the SOC reaches zero. To maintain near zero terminal voltage, a resistor is connected across the terminals for the duration of 24 hours. The charging of the battery is then carried out using a standard non-abusive charging profile. The 24 hour over discharge test cycle is repeated twice and the battery parameters are continuously monitored.

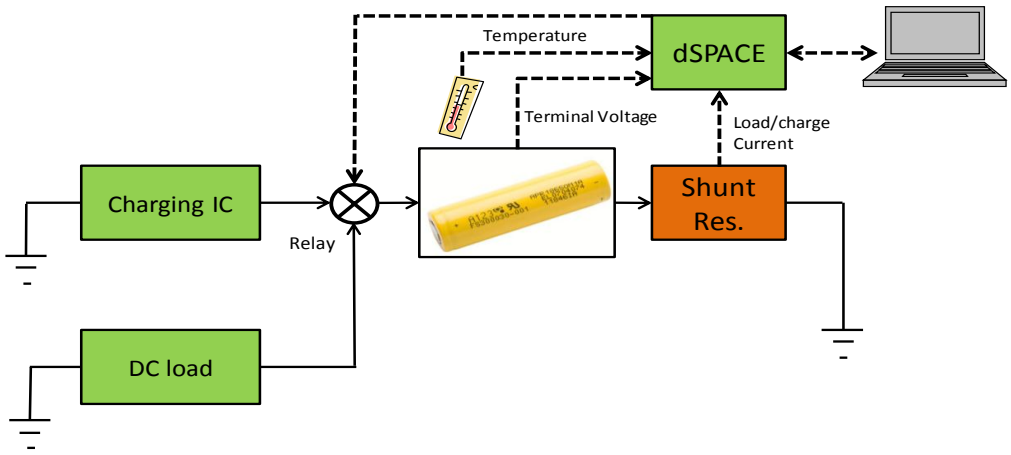

Figure 6.1 Li-ion battery test setup

The time domain Li-ion battery testing and data acquisition setup is as shown in Figure 6.1. For the purpose of system identification, a standard discharge current is applied to the battery for partial SOC drop and the battery is charged again to full SOC. The typical noise filtered discharge-charge current and voltage curves are as shown in Figure 6.2.

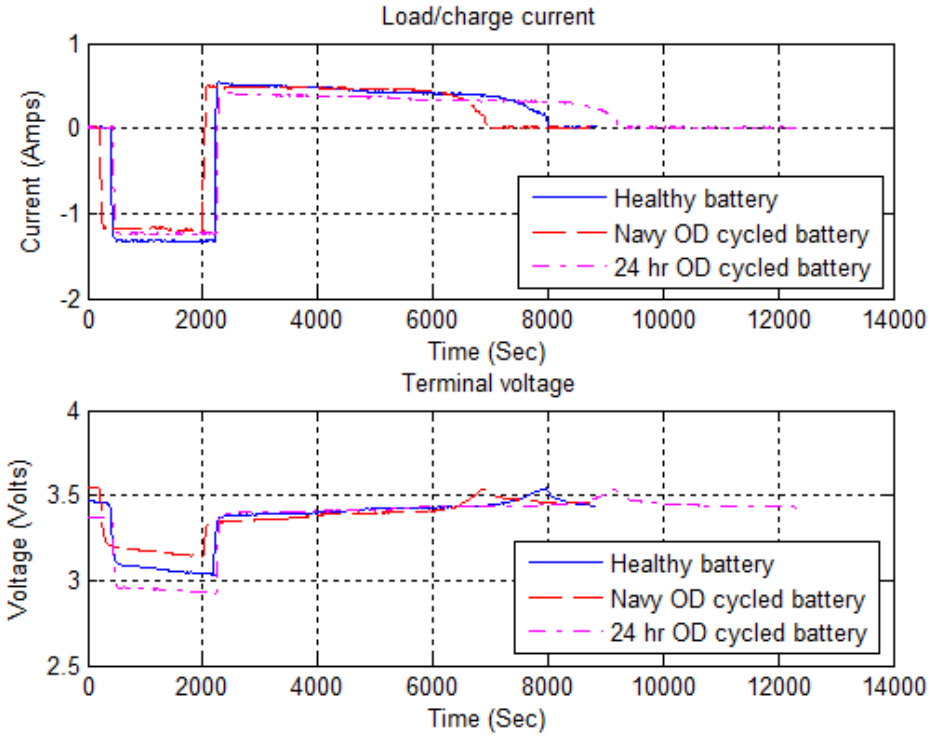

Figure 6.2 Current and Voltage profiles for healthy and nominal charge/ over discharge battery

Based on the current and voltage data of Figure 6.2, the parameter values for the healthy cell before and after the nominal charge/ over discharge cycles are estimated. The identified system parameters are given in Table 6.3. Some of the combined parameters, especially B_1 and B_2 show negative values because of the way they are represented, as shown in Section 4.2, and also because of negative equivalent circuit parameter values, called the pseudo impedance [29].

Table 6. 3 Parameter identification data under nominal charge/ over discharge

Parameter	New battery	Navy over discharge	24 hour over discharge
a^9	0.49161	0.748268	-0.02105
a^8	-0.08717	-0.07862	-0.04814
a^7	-0.32599	-0.42834	-0.00855
a^6	-0.27117	-0.37816	0.057027
a^5	-0.03456	-0.08725	0.092889
a^4	0.198062	0.201331	0.042196
a^3	0.206745	0.219284	-0.10774
a^2	-0.07741	-0.10596	-0.20669
a^1	-0.00024	-0.03705	0.341718
a^0	3.3558	3.490569	3.223314
R_b	-0.06492	-0.05705	-0.09248
A_1	0.241634	0.607614	0.216303
B_1	-0.06881	-0.06389	-0.09306
A_2	0.241634	0.034997	0.216303
B_2	-0.06881	-0.06389	-0.09306

Using the data from impedance spectroscopy and recursive least squares, multiple fault representing models can be formulated. The load current applied to the Li-ion battery cell is based on the urban dynamometer driving schedule (UDDS) drive cycle profile which has been appropriately scaled to match the nominal capacity of one cell. The UDDS drive cycle is accessed from Autonomie [66] and is represented in Figure 6.3.

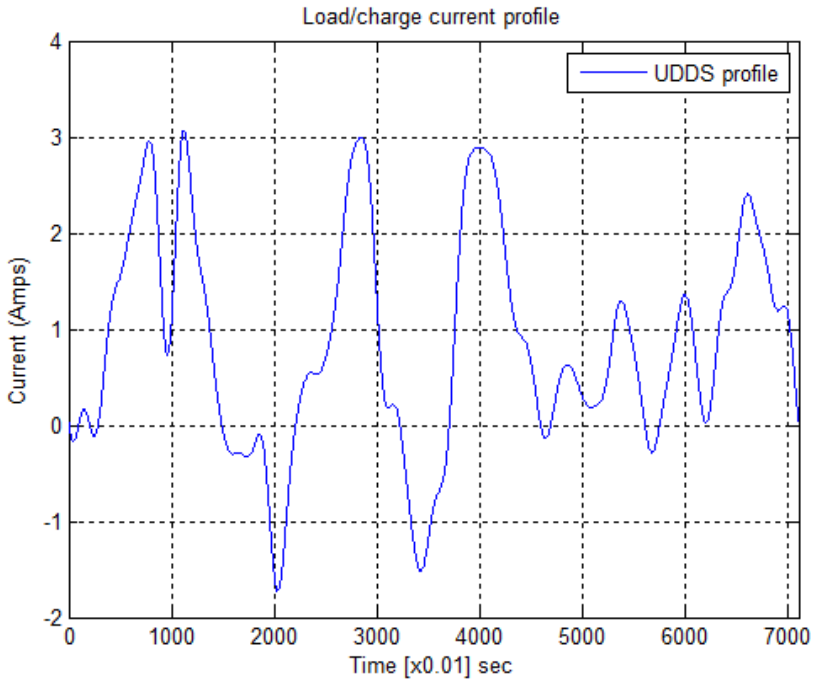

Figure 6.3 Battery cell load current profile

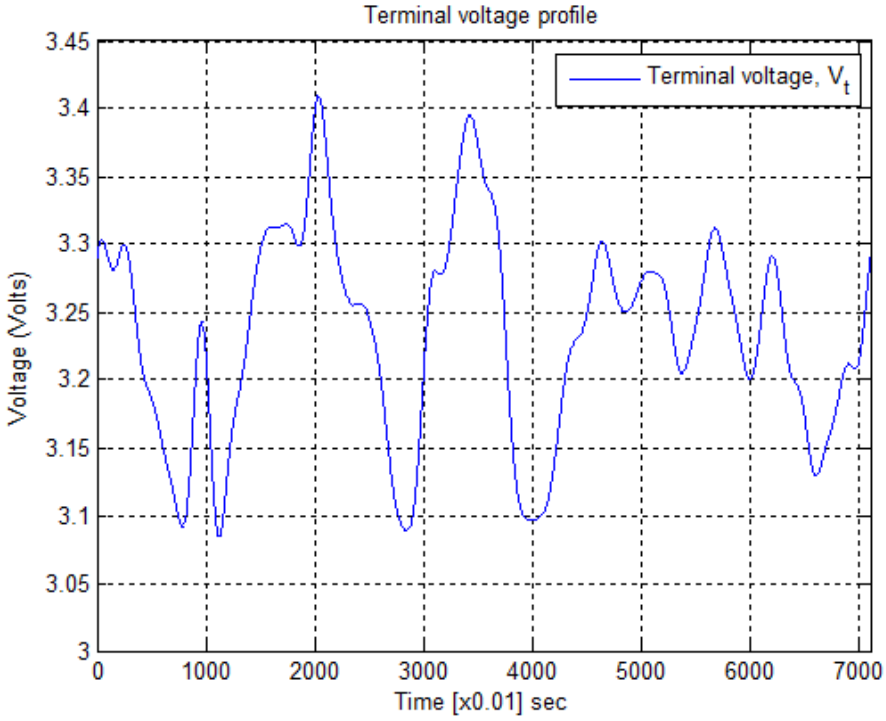

Figure 6.4 Simulated battery cell terminal voltage

The duration of the load current selected for this study 71 seconds but the numbers of samples depend on the sample time T of the system. The corresponding simulated terminal voltage response to the load current input given by a healthy battery cell model is represented in Figure 6.4. While the load current profile simulates the actual working condition of the system, the resulting fault probabilities depend more on the zero average residual signal rather than the magnitude of the load current.

7. DIAGNOSIS PERFORMANCE EVALUATION

The effectiveness of the FDD is examined by injecting consecutive fault cases into the measurement and studying the fault decision. While the number of samples depends on the selected sample time, the general evaluation scenario follows the following setup in which the total simulation is divided into equal parts which occur consecutively:

Failure detection in over charge and over discharge using IS system parameters

- Healthy operation for the first quarter
- Over charge fault condition for the second quarter
- Over discharge fault condition for the third quarter
- Healthy operation for the last quarter

Condition monitoring in over discharge using recursive least squares system parameters

- Healthy operation for the first thirds
- Over discharge operational condition for the second thirds
- Healthy operation for the final thirds

Once the operational condition is diagnosed correctly, this setup helps to check the effectiveness of the FDD algorithm to de-latch itself from its earlier diagnosis [48]. It is also assumed that only one type of fault can occur in the system at any given point in time. The starting SOC of the battery is considered to be at 70% and the polarization voltages are considered to be zero.

The evaluation process is divided into two major parts; the first part is concerned with the use of linear Li-ion battery cell model with impedance spectroscopy data and the second part discusses the results when the non-linear battery model is used with both impedance spectroscopy and recursive least squares data in FDD scheme.

7.1. FDD Performance Evaluation Using Linear Battery Model and IS Model Parameters

Based on the process model structure the system can have an optimal sample time which best captures the process dynamics. For the linear battery model the best response is obtained when the sample time T is chosen as 1×10^{-3}. Through simulations the load current is found to lack enough excitation for robust FDD and is therefore multiplied by a sime term given by:

$$I_L{}' = I_L \, Sin(600\,\pi t) \tag{52}$$

The terminal voltage is also modified by multiplying with a sine term given by:

$$V'_t = V_t \, sin(600\,\pi t) \tag{53}$$

At every time step the probabilities are evaluated to obtain a value between 0 and 1. Where 0 indicates the absence of the particular operational condition and 1 indicates the presence of the respective operational condition. The resulting fault probabilities are given in Figure 7.1. The fault probabilities along with the corresponding residuals are given Figure 7.2.

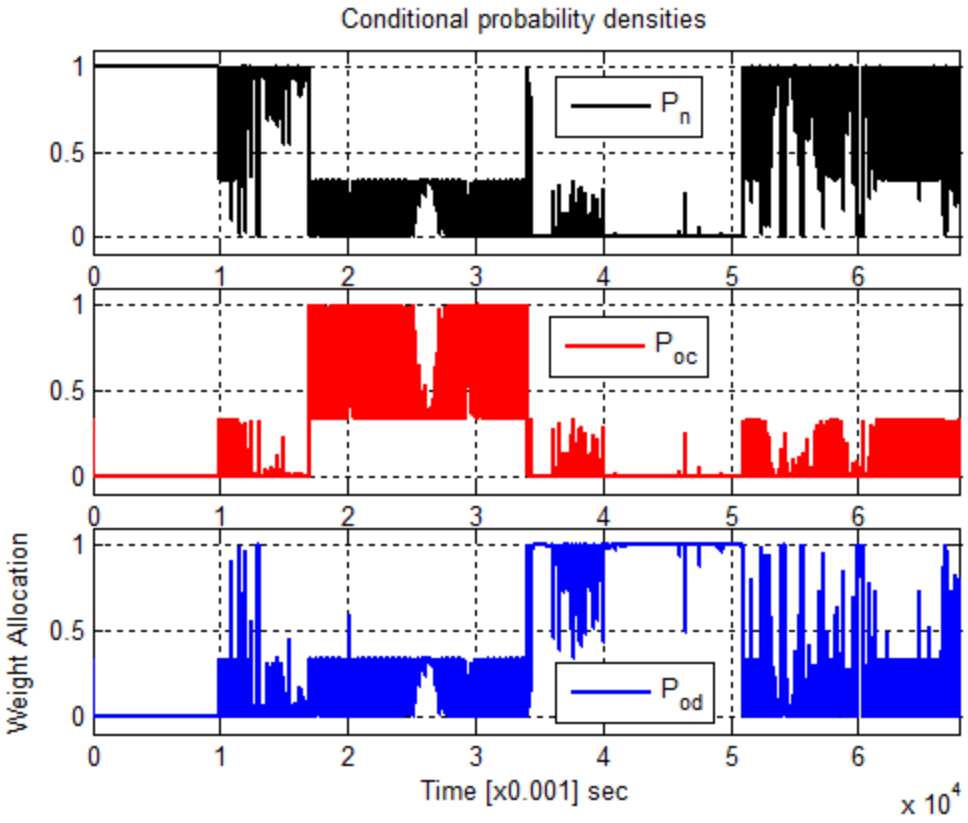

Figure 7.1 Conditional probability densities for healthy condition, over charge and over discharge faults

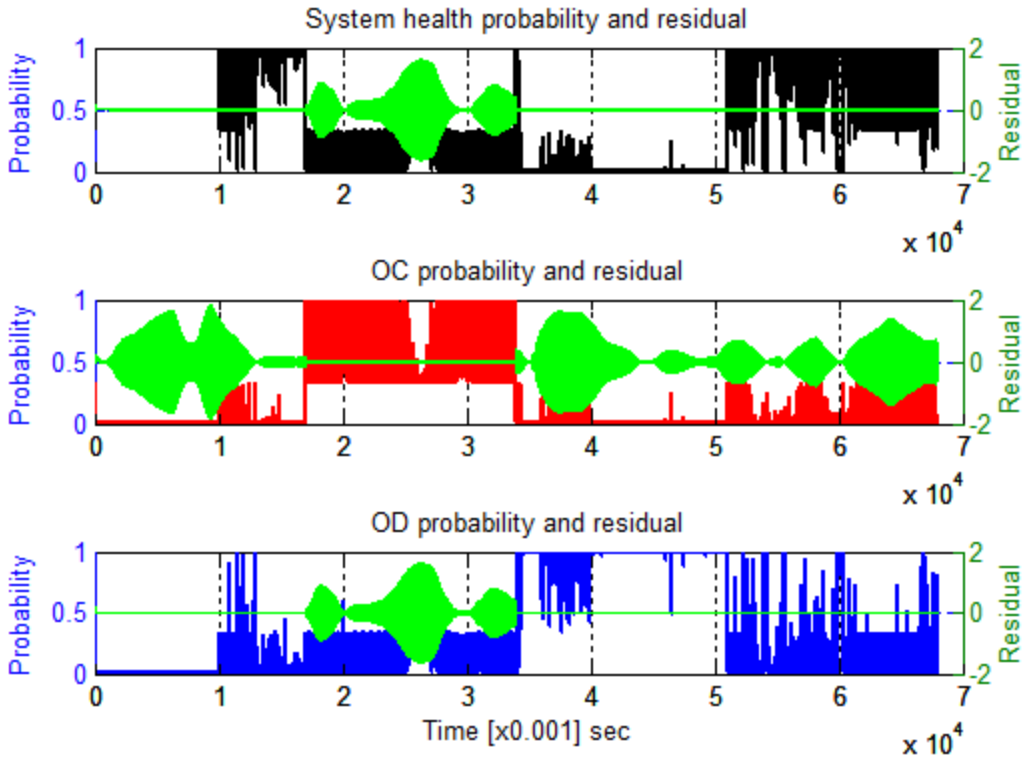

Figure 7.2 Conditional probability densities and residuals for healthy condition, over charge and over discharge faults

In Figure 7.1 the probability p indicates the healthy condition of the Li-ion battery cell while $p1$ and $p2$ indicate the presence of over charge and over discharge fault respectively. The test is run for the total duration of 68 seconds. At 17 seconds, the over charge fault is indicated as healthy condition probability p transitions from 1 to 0 and over charge probability $p1$ increase from 0 to 1. At 34 seconds, the over charge probability $p1$ previously at 1, transitions to 0 and over discharge probability $p2$ increases from 0 to 1thus indicating the occurrence of over discharge fault. Finally, at 51 seconds the healthy condition probability p increases from 0 to 1 while the over discharge probability value $p2$ drops from 1 to 0, this indicates presence of the healthy battery condition. From Figure 7.1 some amount of uncertainty can be observed. While this rapid change in the probability values is an inherent feature, it can be corrected by comparing the probabilities with a threshold [48]. The threshold value needs to be chosen

carefully as it involves a tradeoff between cleaner probabilities and losing out on important fault related information. The resulting probabilities after a threshold filter has been applied are shown in Figure 7.3.

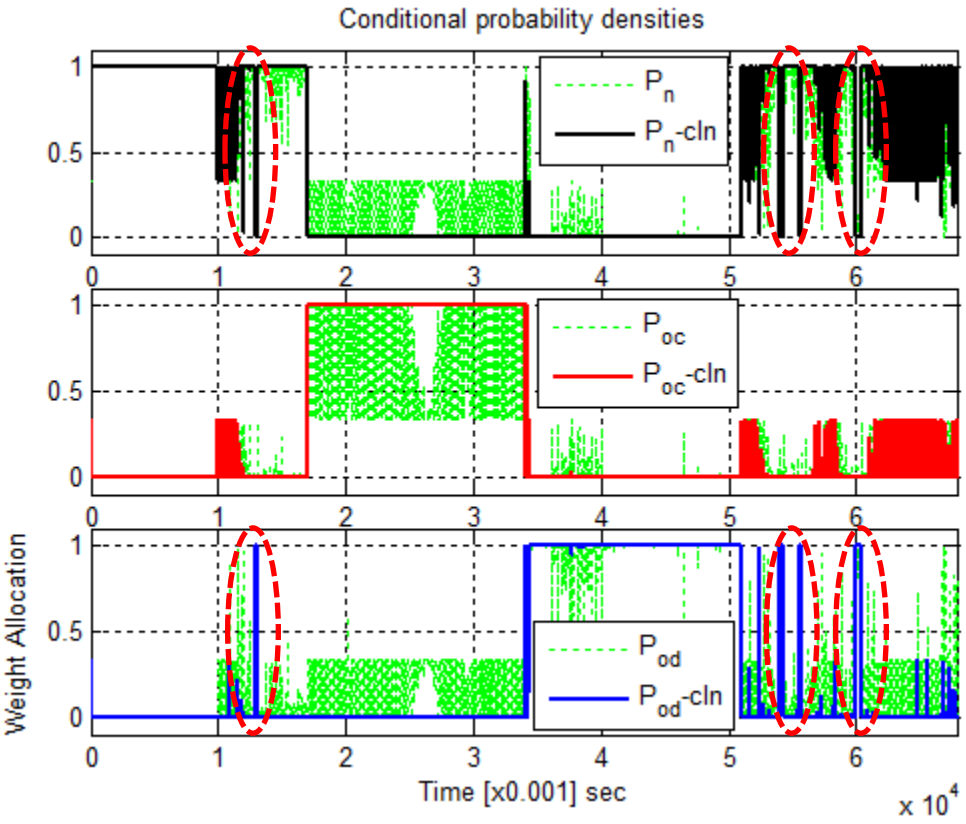

Figure 7.3 Filtered and un-filtered conditional probability densities

The implementation of a threshold filter results in the desired probability correction but there are still some regions of probability which show high variation and hence unexpected behavior. These regions, also identified and singled out in Figure 7.3, can result in false alarms and hence loss in FDD reliability. For further analysis of this un-expected behavior the over discharge probability is selected as the three probabilities are intrinsically related to one another and any one of the three can be a good candidate.

The probabilities are directly dependent on the respective residual input as shown in equations (41) and (42). This relationship can be better visualized in Figure 7.4, where the over discharge probability and residual are plotted together.

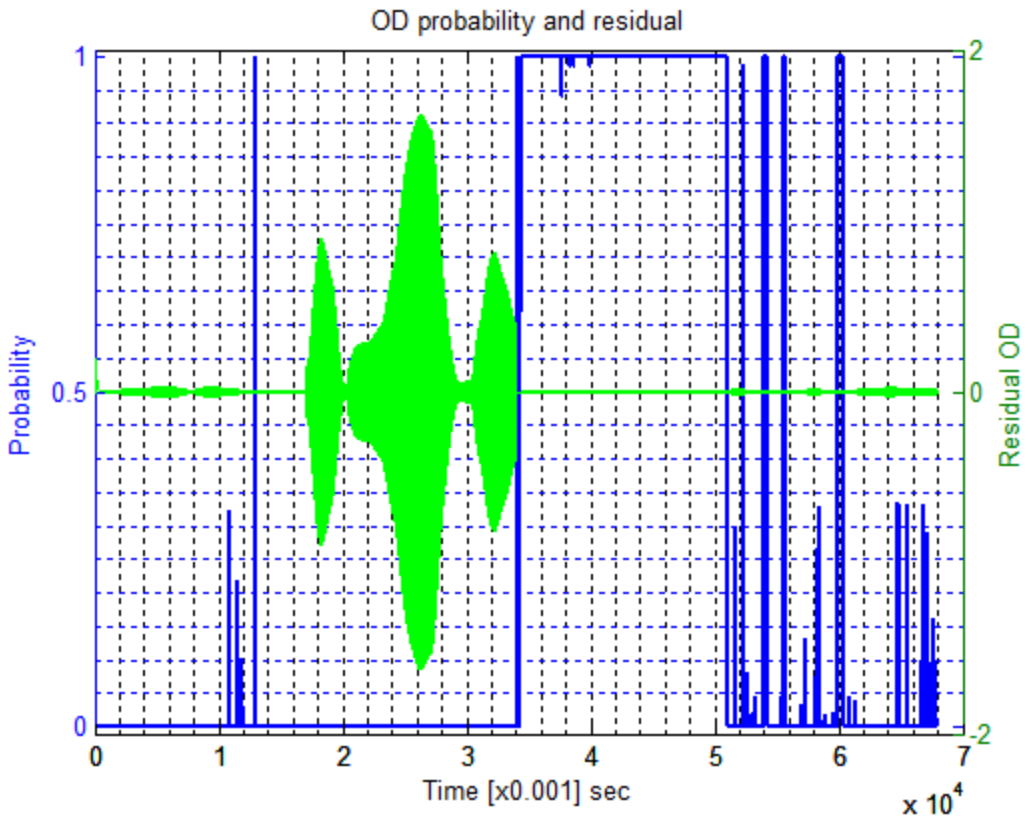

Figure 7.4 Over discharge probability and residual

The regions of abrupt probability change are identified and numbered. The major transition in a conditional probability specifically from 0 to 1 occurs when the mean value of the residual signal goes to zero. As expected the over discharge probability behavior in the identified regions shown in Figure 7.5 coincides with the mean value of the residual reaching zero.

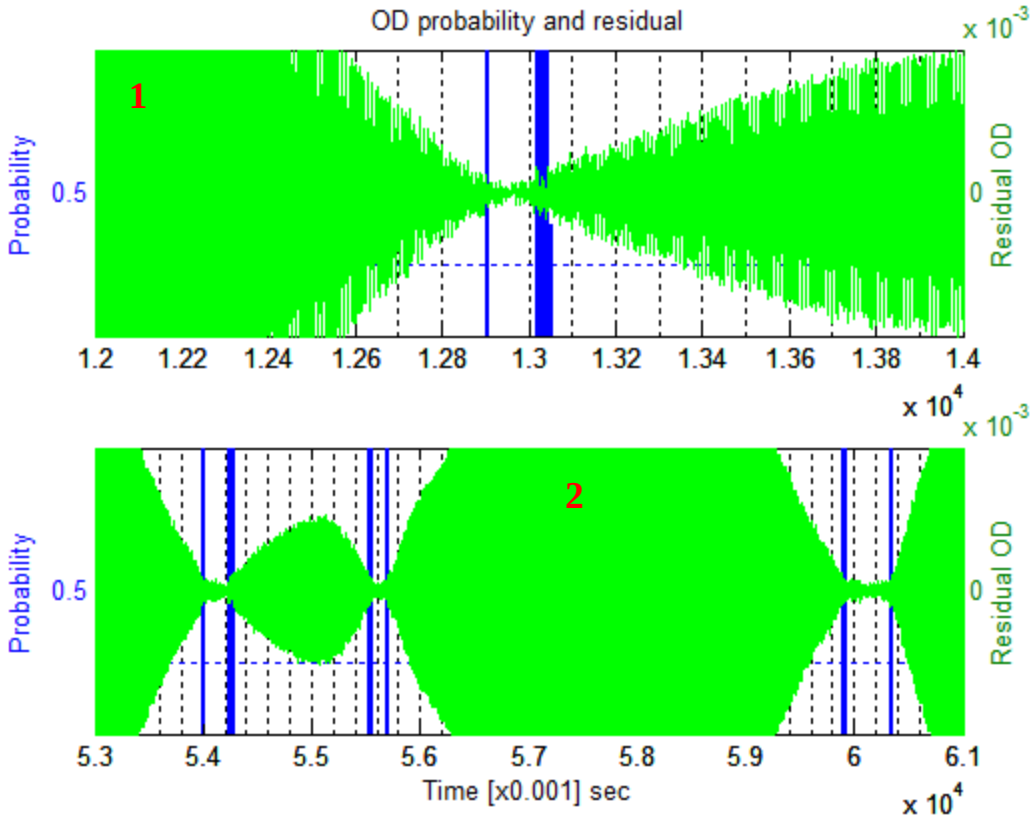

Figure 7.5 Regions of unexpected zero mean valued over discharge residual

The zero mean value of the residual can only be possible is there is an over discharge fault or when the load current reaches zero [10]. Since these identified regions do not fall in the designed over discharge fault scenario, they can be positively attributed to the zero value of load current. This behavior can be confirmed from Figure 7.6, where the load current and the over discharge probability are compared together.

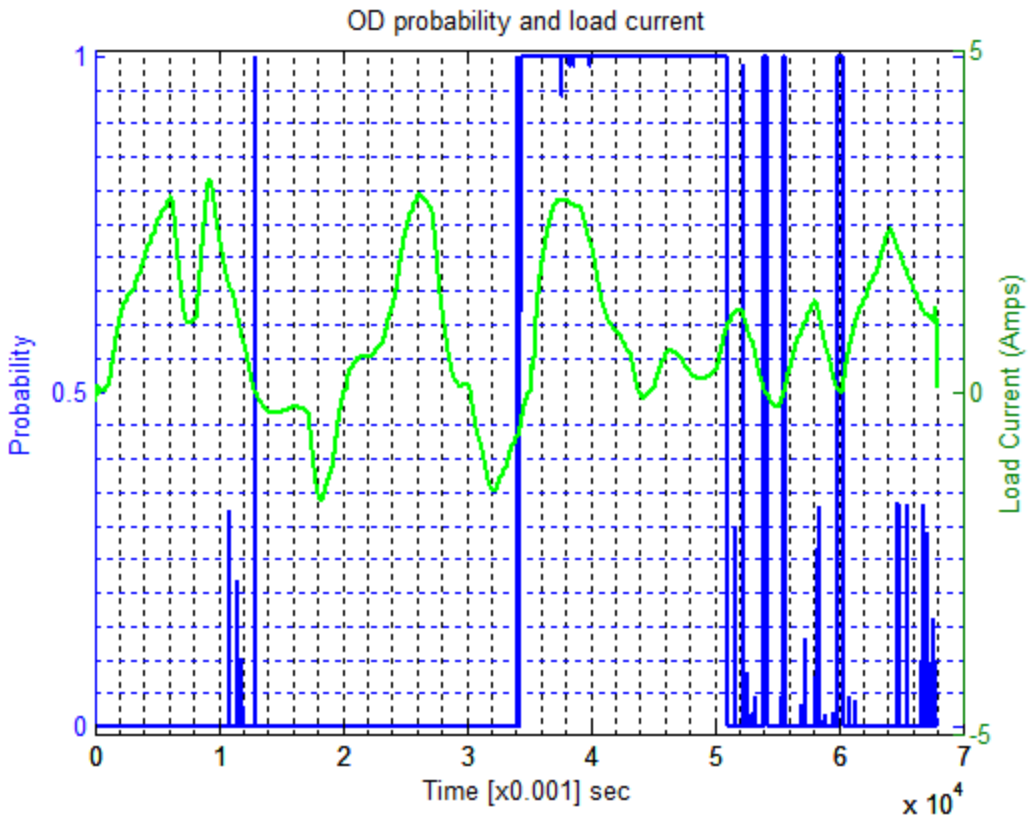

Figure 7.6 Over discharge probability and load current

The solution to the above problem can be achieved by freezing the probabilities whenever the absolute value of the load current falls below a certain set point [10]. The resulting conditional probability density values are shown in Figure 7.7.

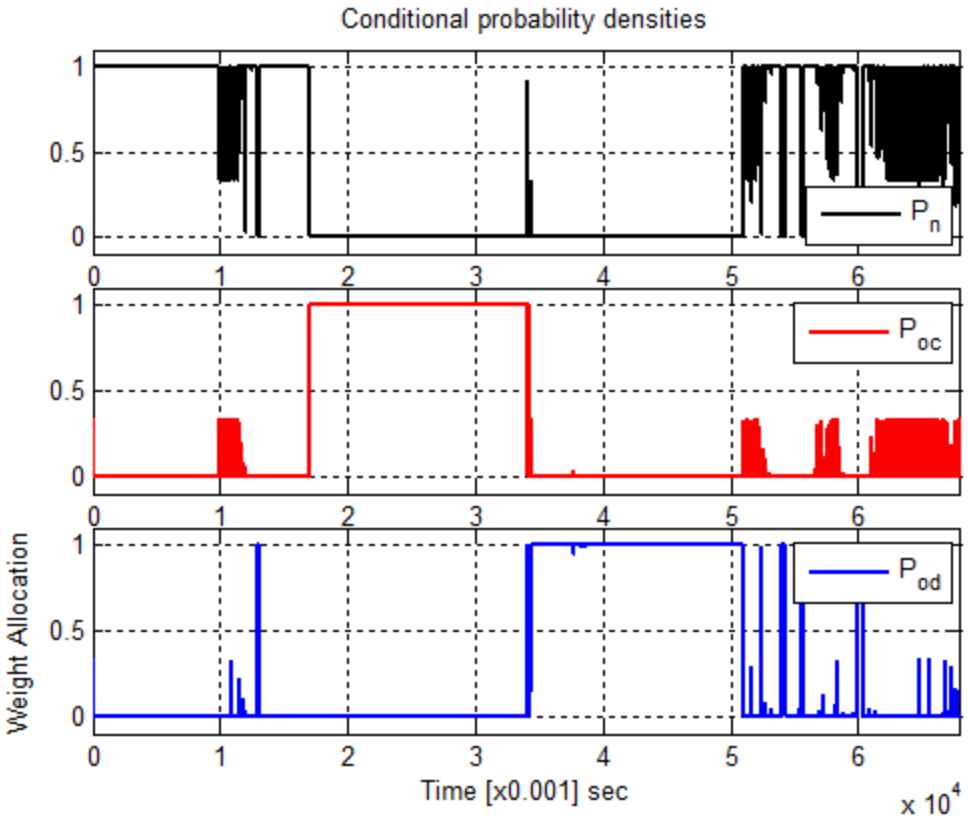

Figure 7.7 Cleaned conditional probability densities

The loss of probability at zero load current will not amount to any major disadvantage as it is highly unlikely that a fault will occur when the load current is zero.

From the results it is evident that linear Li-ion battery model can be successfully incorporated up to a certain degree in the MMAE scheme of FDD for accurate and real-time over charge and over discharge fault detection of the energy storage device.

7.2. FDD Performance Evaluation Using Non-Linear Battery Model

7.2.1. Non-Linear Battery Model With IS Battery Parameters

The FDD using non-linear Li-ion battery model is studied under two different conditions of SOC. Firstly the MMAE technique was applied to the system without any

bound on the SOC and the subsequent fault decisions were analyzed. As a second step, the SOC was lower and upper bounded and the resulting fault decisions were studied for improved performance.

7.2.1.1. FDD with Unbounded SOC

The MMAE FDD setup for non-linear systems given by equation (43) is applied to the non-linear Li-ion battery system given by equations (21), (22) and (23) with no upper or lower limits on the state of charge estimation. The three resulting probabilities can be observed in Figure 7.8, where P_n represents the probability of the healthy operation of the cell, while P_{OC} and P_{OD} indicate the probability of the over charge and the over discharge fault occurrence respectively.

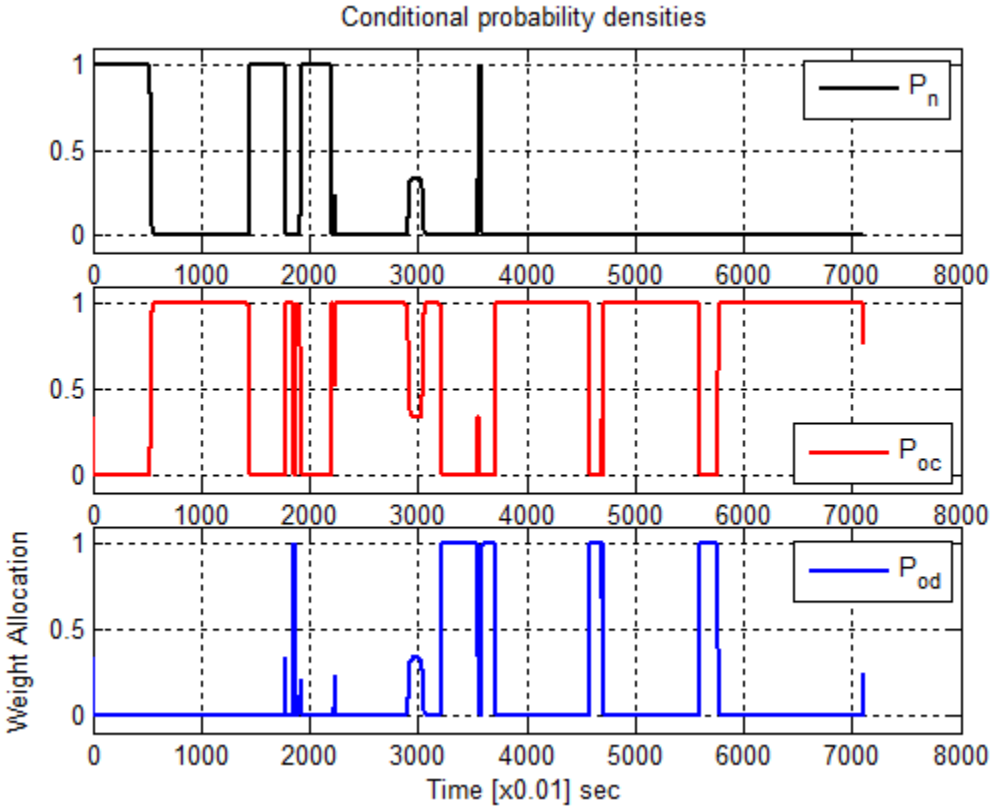

Figure 7.8 Conditional probability density evaluated for normal operation, over charge and over discharge faults

The probability of Figure 7.8 does not follow the expected fault trend established by the fault scenario; it rather shows random behavior and does not indicate any definite fault. This behavior of the fault probabilities can be attributed to the unexpected residual change resulting from inaccurate filter output. The probabilities along with the residuals are as shown in Figure 7.9.

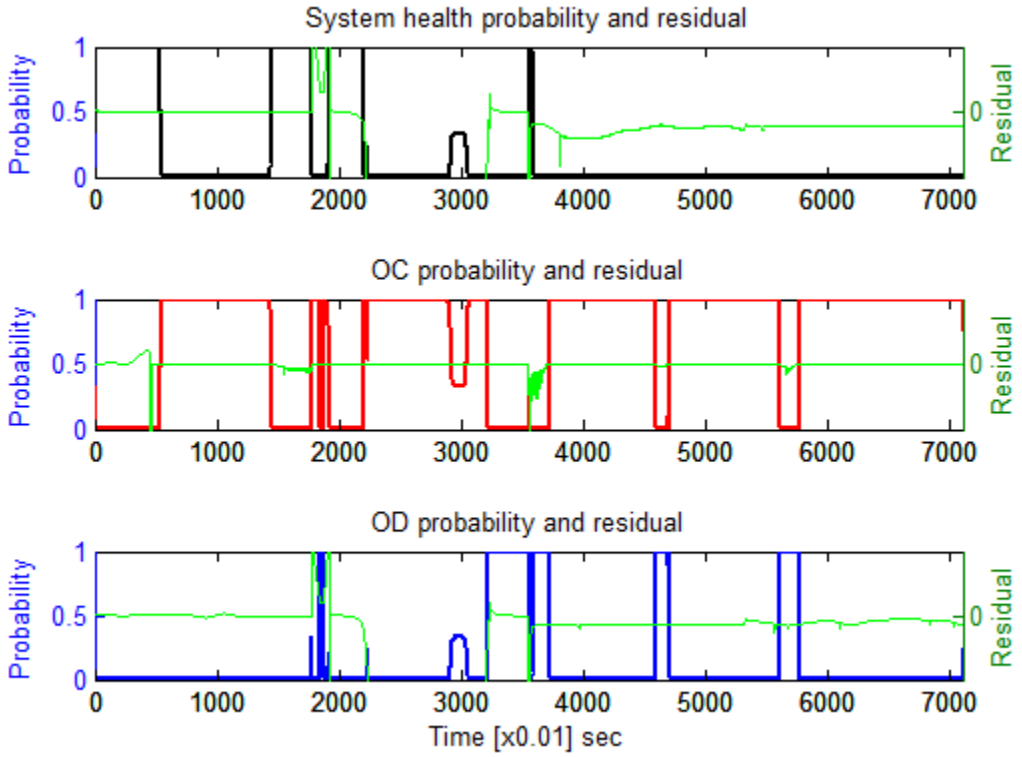

Figure 7.9 Conditional probability density and residuals for unbounded SOC

From the fault probabilities and the residuals it is clear that the signature faults cannot be detected using the current scheme. The extended Kalman filter is used to estimate the state of the non-linear battery model given by $x = [SOC \quad V_C \quad V_{C_{dl}}]^T$. The inaccuracy in the filter output results due to the largely uncontrolled variation in the estimated SOC of the battery cell. Unrealistic SOC variation causes the error to be transferred to the OCV of the battery cell given by (23) and hence the residual generation process given by (33). The unbounded SOC variation can be seen in Figure 7.10. The unbounding of the SOC leads to extensive over or under estimation of the battery SOC. During any particular

battery condition in the test scenario, the SOC signals for the hypothesis under test matches in trend with the measured SOC while showing large offset. This is caused due to inaccurate state estimation stemming from the unrealistically large and small SOC estimation and the error gets accumulated.

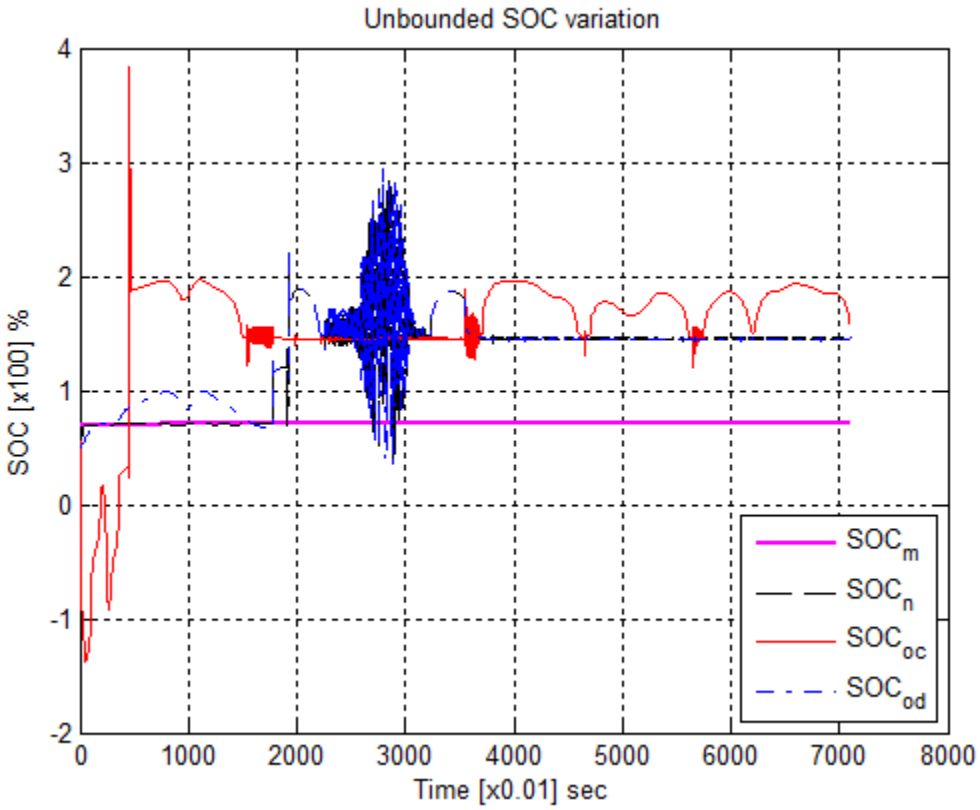

Figure 7.10 Unbounded SOC variation for normal operation, over charge and over discharge faults

Although it is natural to expect the SOC for the over charge or the over discharge battery to show abnormal behavior since it has already failed, it is equally important that SOC stays within the physical boundaries set for an energy storage device. Lower bound on SOC mimics the physical constraint on the system as the SOC cannot be negative. An upper bound on SOC helps to keep the OCV under permissible limits thus giving greater weightage to the fault representing polarization voltages. The polarization voltages for fault model capture the shift in electro-chemical properties of the battery cell once the over charge and over discharge failure has occurred.

7.2.1.2. FDD with Bounded SOC

The upper and lower bounding of the SOC to 1 and 0 respectively, results in more accurate diagnosis using MMAE. The estimated terminal voltage resulting from the bounded SOC is compared with the simulated terminal voltage measurement in Figure 7.11.

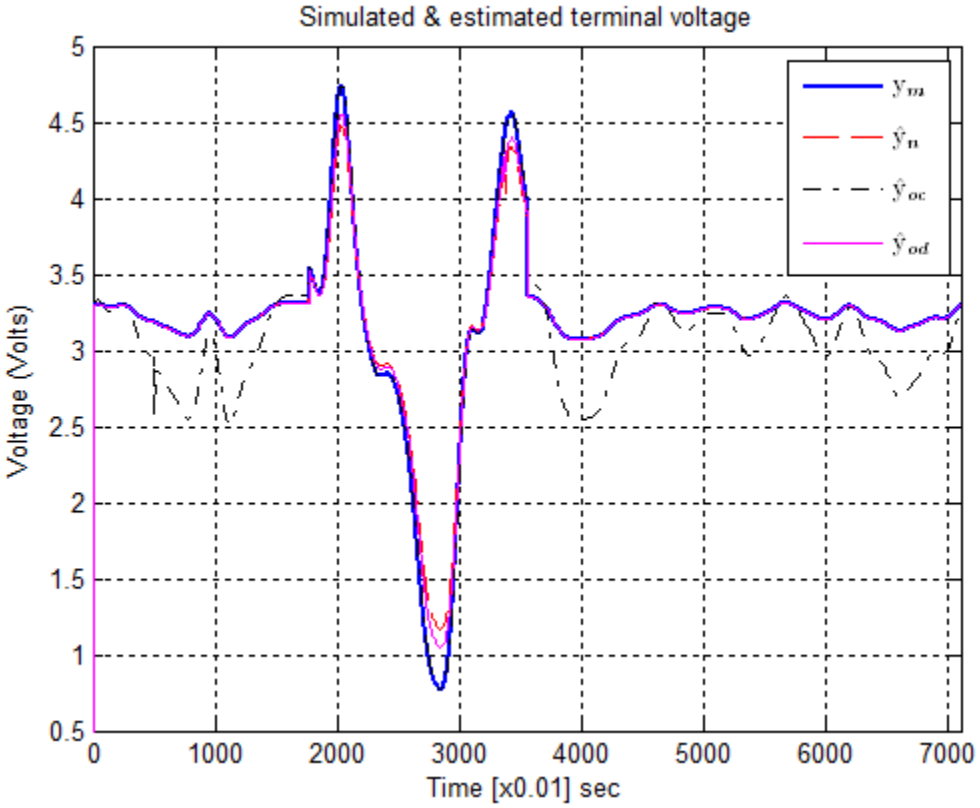

Figure 7.11 Terminal voltage with bounded SOC: simulated measurement, normal, over charge and over discharge

In Figure 7.11, during the first and last 17.75 seconds, the estimated terminal voltage in normal case $\hat{y}_n$ matches while the overcharge $\hat{y}_{OC}$ and over-discharge $\hat{y}_{OD}$ showed deviation from the simulated measurementy_m. From 17.76 to 35.5 seconds, the $\hat{y}_{OC}$ matched with the simulated measurement, while both $\hat{y}_n$ and $\hat{y}_{OD}$ showed deviation from the simulated measurement. Finally, from 35.51 to 53.25 seconds, the estimated terminal voltage from the over-discharge filter $\hat{y}_{OD}$ matched closely with the simulated measurement, while $\hat{y}_{OC}$ showed deviation and $\hat{y}_n$ showed a relatively large difference

from the simulated measurement. The resulting conditional probability densities are shown in Figure 7.12.

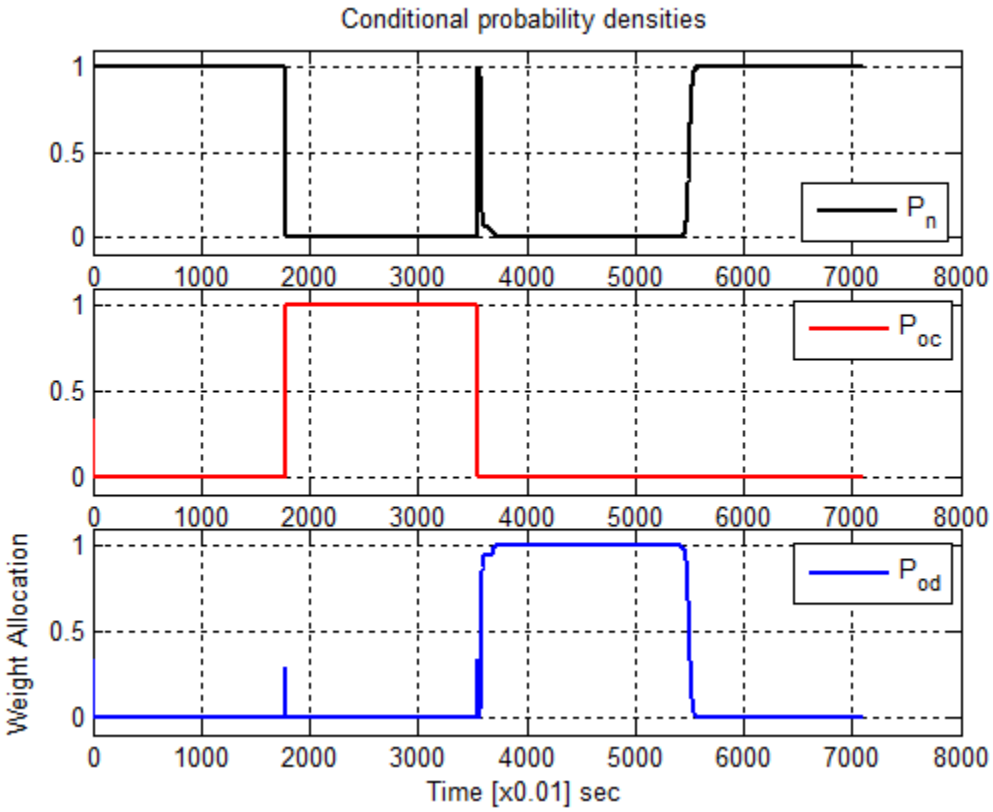

Figure 7.12 Conditional probability evaluated for normal operation, over charge and over discharge faults with bounded SOC

As per the designed scenario, the over charge fault was injected at 17.75 seconds, the resulting probability change can be observed in Figure 7.12. The healthy battery operation is no longer valid and is indicated with the probability P_n reaching zero while the presence of the over charge fault is indicated by the probability P_{OC}transitioning from 0 to 1 and no change in the probability P_{OD}. At 35.5 seconds, the over discharge fault is indicated with the change in P_{OD} from 0 to 1 while the over charge probability given by P_{OC} transitions from 1 to 0 and no prolonged change in the battery health probability P_n is observed. A brief fluctuation in P_n at 35.5 seconds is due to the transition dynamics between the P_{OC} and P_{OD} and interdependencies of the probability. The healthy cell operation was indicated at 53.25 seconds when the battery health probability P_n

transitions from 0 to 1while the over discharge probability P_{OD}reached 0 and over charge probability P_{OC} remains unchanged at 0.

The conditional probabilities along with their respective residuals are shown in Figure 7.13.

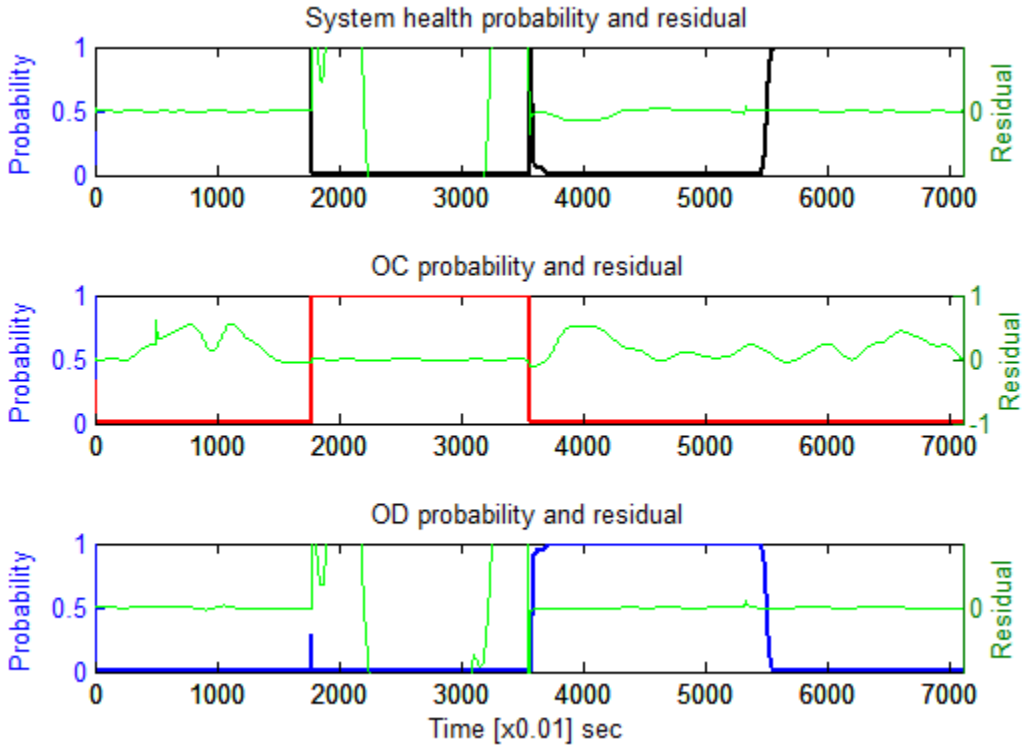

Figure 7.13 Conditional probability density and residuals evaluated for normal operation and over charge and over discharge faults with bounded SOC

Within each of the operational scenario, the bounded SOC results in realistic and improved state estimation using extended Kalman filters, this further leads to better OCV estimation. With improved OCV estimation, greater weightage can be given to the fault information carrying polarization volatges. This marked improvement over the un-bounded SOC case results in zero mean residual signal and accurate FDD as shown in Figure 7.12. The bounded SOC variation under different cases can be seen in Figure 7.14.

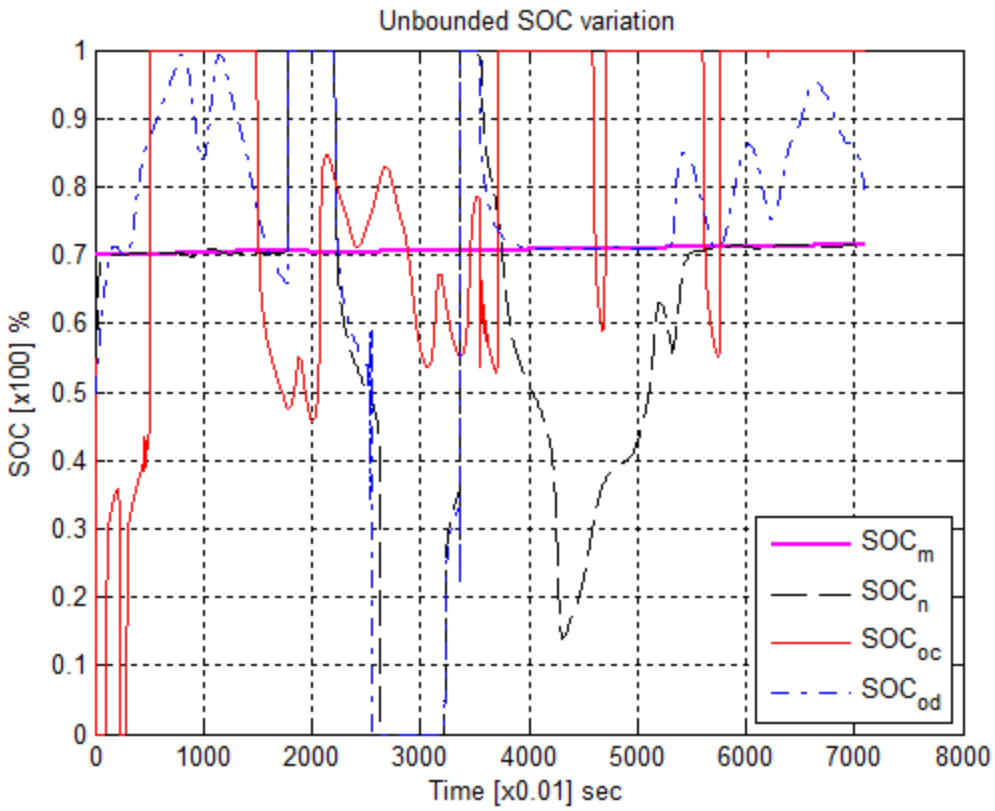

Figure 7.14 Bounded SOC variation for normal operation, over charge and over discharge faults

The SOC variation trend for normal, over charge and over discharge faults shown in Figure 7.14 shows marked improvement over the unbounded SOC variation of Figure 7.10. In Figure 7.14, during the first and last 17.75 seconds, the SOC for normal case given by SOC_n matches with the simulated measurement SOC given by SOC_m while the over charge and over discharge SOC given by SOC_{OC} and SOC_{OD} respectively do not match with SOC_m. From 17.76 to 35.5 seconds the SOC_{OC} shows relatively better match with SOC_m than SOC_n and SOC_{OD}. From 35.51 to 53.25 seconds SOC_{OD} shows good match with SOC_m while SOC_n and SOC_{OC} show high deviation.

The simulation results indicate the successful application of adaptive model-based FDD on the Li-ion battery while incorporating the nonlinear characteristics of Li-ion battery cells.

7.2.2. Non-Linear Battery Model with RLS Battery Parameters

7.2.2.1. Navy Overdischarge Cycle

The input to the FDD is a load/charge current profile with two UDDS cycles resulting in the total simulation time of 142 second. The healthy battery operation is simulated from zero to 47.3 seconds and again from 94.7 to 142 seconds. The over discharge battery operation is simulated from 47.4 to 94.6 seconds. Based on the measurement of current and the battery terminal voltage, the terminal voltages of the two models are estimated at each sample. The simulated measurement and the estimated terminal voltages can be seen in Figure 7.15.

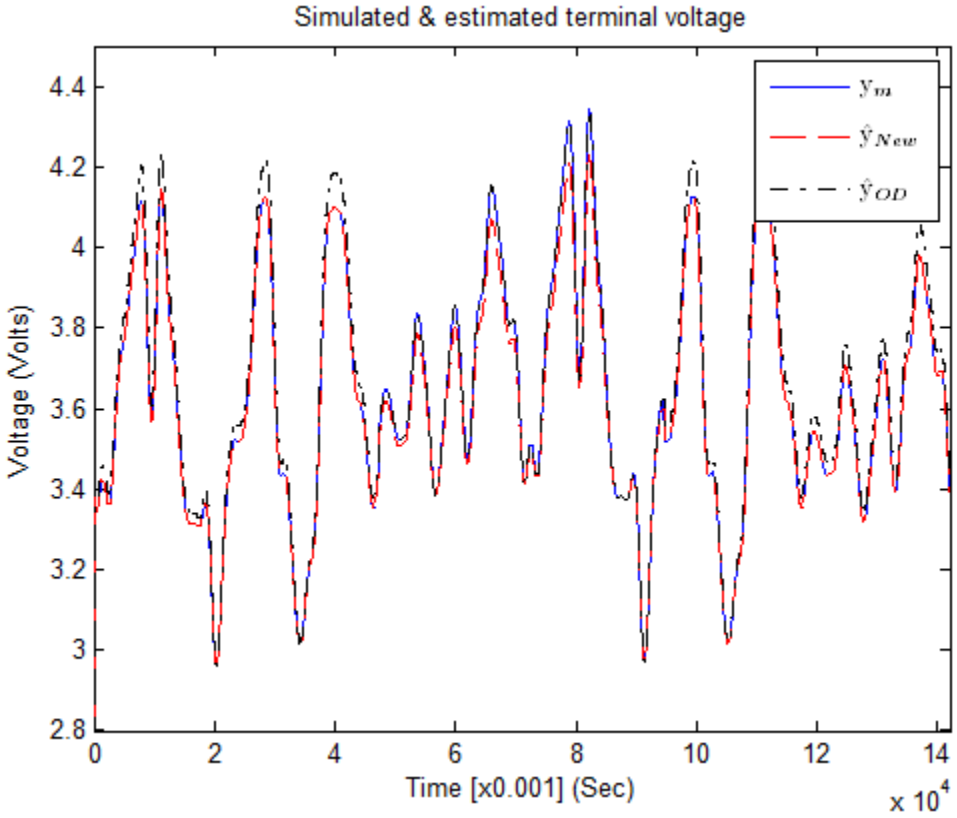

Figure 7.15 Simulated and estimated terminal voltage for healthy and over discharge condition

The simulated terminal voltage is given by y_m and the estimated terminal voltages for the new and over discharged batteries are given by $\hat{y}_{New}$ and $\hat{y}_{OD}$ respectively.

Further, the system residuals are generated by comparing the simulated terminal voltages with the estimated terminal voltages. The residuals at each sample are evaluated at the conditional probability density evaluator block and the resulting operational condition probabilities as shown in Figure 7.16.

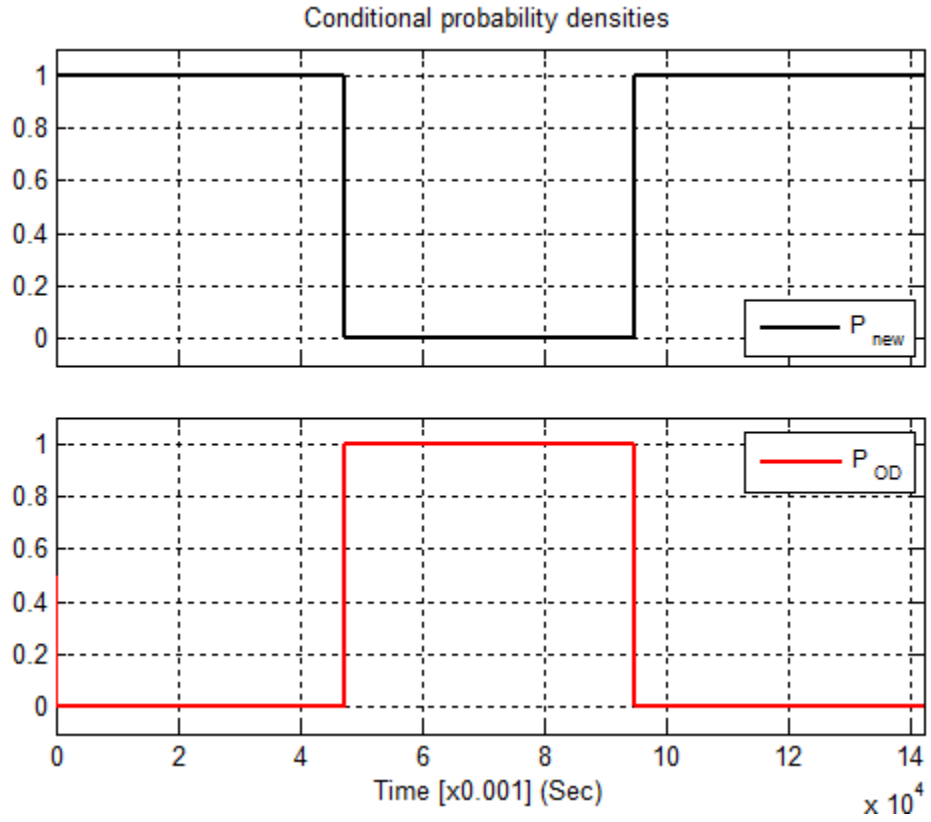

Figure 7.16 Conditional probability densities for healthy and over discharged (Navy over discharge cycle) battery

From Figure 7.16, the two probabilities can be observed, where P_{new} represents the probability of healthy operation of the cell and P_{OD} indicates the probability of over discharge operational condition. The over discharge operational condition was inserted at 47.3 seconds, as indicated byP_{OD}, when it transitions from 0 to 1. At the same time, P_{new} drops down to 0, thus indicating the battery operation is no longer healthy. At 94.6

seconds, the healthy operational condition is indicated with P_{new}transitioning from 0 to 1and P_{OD} dropping to zero.

As discussed previously, the system probabilities are directly related to the information carrying residuals. When the process response matches with the estimated output from the filter, the mean value of the residual signal goes to zero, as observed in Figure7.17, where the residuals and the probabilities are plotted together.

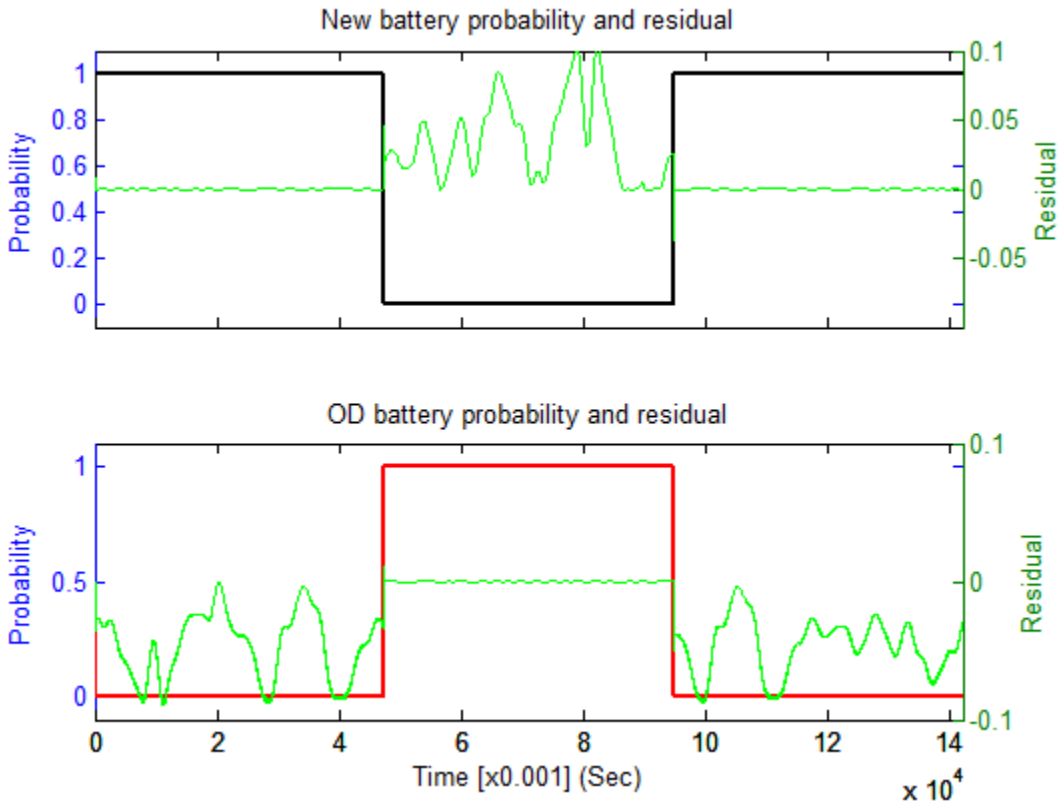

Figure 7.17 Conditional probability densities and residuals for healthy and over discharged (Navy over discharge cycle) battery

The generation of accurate residuals can be attributed to the precise state estimation using the extended Kalman filters. The SOC is one of the states of the non-linear model and needs to be estimated accurately for effective terminal voltage estimation. The variation of the SOC is as shown in Figure 7.18.

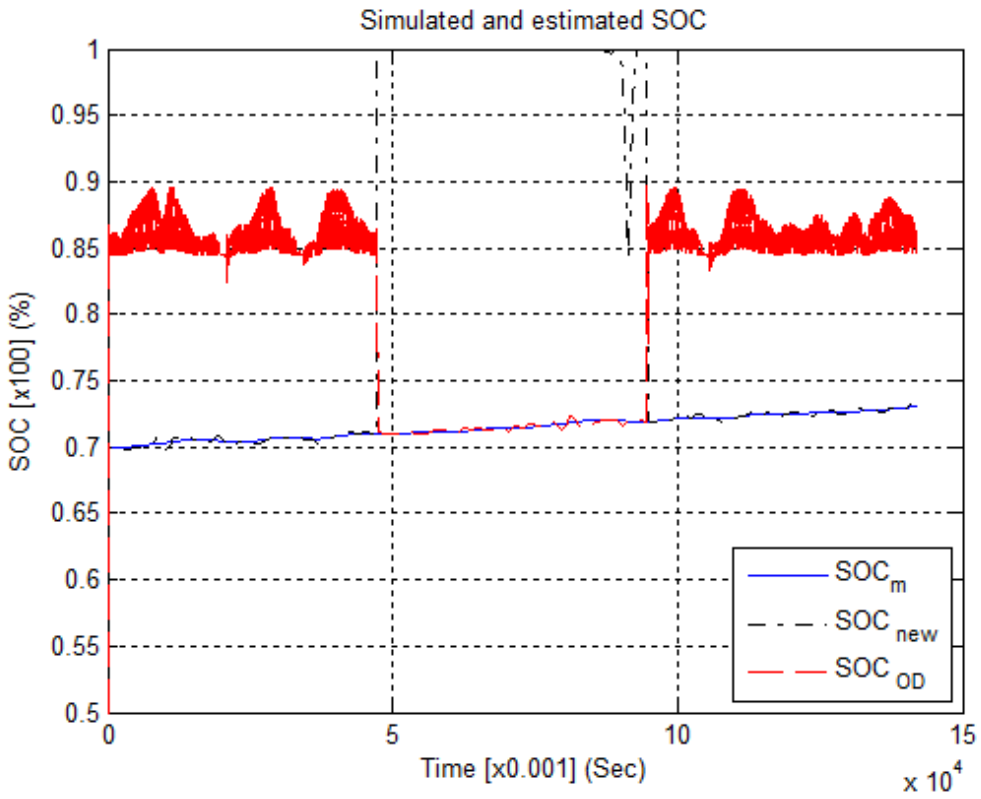

Figure 7.18 SOC variation for new and over discharge battery conditions

In Figure 7.18, during the first and last 47.3 seconds, SOC_{new} for the new battery operational condition matched with the simulated SOC_m, while SOC_{OD} deviates from SOC_m. From 47.4 to 94.6 seconds, the SOC_{new} shows marked deviation from SOC_m while SOC_{OD} matches very closely with SOC_m.

7.2.2.2. 24 Hour Overdischarge Cycle

The FDD performance validation for 24 hour over discharge cycle based model parameters is also performed using two cycles of the UDDS load/charge current profile with the total simulation time of 142 seconds. As in the previous case, the measured terminal voltage is given by y_m and the estimated terminal voltages for healthy and over discharged operational condition are given by $\hat{y}_{New}$ and $\hat{y}_{OD}$ respectively. These terminal voltages are as shown in the Figure 7.19.

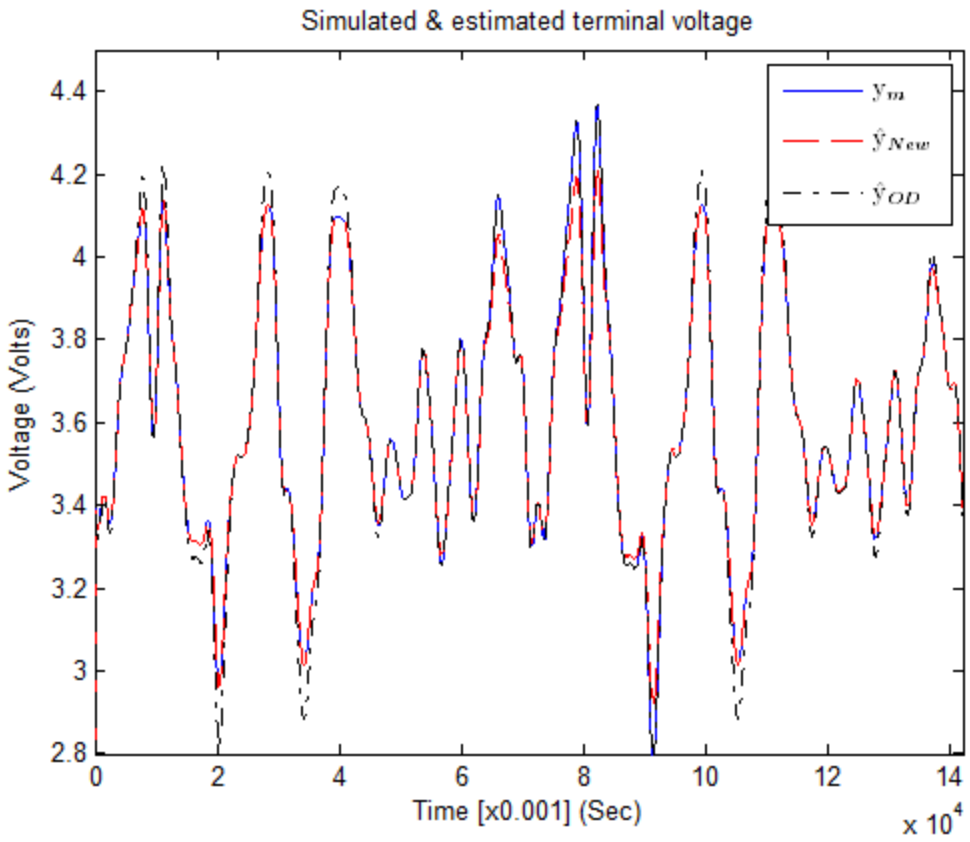

Figure 7.19 Simulated and estimated terminal voltage for healthy and over discharge condition

In Figure 7.19, from zero to 47.3 seconds, the $\hat{y}_{New}$ matches closely with the simulated measurement y_m while the over discharge estimated terminal voltage $\hat{y}_{OD}$ shows large deviation from the simulated measurement y_m. From 47.4 to 94.6 seconds, the estimated terminal voltage for the over discharge model $\hat{y}_{OD}$ matches with y_m while $\hat{y}_{New}$ deviates from y_m. Finally from 94.7 to 142 seconds, $\hat{y}_{New}$ matches with y_m and $\hat{y}_{OD}$ shows marked difference from y_m. The accurate terminal voltage estimations can be attributed to the accurate state estimation, including the SOC estimation. The variation of SOC during the FDD validation process is as shown in the Figure 7.20.

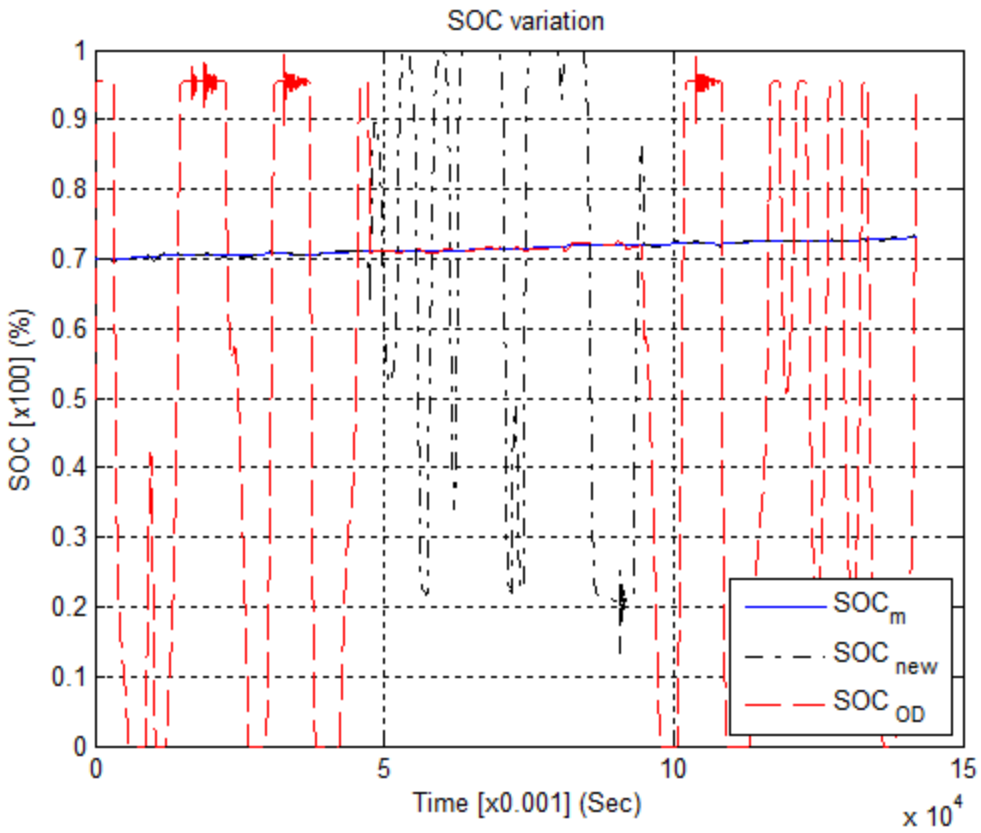

Figure 7.20 SOC variation for new and over discharged battery conditions

During the first one thirds of the simulation, the SOC_{new} matches with the simulated measurement of the SOC given by SOC_m thus ensuring accurate terminal voltage estimation. During the second thirds of the simulation time, the SOC_{OD} matches with the SOC_m while SOC_{new} shows large deviations from SOC_m. For the last one thirds of the simulation, the SOC_{new} closely matches with SOC_m while SOC_{OD} shows large deviations from SOC_m.

The accurate state estimation and the resulting terminal voltages ensure the generation of correct operational information carrying residuals and hence the conditional probabilities. The healthy and over discharged system probabilities along with residuals can be seen in Figure 7.21 below.

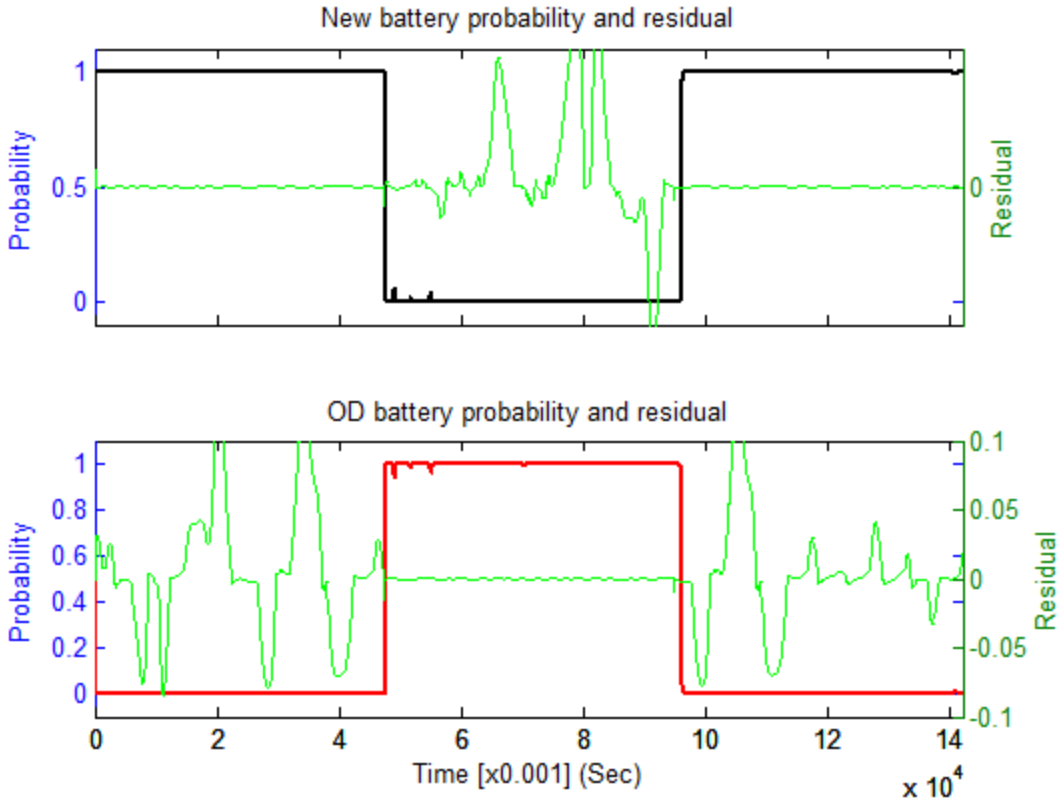

Figure 7.21 Conditional probability densities and residuals for healthy and over discharged (24 hr over discharge cycle) battery

The system probabilities depend on the system residuals, when the operational scenarios match, the residuals become zero mean and hence appropriate variation in the probabilities can be observed.

In Figure 7.22, from zero to 47.3 seconds, the probability of the new battery condition P_{new} is at 1 while the over discharge condition probability P_{OD} stays at zero. P_{OD} transitions to 1 at 47.4 seconds while P_{new} drops from 1 to zero at this time. From 47.4 to 94.6 seconds, P_{OD} and P_{new} remain at 1 and 0 respectively thus indicating the presence of over discharge battery condition. At 94.7 second, P_{new} transitions from 0 to 1 and P_{OD} drops from 1 to 0, indicating the healthy battery condition.

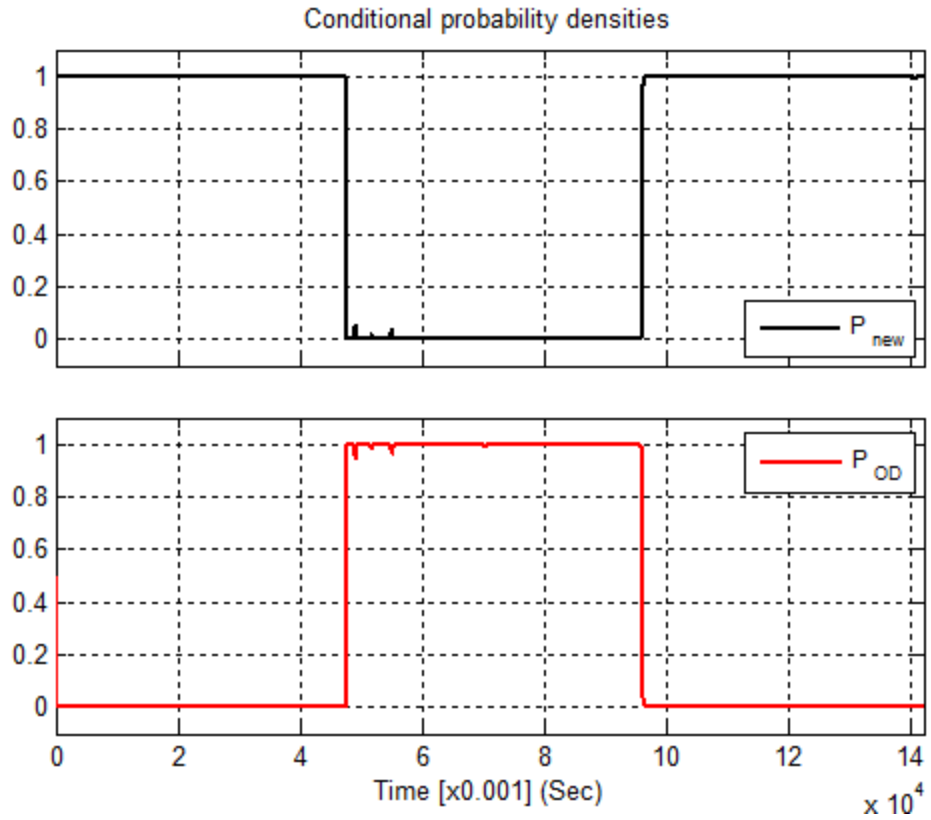

Figure 7.22 Conditional probability densities for healthy and over discharged (24 hour over discharge cycle) battery

The probabilities show the expected behavior as per the designed scenario, also the FDD successfully de-latches itself from the over discharge operational condition as indicated at 94.7 seconds.

8. CONCLUSIONS AND RECOMMENDATIONS

8.1. Conclusions

Li-ion battery models were developed for cell level fault detection and diagnosis. The major electro-chemical phenomenon of the Li-ion battery cell namely, electrolyte resistance, distribution of reactivity and interfacial impedance were taken into account and embedded in the battery model.

The electrochemical energy storage device is a complex system; with underlying dynamics which change with chemistry, charging, discharging, temperature and age of the system. Although these cell dynamics can be modeled using first principle approach, more often than not it will result in computationally expensive models which are hard to implement at the level of fault diagnosis. The equivalent circuit modeling technique employed in this study results in process models that offer good conformity, require relatively little computational effort and are an effective choice in state estimation and monitoring applications [67, 68].

The system identification of the Li-ion battery cell is carried out using impedance spectroscopy and recursive least squares. Two different battery cells of the same chemistry were tested under over charge and over discharge testing schedules and the impedance spectroscopy is performed at the end of each over charge and over discharge cycle. These cycles are continued till the battery experiences a failure under the respective conditions. The impedance response of the battery cell was fitted to a second order circuit consisting of lumped electrical elements like resistors and capacitors in series and parallel configuration.

For the recursive least squares based approach, 25 Navy over discharge cycles and two 24 hour over discharge cycles were carried out on two different batteries. A brand new battery and the two over discharge batteries are suitably perturbed while the current and voltage of the cell are continuously measured. The measured data is then fit to a third order non-linear model and the lumped electrical parameters for healthy and over discharged battery condition acquired. A voltage source was also incorporated into this equivalent circuit representation to account for the OCV; which shares a non-linear relationship with the SOC of the battery cell. The relationship between OCV and SOC was found experimentally and was fitted to a 9^{th} order polynomial. With this available information from impedance spectroscopy, recursive least squares, and OCV-SOC relationship, six 3^{rd} order Li-ion battery state space models were formulated in continuous time. For easy implementation and analysis, the continuous time state space representation was converted to the discrete time domain.

The discrete time linear and non-linear models were incorporated into the MMAE frame work, a special technique related to observer based fault diagnosis. The terminal voltages were estimated and compared with the terminal voltage measurement for generating healthy, over charge and over discharge residuals. The residuals were evaluated in real time using the conditional density evaluator function as part of the fault detection and diagnosis logic. The function assigns conditional probability to healthy, over charge and over discharge operational condition of the Li-ion battery.

Fault scenarios of over charge and over discharge were created and simulated to show the effectiveness of the technique when applied using linear and non-linear process model. Simulation results show that the proposed method is very effective in detecting the stated battery faults in real-time, thus providing an effective way of diagnosing Li-ion battery failure.

8.2. Recommendations for Future Work

There is some more work that can be done in the future to improve the real time battery fault detection as listed below.

- As the next step, MMAE battery fault diagnosis can be validated for over charge operational condition with recursive least squares based system parameters
- The battery model can be further enhanced to include the effect of temperature on the battery model. The performance of the battery changes with variation in temperature. It will be interesting to study the effect of temperature on the model parameters and how it influences the Li-ion battery cell fault diagnosis
- Electrochemical battery models can be explored for more accurate modeling of the Li-ion battery behavior. Further, these models can be tested for their performance in fault diagnosis
- The extension of fault diagnosis from single cell to battery modules and subsequently battery pack can also be investigated

LIST OF REFERENCES

LIST OF REFERENCES

[1] J. M. Tarascon and M. Armand, "Issues and challenges facing rechargeable lithium batteries," *Nature*, vol. 414, pp. 359-67, Nov 15 2001.

[2] T. G. Goonan, "Lithium use in batteries," vol. Circular 1371, 14 p., U. S. G. Survey, Ed., ed, 2012.

[3] M. Nagata, A. Saraswat, H. Nakahara, H. Yumoto, D. M. Skinlo, K. Takeya, *et al.*, "Miniature pin-type lithium batteries for medical applications," *Journal of Power Sources*, vol. 146, pp. 762-765, 8/26/ 2005.

[4] L. Kanevskii and V. Dubasova, "Degradation of lithium-ion batteries and how to fight it: A review," *Russian Journal of Electrochemistry*, vol. 41, pp. 1-16, 2005.

[5] L. Yuang-Shung and C. Ming-Wang, "Intelligent control battery equalization for series connected lithium-ion battery strings," *Industrial Electronics, IEEE Transactions on*, vol. 52, pp. 1297-1307, 2005.

[6] J. Zhang and J. Lee, "A review on prognostics and health monitoring of Li-ion battery," *Journal of Power Sources*, vol. 196, pp. 6007-6014, 8/1/ 2011.

[7] K. Goebel, B. Saha, A. Saxena, J. Celaya, and J. Christophersen, "Prognostics in Battery Health Management," *Instrumentation & Measurement Magazine, IEEE*, vol. 11, pp. 33-40, 2008.

[8] S. M. Alavi, M. F. Samadi, and M. Saif, "Diagnostics in Lithium-Ion Batteries: Challenging Issues and Recent Achievements," in *Integration of Practice-Oriented Knowledge Technology: Trends and Prospectives*, ed: Springer, 2013, pp. 277-291.

[9] W. Chen, W. T. Chen, M. Saif, M. F. Li, and H. Wu, "Simultaneous Fault Isolation and Estimation of Lithium-Ion Batteries via Synthesized Design of Luenberger and Learning Observers," *Control Systems Technology, IEEE Transactions on*, vol. PP, pp. 1-1, 2013.

[10] A. Singh, A. Izadian, and S. Anwar, "Fault Diagnosis of Li-Ion Batteries Using Multiple-Model Adaptive Estimation," presented at the IEEE Industrial Electronics, IECON 2013 - 39th Annual Conference on, Vienna, Austria, in press.

[11] P. S. Maybeck and D. L. Pogoda, "Multiple model adaptive controller for the stol f-15 with sensor/actuator failures," in *Decision and Control, 1989., Proceedings of the 28th IEEE Conference on*, 1989, pp. 1566-1572.

[12] P. D. Hanlon and P. S. Maybeck, "Multiple-model adaptive estimation using a residual correlation Kalman filter bank," *Aerospace and Electronic Systems, IEEE Transactions on,* vol. 36, pp. 393-406, 2000.

[13] A. Izadian, P. Khayyer, and P. Famouri, "Fault Diagnosis of Time-Varying Parameter Systems With Application in MEMS LCRs," *Industrial Electronics, IEEE Transactions on,* vol. 56, pp. 973-978, 2009.

[14] A. Izadian, "Self-Tuning Fault Diagnosis of MEMS," *International Federation on Automatic Control, Journal of Mechatronics,* To appear, 2013.

[15] B. Saha and K. Goebel, "Uncertainty Management for Diagnostics and Prognostics of Batteries using Bayesian Techniques," in *Aerospace Conference, 2008 IEEE*, 2008, pp. 1-8.

[16] B. Saha, K. Goebel, S. Poll, and J. Christophersen, "An integrated approach to battery health monitoring using bayesian regression and state estimation," in *Autotestcon, 2007 IEEE*, 2007, pp. 646-653.

[17] J. Liu, A. Saxena, K. Goebel, B. Saha, and W. Wang, "An Adaptive Recurrent Neural Network for Remaining Useful Life Prediction of Lithium-ion Batteries," DTIC Document 2010.

[18] A. Nuhic, T. Terzimehic, T. Soczka-Guth, M. Buchholz, and K. Dietmayer, "Health diagnosis and remaining useful life prognostics of lithium-ion batteries using data-driven methods," *Journal of Power Sources,* 2012.

[19] D. Wang, Q. Miao, and M. Pecht, "Prognostics of lithium-ion batteries based on relevance vectors and a conditional three-parameter capacity degradation model," *Journal of Power Sources,* 2013.

[20] J. D. Kozlowski, "Electrochemical cell prognostics using online impedance measurements and model-based data fusion techniques," in *Aerospace Conference, 2003. Proceedings. 2003 IEEE*, 2003, pp. 3257-3270.

[21] J. Xiong, H. Banvait, L. Li, Y. Chen, J. Xie, Y. Liu, *et al.*, "Failure detection for over-discharged Li-ion batteries," in *Electric Vehicle Conference (IEVC), 2012 IEEE International*, 2012, pp. 1-5.

[22] M. A. Roscher, J. Assfalg, and O. S. Bohlen, "Detection of utilizable capacity deterioration in battery systems," *Vehicular Technology, IEEE Transactions on,* vol. 60, pp. 98-103, 2011.

[23] S. Abu-Sharkh and D. Doerffel, "Rapid test and non-linear model characterisation of solid-state lithium-ion batteries," *Journal of Power Sources,* vol. 130, pp. 266-274, 5/3/ 2004.

[24] O. Tremblay, L. A. Dessaint, and A. I. Dekkiche, "A Generic Battery Model for the Dynamic Simulation of Hybrid Electric Vehicles," in *Vehicle Power and Propulsion Conference, 2007. VPPC 2007. IEEE*, 2007, pp. 284-289.

[25] H. He, R. Xiong, and J. Fan, "Evaluation of Lithium-Ion Battery Equivalent Circuit Models for State of Charge Estimation by an Experimental Approach," *Energies,* vol. 4, pp. 582-598, 2011.

[26] S. Buller, "Impedance-Based Simulation Models for Energy Storage Devices in Advanced Automotive Power Systems," Phd, Institute for Power Electronics and Electrical Drives, RWTH Aachen University, Germany, 2003.

[27] T. B. Reddy, *Linden's Handbook of Batteries* vol. 4: McGraw-Hill, 2011.

[28] M. E. Orazem and B. Tribollet, *Electrochemical Impedance Spectroscopy*: John Wiley & Sons, Inc., 2008.

[29] E. Barsoukov and J. R. Macdonald, *Impedance Spectroscopy: Theory, Experiment, and Applications*: Wiley, 2005.

[30] S. Buller, M. Thele, R. W. A. A. De Doncker, and E. Karden, "Impedance-based simulation models of supercapacitors and Li-ion batteries for power electronic applications," *Industry Applications, IEEE Transactions on,* vol. 41, pp. 742-747, 2005.

[31] T. C. Kaypmaz and R. N. Tuncay, "An advanced cell model for diagnosing faults in operation of Li-ion Polymer batteries," in *Vehicle Power and Propulsion Conference (VPPC), 2011 IEEE*, 2011, pp. 1-5.

[32] C. Min and G. A. Rincon-Mora, "Accurate electrical battery model capable of predicting runtime and I-V performance," *Energy Conversion, IEEE Transactions on,* vol. 21, pp. 504-511, 2006.

[33] Z. Xiang, Z. Bingzhan, Z. Han, S. Weixiang, and A. Kapoor, "State of charge estimation based on improved Li-ion battery model using extended Kalman filter," in *Industrial Electronics and Applications (ICIEA), 2013 8th IEEE Conference on*, 2013, pp. 607-612.

[34] Z. Fei, L. Guangjun, and F. Lijin, "A battery State of Charge estimation method with extended Kalman filter," in *Advanced Intelligent Mechatronics, 2008. AIM 2008. IEEE/ASME International Conference on*, 2008, pp. 1008-1013.

[35] K. Ogata, *Discrete-time control systems*. Englewood Cliffs, N.J.: Prentice Hall, 1995.

[36] S. M. Ross, *A first course in probability*: Pearson Prentice Hall, 2010.

[37] T. M. Inc., "MATLAB," 10 ed. Natick, Massachusetts, 2010.

[38] M. Ehsani, Y. Gao, and A. Emadi, *Modern Electric, Hybrid Electric, and Fuel Cell Vehicles: Fundamentals, Theory, and Design, Second Edition*: Taylor & Francis, 2009.

[39] V. F. Lvovich, "Impedance spectroscopy applications to electrochemical and dielectric phenomena," ed. Hoboken, N.J.: Wiley, 2012.

[40] J. W. Nilsson and S. A. Riedel, *Electric Circuits, 9/E*: Pearson Education USA, 2011.

[41] J. R. Macdonald, "LEVM/ LEVMW," 8.12 ed, 2013.

[42] P. Ioannou and B. Fidan, *Adaptive Control Tutorial*: Society for Industrial and Applied Mathematics, 2006.

[43] S. X. Ding, *Model-based Fault Diagnosis Techniques: Design Schemes, Algorithms, and Tools*: Springer Publishing Company, Incorporated, 2008.

[44] R. Isermann, *Fault-Diagnosis Systems: An Introduction from Fault Detection to Fault Tolerance*: Springer, 2006.

[45] R. Isermann, *Fault-Diagnosis Applications: Model-Based Condition Monitoring: Actuators, Drives, Machinery, Plants, Sensors, and Fault-tolerant Systems*: Springer, 2011.

[46] W. Greg and B. Gary, "An introduction to the Kalman filter," *Department of Computer Science, University of North Carolina at Chapel Hill, NC*, 2006.

[47] D. Simon, *Optimal state estimation: Kalman, H infinity, and nonlinear approaches*: Wiley. com, 2006.

[48] A. Izadian and P. Famouri, "Fault Diagnosis of MEMS Lateral Comb Resonators Using Multiple-Model Adaptive Estimators," *Control Systems Technology, IEEE Transactions on*, vol. 18, pp. 1233-1240, 2010.

[49] B. D. O. Anderson, "Optimal filtering," J. B. Moore, Ed., ed. Englewood Cliffs, N.J. :: Prentice-Hall, 1979.

[50] D. Magill, "Optimal adaptive estimation of sampled stochastic processes," *Automatic Control, IEEE Transactions on*, vol. 10, pp. 434-439, 1965.

[51] J. Moore and R. Hawkes, "Decision methods in dynamic system identification," in *Decision and Control including the 14th Symposium on Adaptive Processes, 1975 IEEE Conference on*, 1975, pp. 645-650.

[52] D. Lainiotis, "Optimal adaptive estimation: Structure and parameter adaption," *Automatic Control, IEEE Transactions on*, vol. 16, pp. 160-170, 1971.

[53] D. W. Lane and P. S. Maybeck, "Multiple model adaptive estimation applied to the LAMBDA URV for failure detection and identification," in *Decision and Control, 1994., Proceedings of the 33rd IEEE Conference on*, 1994, pp. 678-683 vol.1.

[54] P. Eide and P. Maybeck, "Implementation and demonstration of a multiple model adaptive estimation failure detection system for the F-16," in *Decision and Control, 1995., Proceedings of the 34th IEEE Conference on*, 1995, pp. 1873-1878 vol.2.

[55] T. E. Menke and P. S. Maybeck, "Multiple model adaptive estimation applied to the VISTA F-16 flight control system with actuator and sensor failures," in *Aerospace and Electronics Conference, 1992. NAECON 1992., Proceedings of the IEEE 1992 National*, 1992, pp. 441-448.

[56] M. Athans, D. Castanon, K.-P. Dunn, C. Greene, W. Lee, N. Sandell Jr, *et al.*, "The stochastic control of the F-8C aircraft using a multiple model adaptive control (MMAC) method--Part I: Equilibrium flight," *Automatic Control, IEEE Transactions on*, vol. 22, pp. 768-780, 1977.

[57] P. Eide and P. Maybeck, "An MMAE failure detection system for the F-16," *Aerospace and Electronic Systems, IEEE Transactions on*, vol. 32, pp. 1125-1136, 1996.

[58] J. Marzat, H. Piet-Lahanier, F. Damongeot, and E. Walter, "Model-based fault diagnosis for aerospace systems: A survey," *Proceedings of the Institution of Mechanical Engineers, Part G: Journal of Aerospace Engineering*, vol. 226, pp. 1329-1360, 2012.

[59] D. Rupp, G. Ducard, E. Shafai, and H. P. Geering, "Extended Multiple Model Adaptive Estimation for the Detection of Sensor and Actuator Faults," in *Decision and Control, 2005 and 2005 European Control Conference. CDC-ECC '05. 44th IEEE Conference on*, 2005, pp. 3079-3084.

[60] G. L. Plett, "Extended Kalman filtering for battery management systems of LiPB-based HEV battery packs: Part 3. State and parameter estimation," *Journal of Power Sources*, vol. 134, pp. 277-292, 8/12/ 2004.

[61] X. Rui, H. Hongwen, S. Fengchun, and Z. Kai, "Evaluation on State of Charge Estimation of Batteries With Adaptive Extended Kalman Filter by Experiment Approach," *Vehicular Technology, IEEE Transactions on*, vol. 62, pp. 108-117, 2013.

[62] F. Auger, M. Hilairet, J. M. Guerrero, E. Monmasson, T. Orlowska-Kowalska, and S. Katsura, "Industrial Applications of the Kalman Filter: A Review," *Industrial Electronics, IEEE Transactions on*, vol. 60, pp. 5458-5471, 2013.

[63] Z. Fei, L. Guangjun, and F. Lijin, "Battery state estimation using Unscented Kalman Filter," in *Robotics and Automation, 2009. ICRA '09. IEEE International Conference on*, 2009, pp. 1863-1868.

[64] A. Systems. (2009, 9/9/12). *High Power Li-Ion APR18650* [Data Sheet]. Available: www.cosmoenergy.com/APR18650M1A_Datasheet_2009.pdf

[65] D. o. t. Navy, "Technical Manual For Batteries, Navy Lithium Safety Program Responsibilities And Procedures," ed, 2004.

[66] ANL, "Autonomie," ed: Argonne National laboratory, 2010.

[67] T. Xidong, M. Xiaofeng, L. Jian, and B. Koch, "Li-ion battery parameter estimation for state of charge," in *American Control Conference (ACC), 2011*, 2011, pp. 941-946.

[68] A. H. Ranjbar, A. Banaei, A. Khoobroo, and B. Fahimi, "Online Estimation of State of Charge in Li-Ion Batteries Using Impulse Response Concept," *Smart Grid, IEEE Transactions on*, vol. 3, pp. 360-367, 2012.

APPENDICES

Appendix A Impedance Spectroscopy Figures

The following figures represent the individual over charge and over discharge impedance spectroscopy test results at the end of certain cycles. The test was carried out in the frequency range of 1 MHz~0.01 Hz with amplitude of 5 mV. For over charge testing, the impedance data was recorded at the end of cycles 1, 5, 10, 12, 15, 18 and 19.

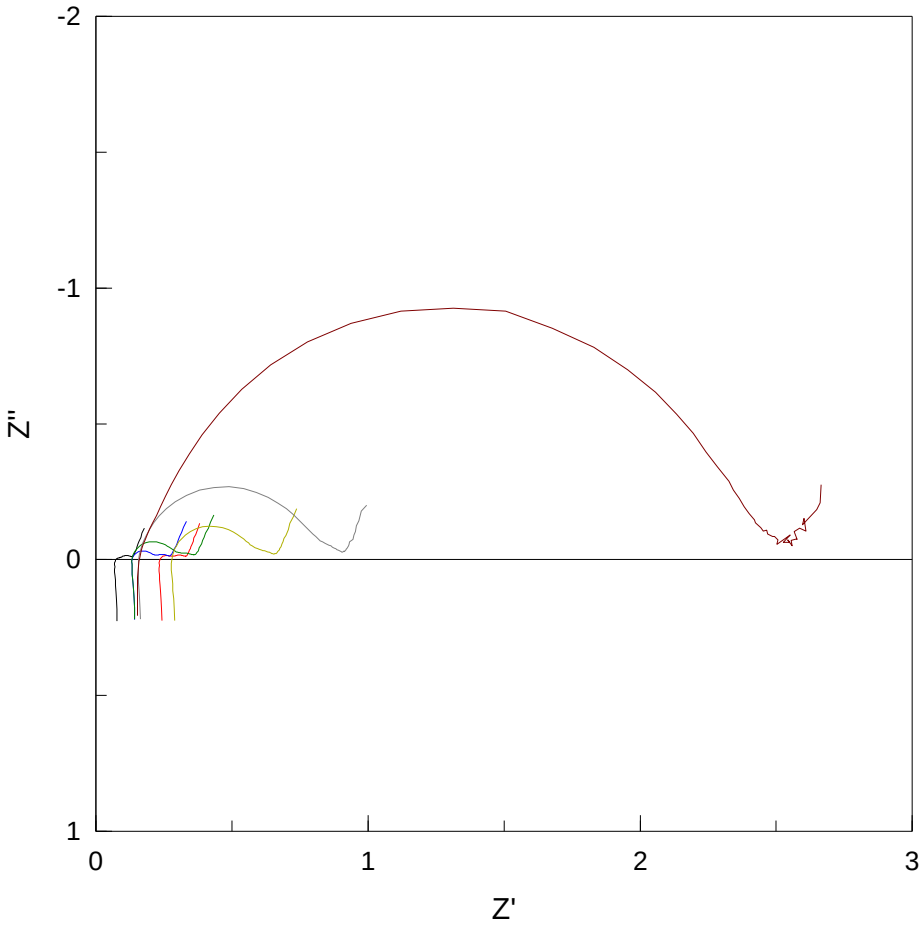

Figure A. 1 Impedance plane plot for over charged 18650 LiFePO4 battery

For over discharge testing, the impedance data was recorded at the end of cycles 1, 2, 3, 4, 5 and 6.

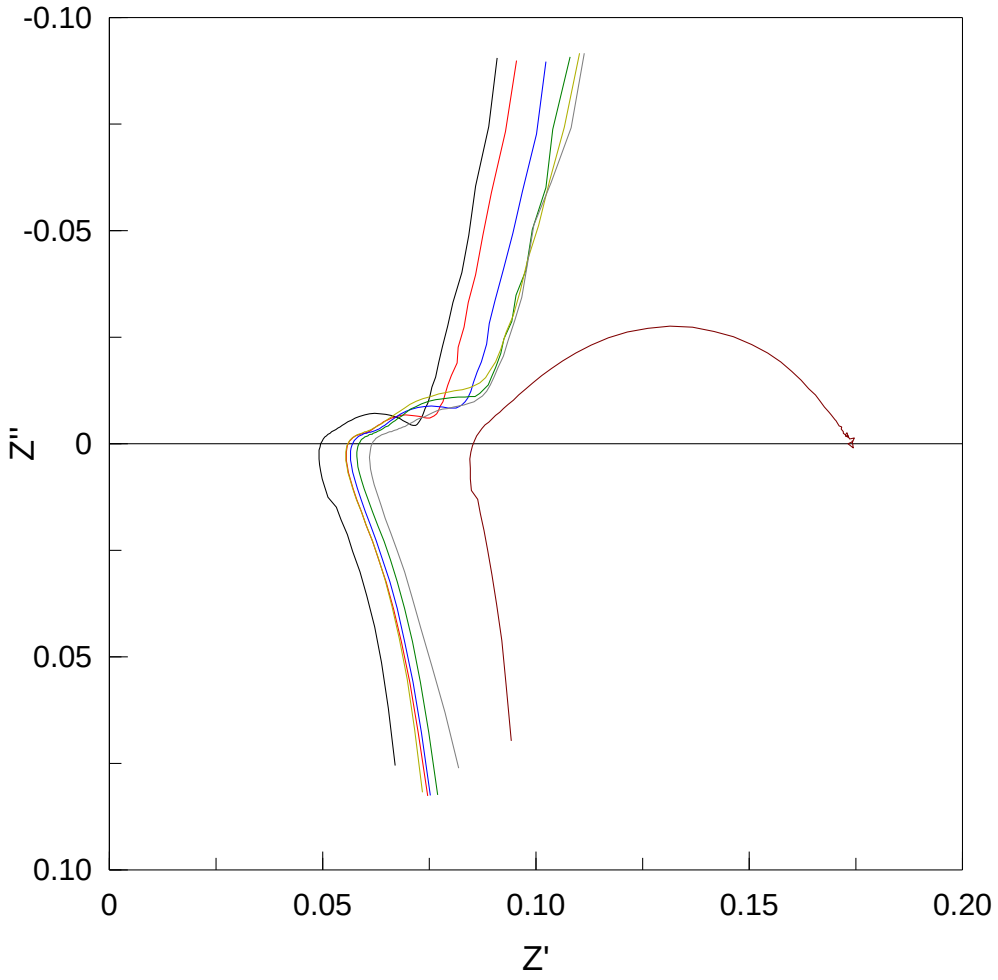

Figure A. 2 Impedance plane plot for over discharged 18650 LiFePO4 battery

Appendix B Li-ion Battery Fault Diagnosis- Linear Model

The UDDS current cycle is appropriately scaled for Li-ion battery under study and is made sufficiently rich for FDD. The modified load/charge current based on (52) and terminal voltage based on (53) are shown below. Also shown are the individial probabilities and residuals for system health and over charge conditions.

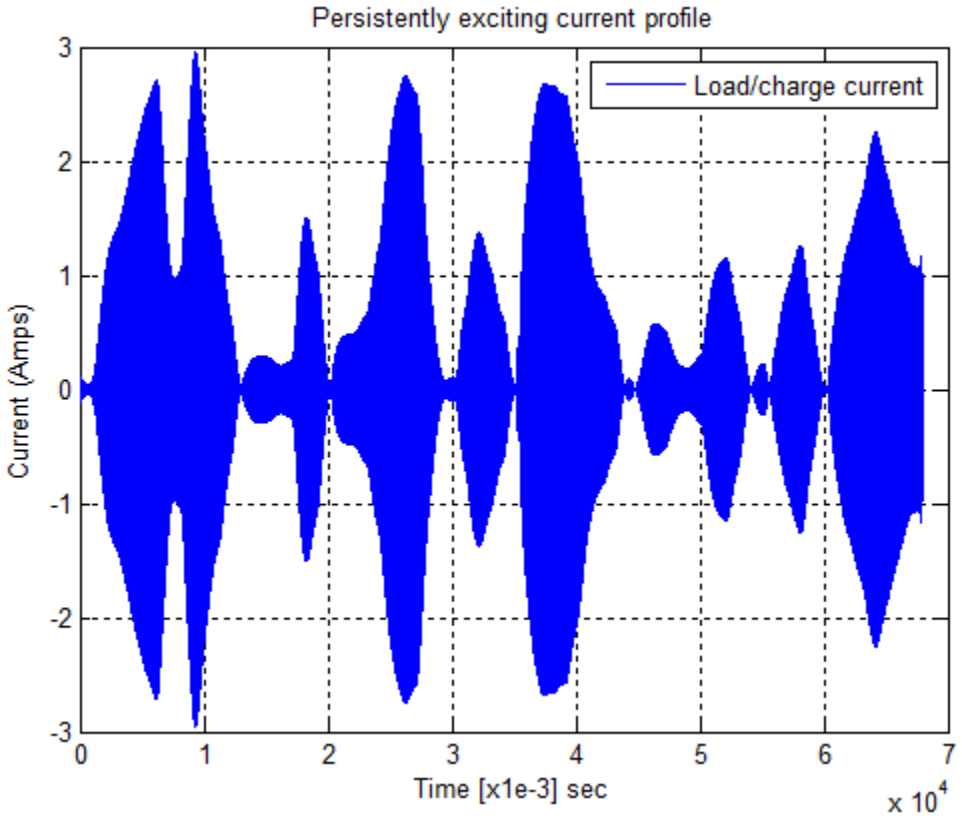

Figure B. 1 Persistently exciting load current $I_L{}'$ profile

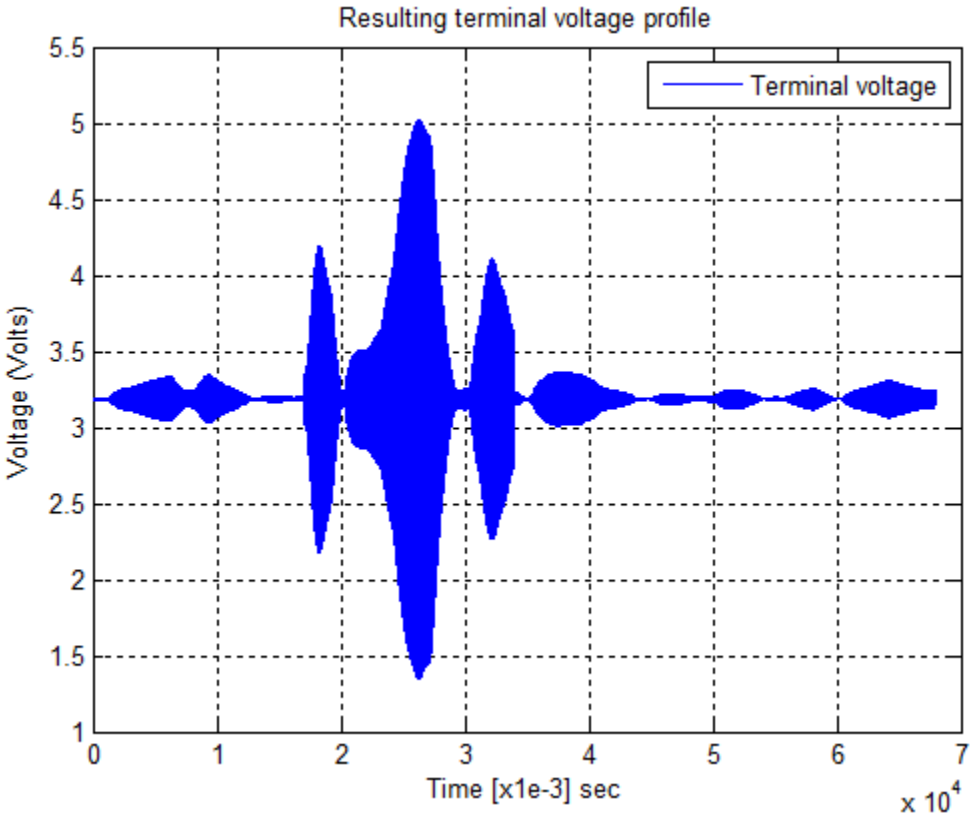

Figure B. 2 Persistently excited terminal voltage $V_t{}'$ profile

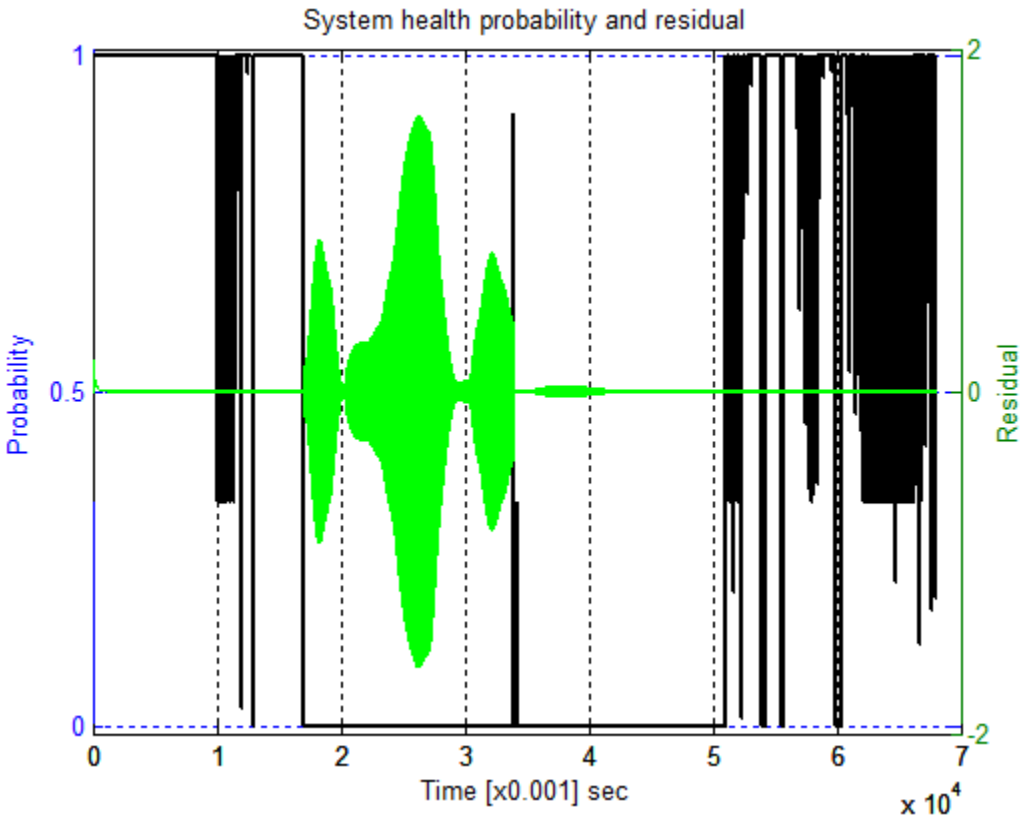

Figure B. 3 System health probability and residual

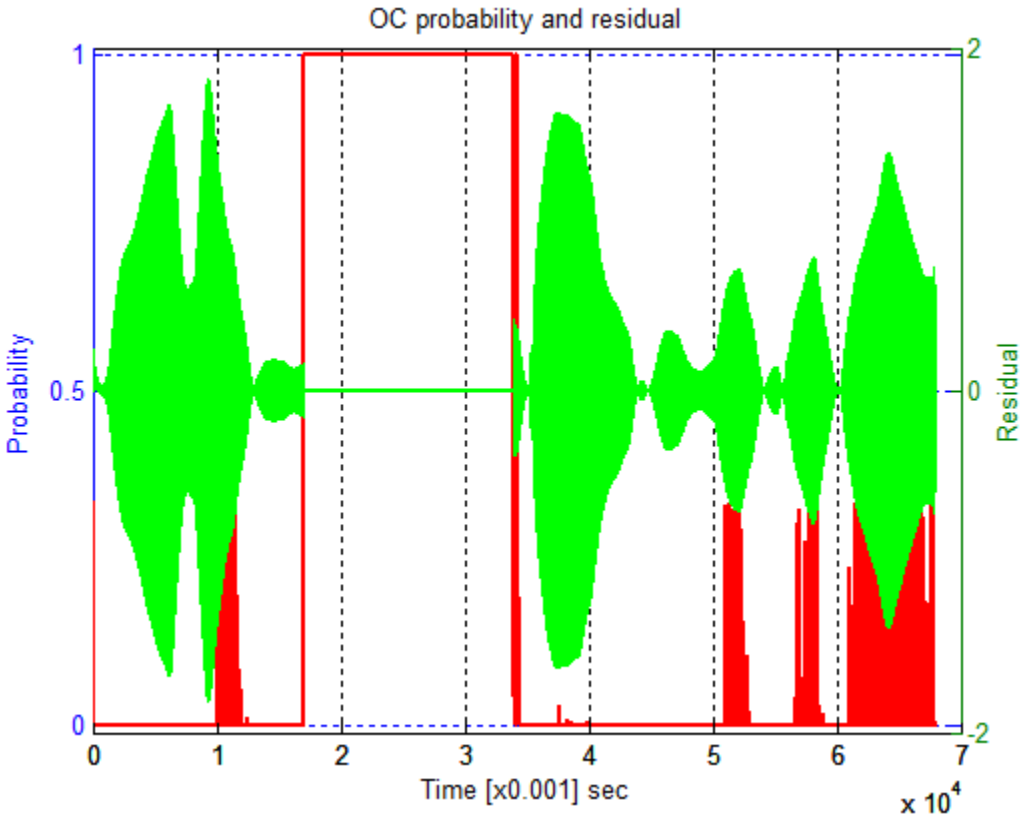

Figure B. 4 Over charge probability and residual

Appendix C Li-ion Battery Fault Diagnosis- Nonlinear Model

C. 1. Impedance Spectroscopy based Models

The following figures show the variation in estimated terminal voltages, residuals and combined probability-residual change in unbounded and bounded SOC case with IS model data.

C. 1. i. Unbounded SOC

The Figure C. 1 shows the variation of estimated terminal voltages with reference to the simulated measurement of terminal voltage y_m. The system residuals are shown in Figure C. 2, and the conditional probabilities for battery health, overcharge, and overdischarge with residuals are as shown in Figures C. 3, C. 4 and C. 5 respectively.

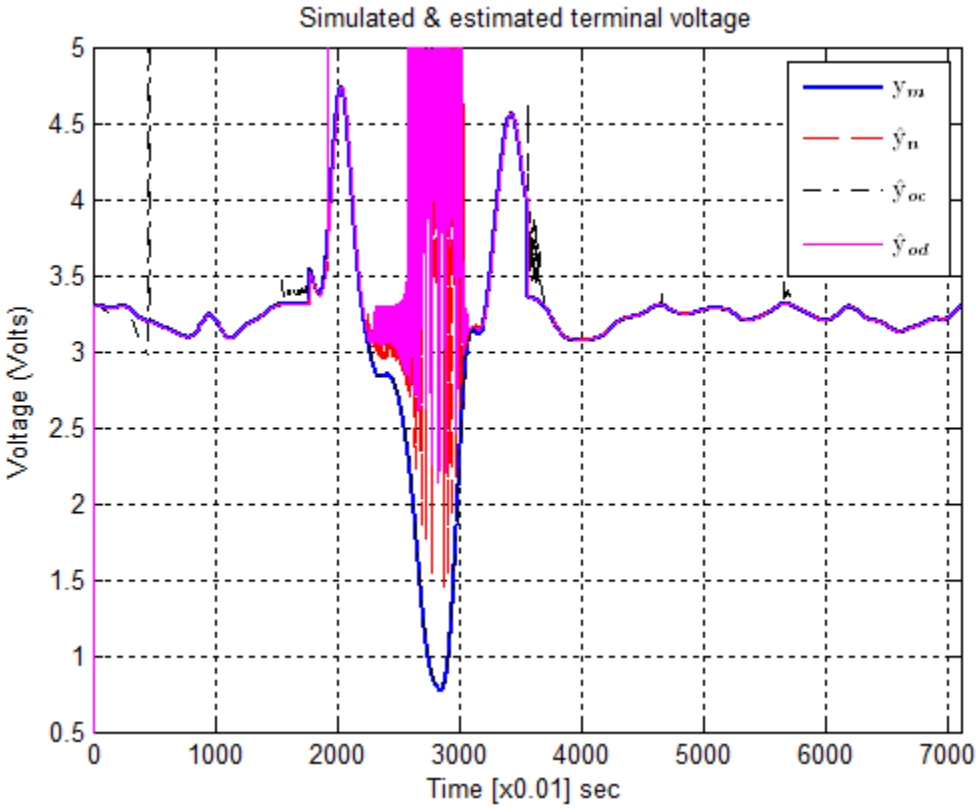

Figure C. 1 Unbounded SOC: simulated and estimated terminal voltage

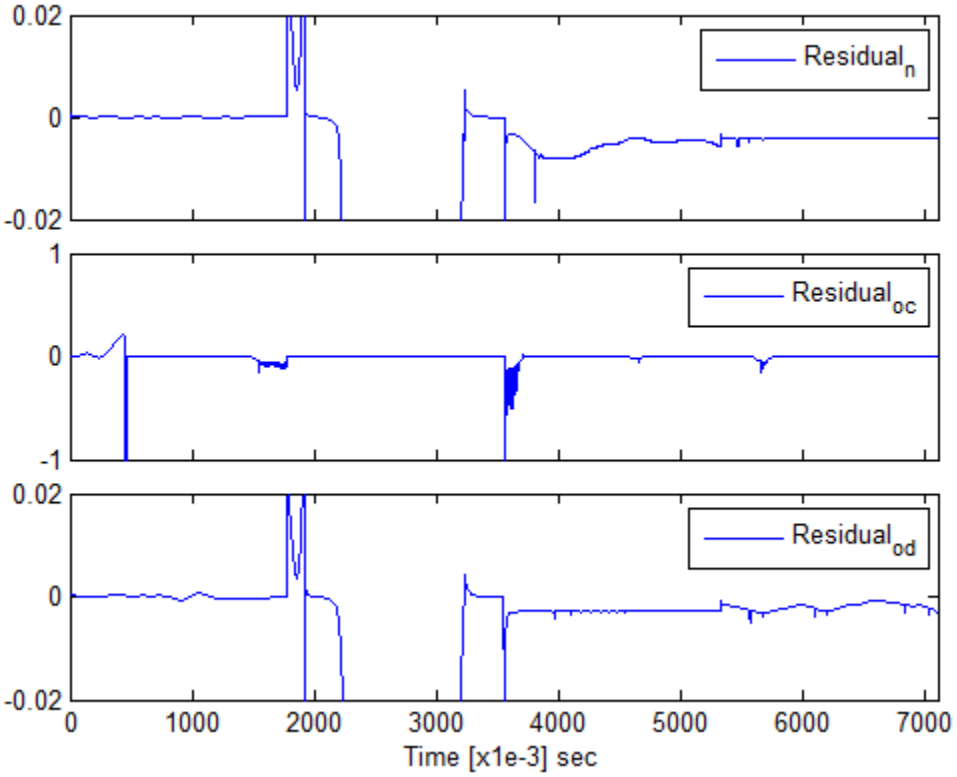

Figure C. 2 Unbounded SOC: healthy, over charge and over discharge residuals

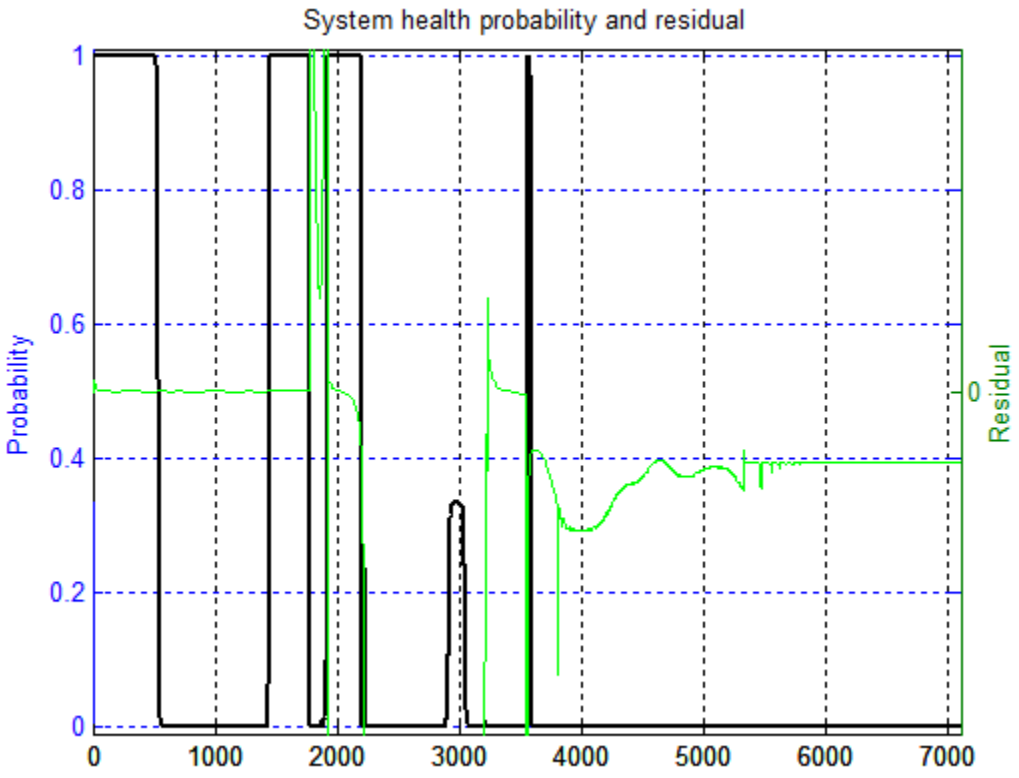

Figure C. 3 Unbounded SOC: health probability and residual

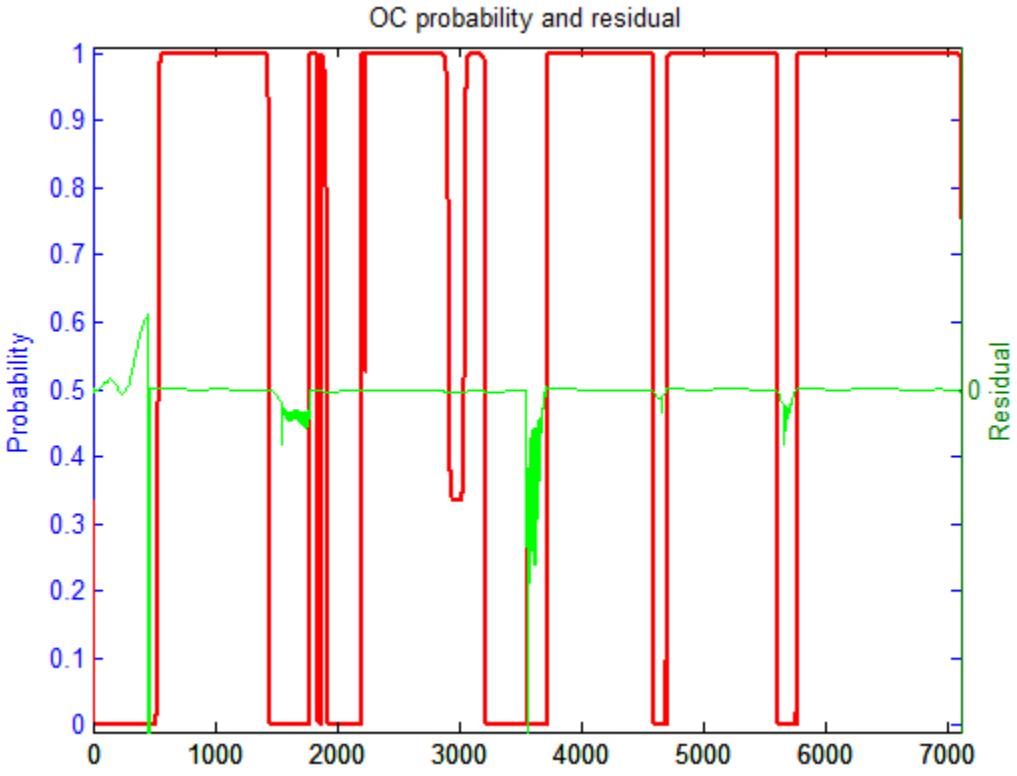

Figure C. 4 Unbounded SOC: over charge probability and residual

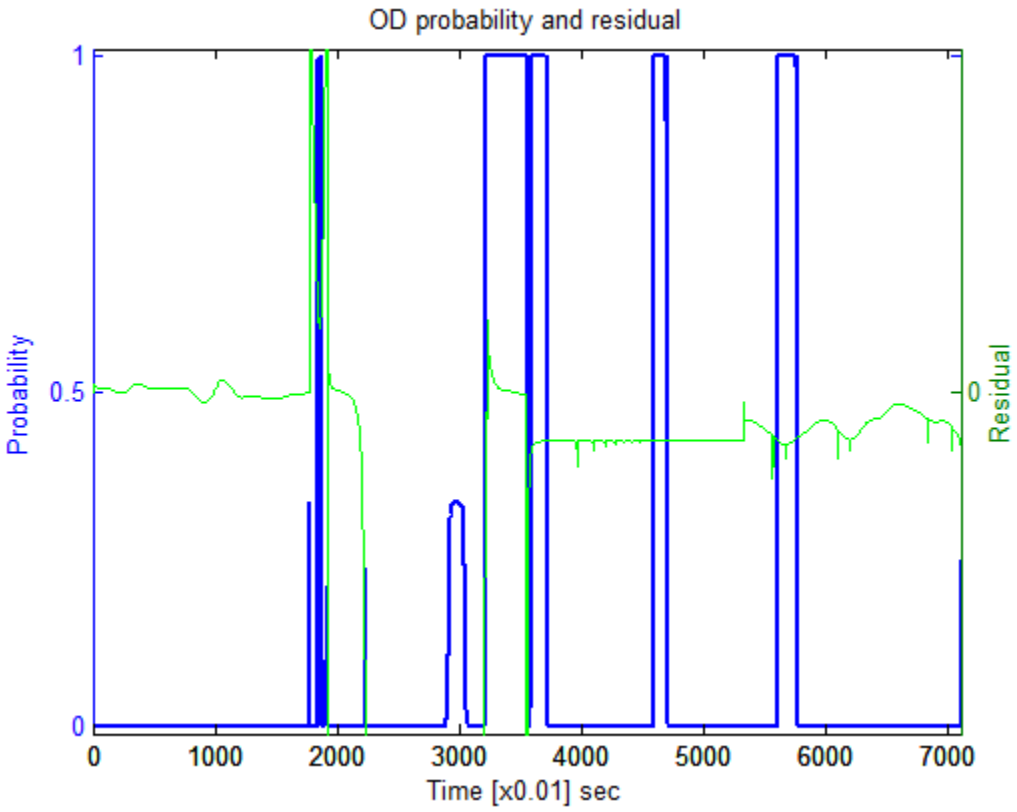

Figure C. 5 Unbounded SOC: over discharge probability and residual

C. 1. ii. Bounded SOC

The system residuals for the bounded SOC case are shown in Figure C. 6, and the conditional probabilities for battery health, overcharge, and overdischarge with associated residuals are as shown in Figures C. 7, C. 8 and C. 9 respectively.

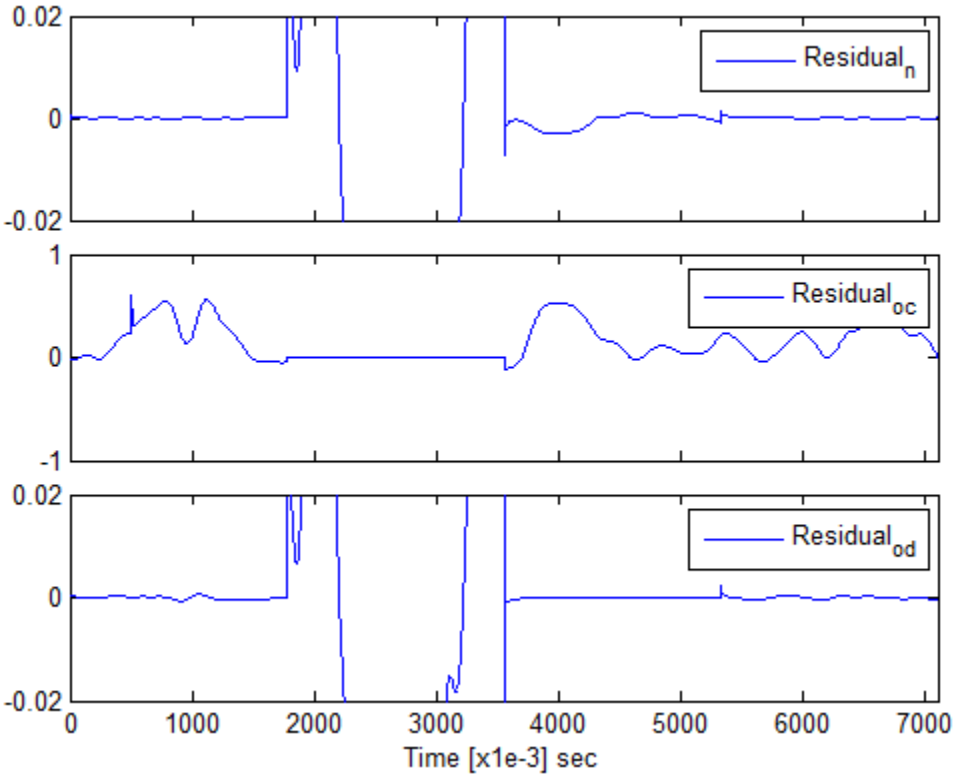

Figure C. 6 Bounded SOC: healthy, over charge and over discharge residual

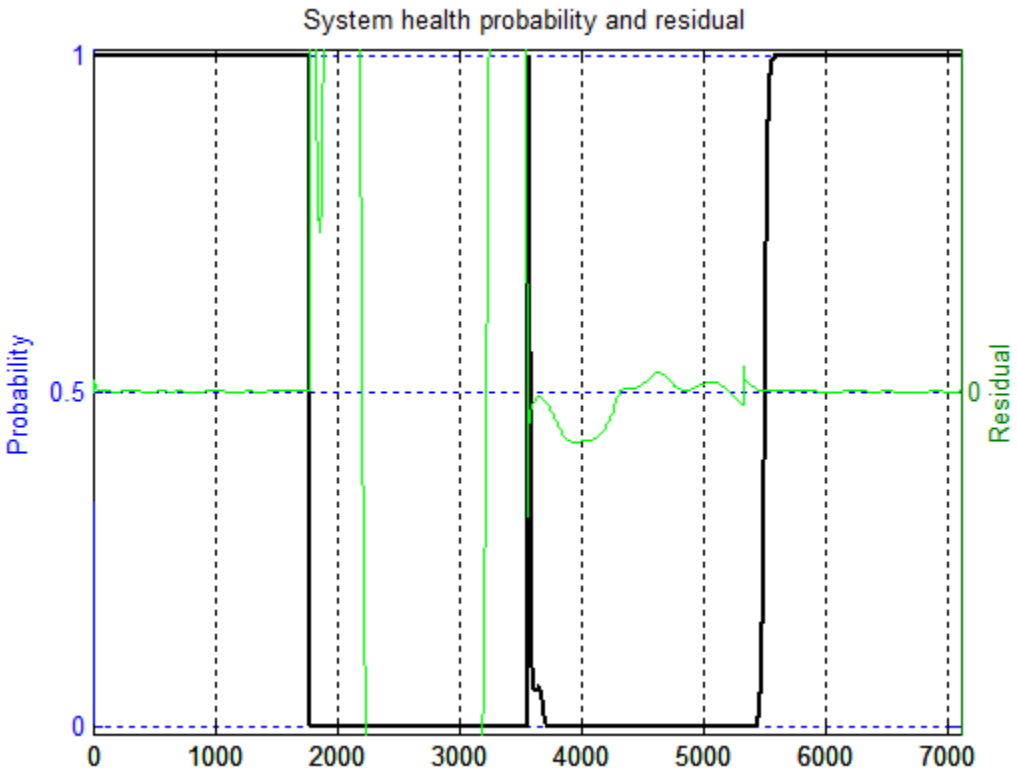

Figure C. 7 Bounded SOC: health probability and residual

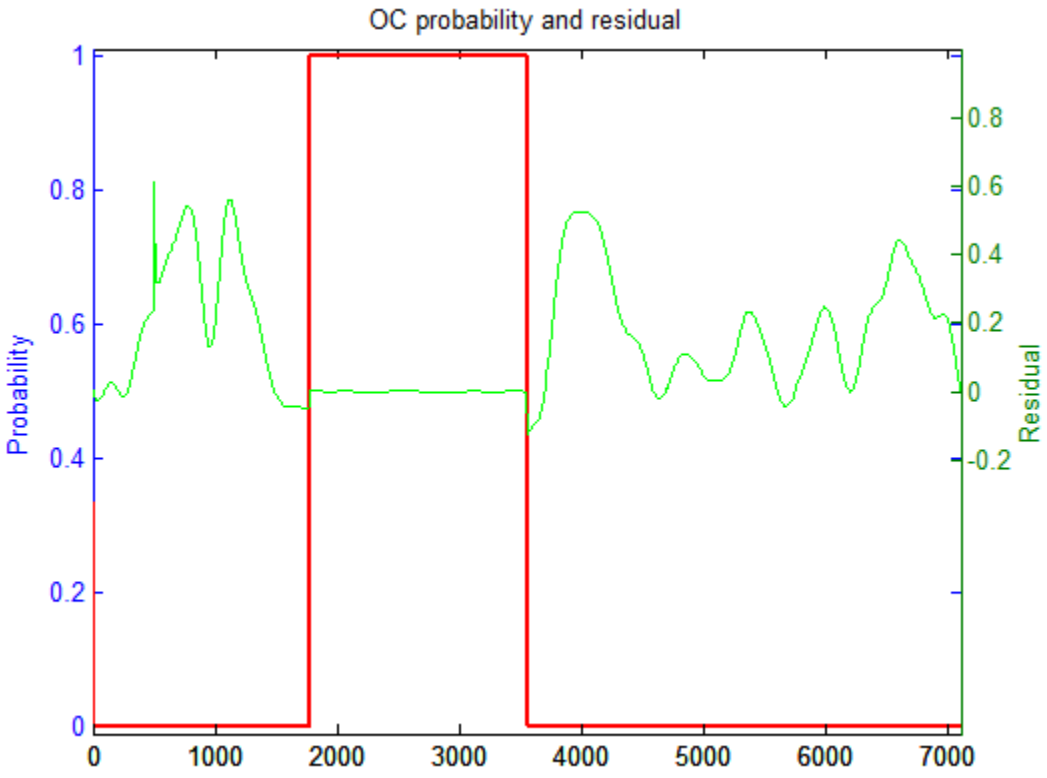

Figure C. 8 Bounded SOC: over charge probability and residual

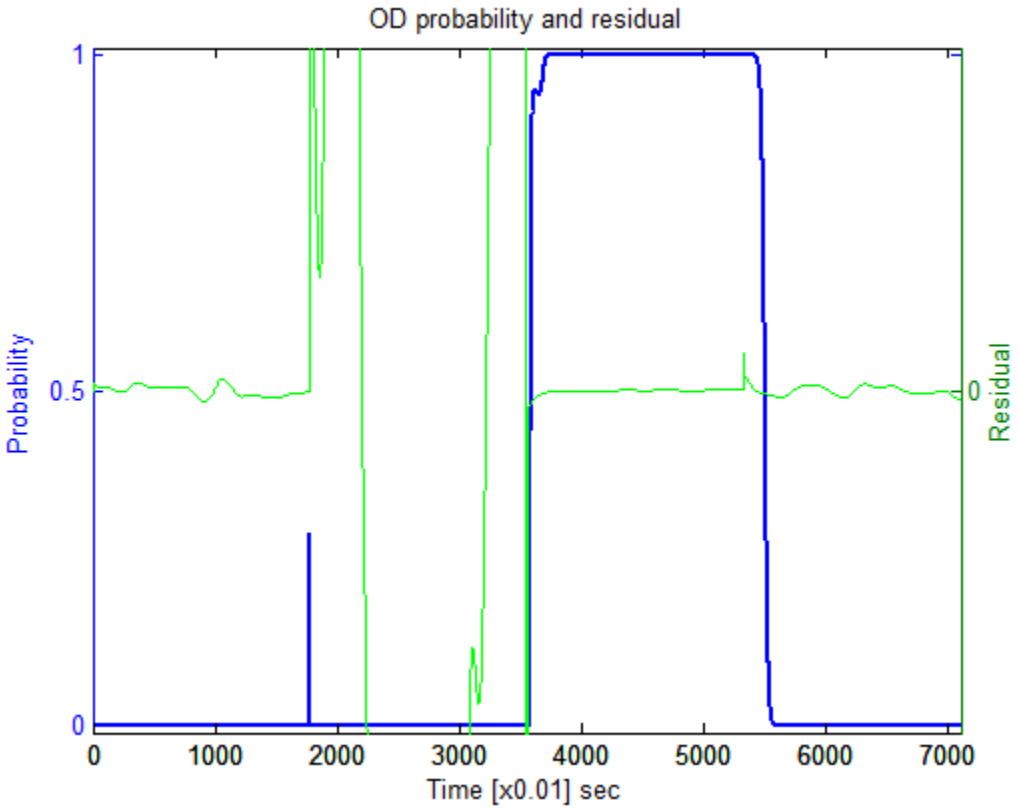

Figure C. 9 Bounded SOC: over discharge probability and residual

C. 2. Navy over discharge Cycle Based Models

The following figures show the variation in estimated terminal voltages, residuals and combined probability-residual change with system identification on Navy over discharge cycled battery.

The Figures C. 10, C. 11 and C. 12 show the variation of estimated terminal voltages with reference to the simulated measurement of terminal voltage $\hat{y}_m$. The system residuals are shown in Figure C. 13, and the conditional probabilities with associated residuals are as shown in Figures C. 14 and C. 15.

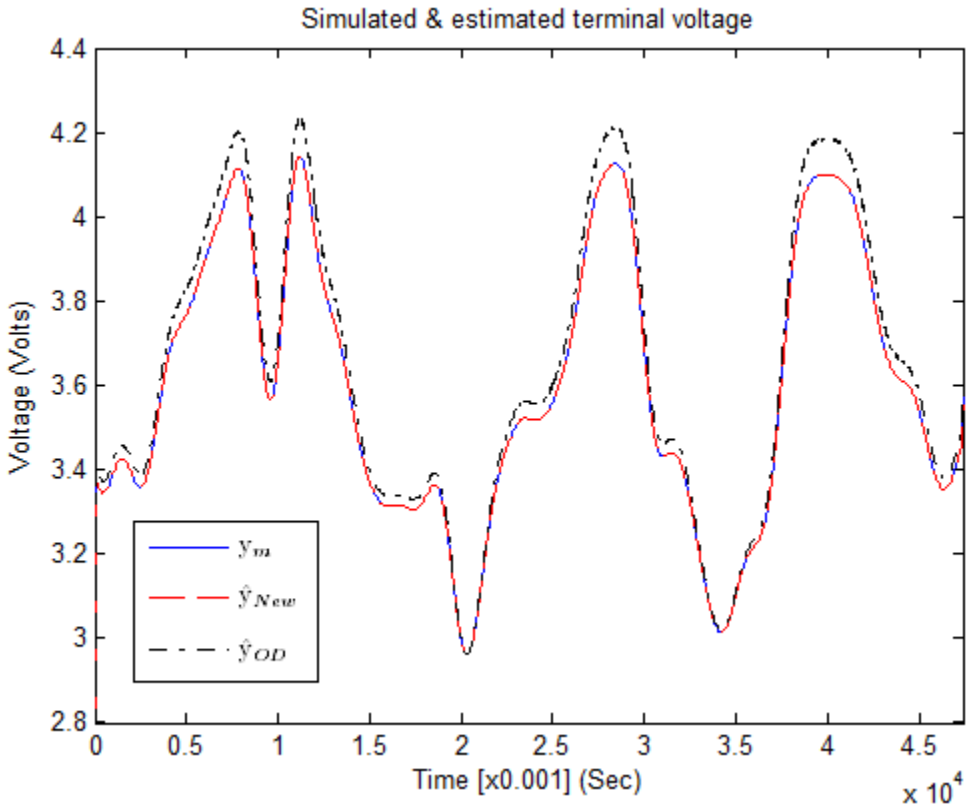

Figure C. 10 Simulated and estimated terminal voltages for 0 to 47.4 seconds (Navy over discharge)

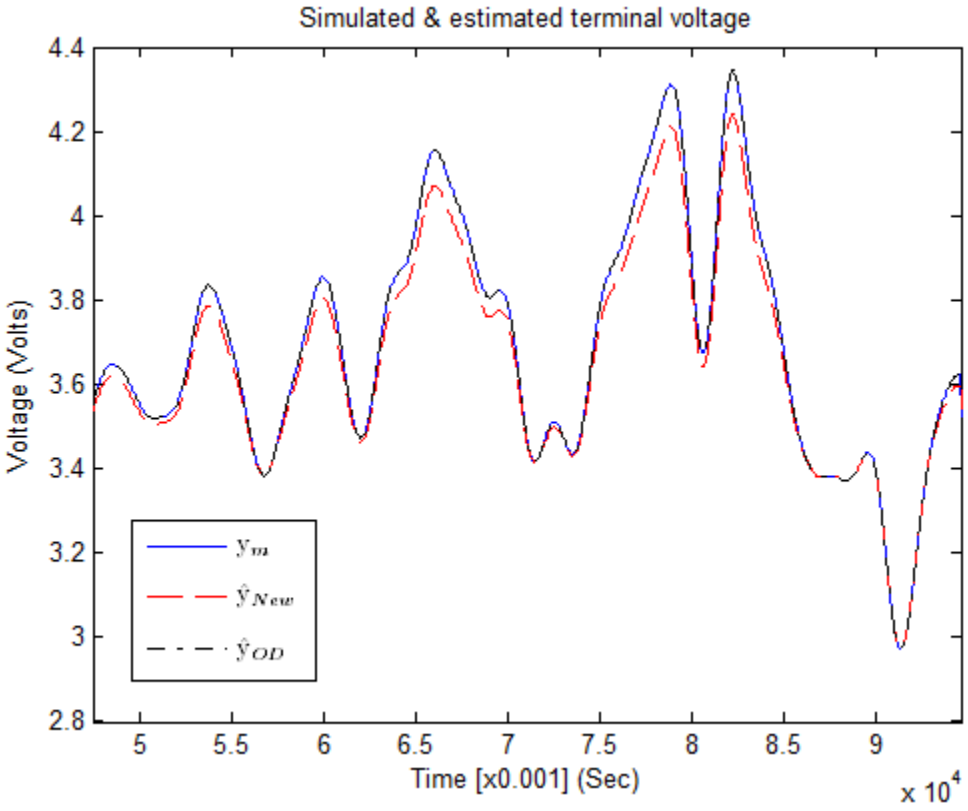

Figure C. 11 Simulated and estimated terminal voltages for 47.5 to 94.6 seconds (Navy over discharge)

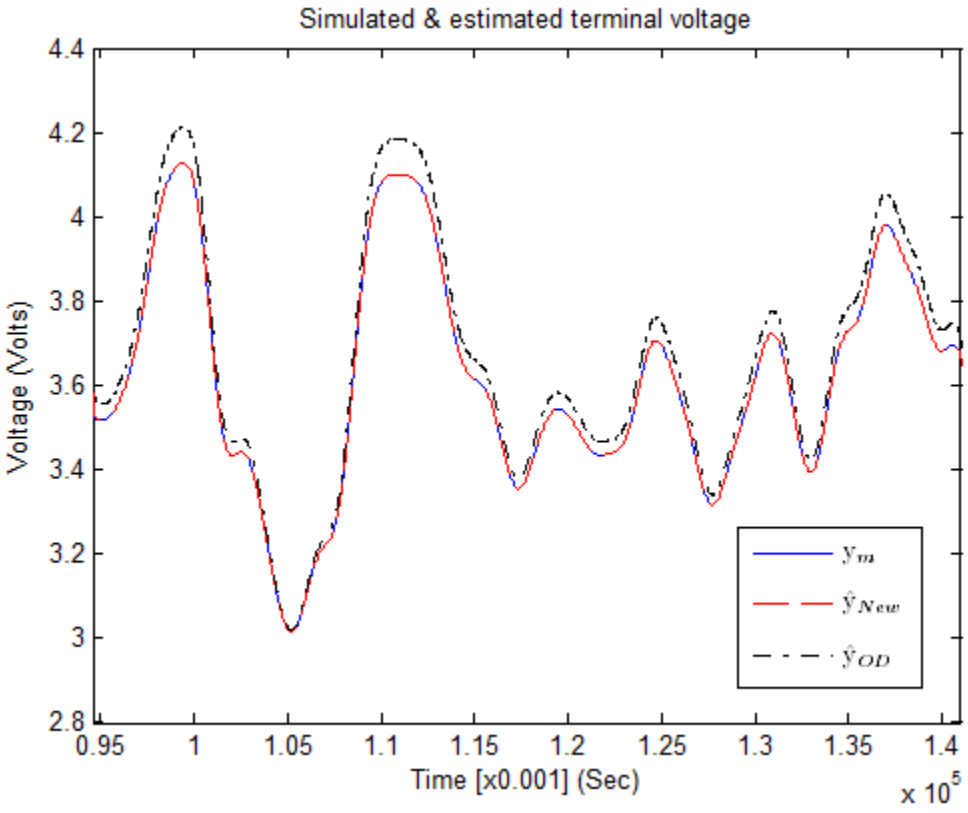

Figure C. 12 Simulated and estimated terminal voltages for 94.6 to 141 seconds (Navy over discharge)

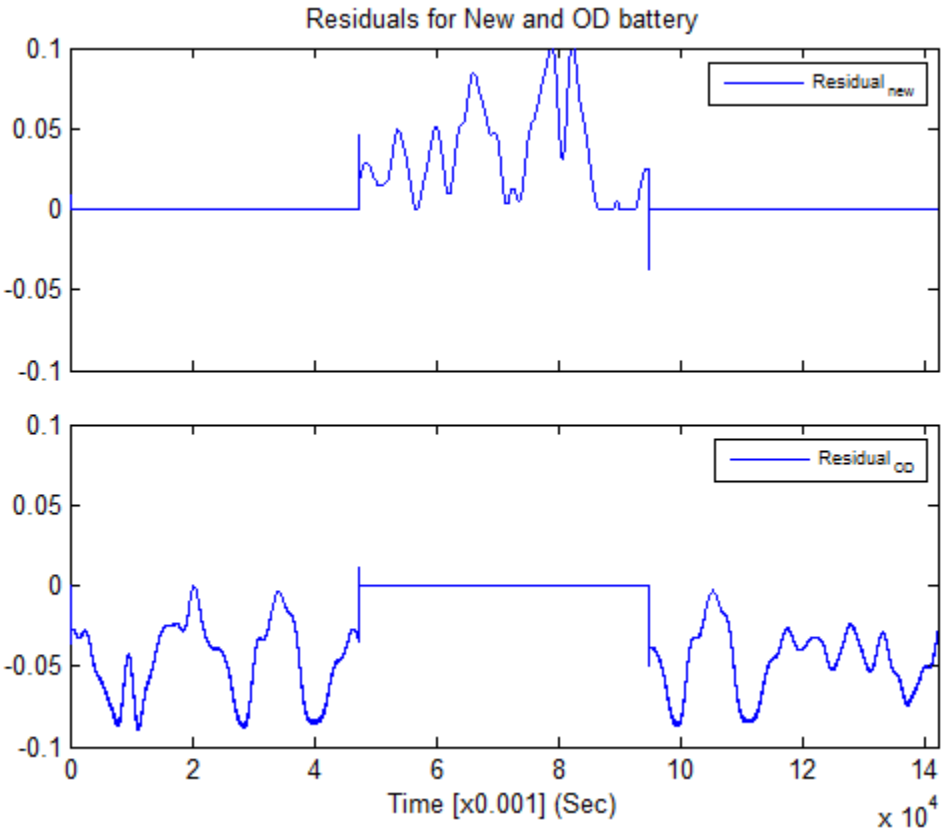

Figure C. 13 System residuals for new and over discharged battery (Navy over discharge)

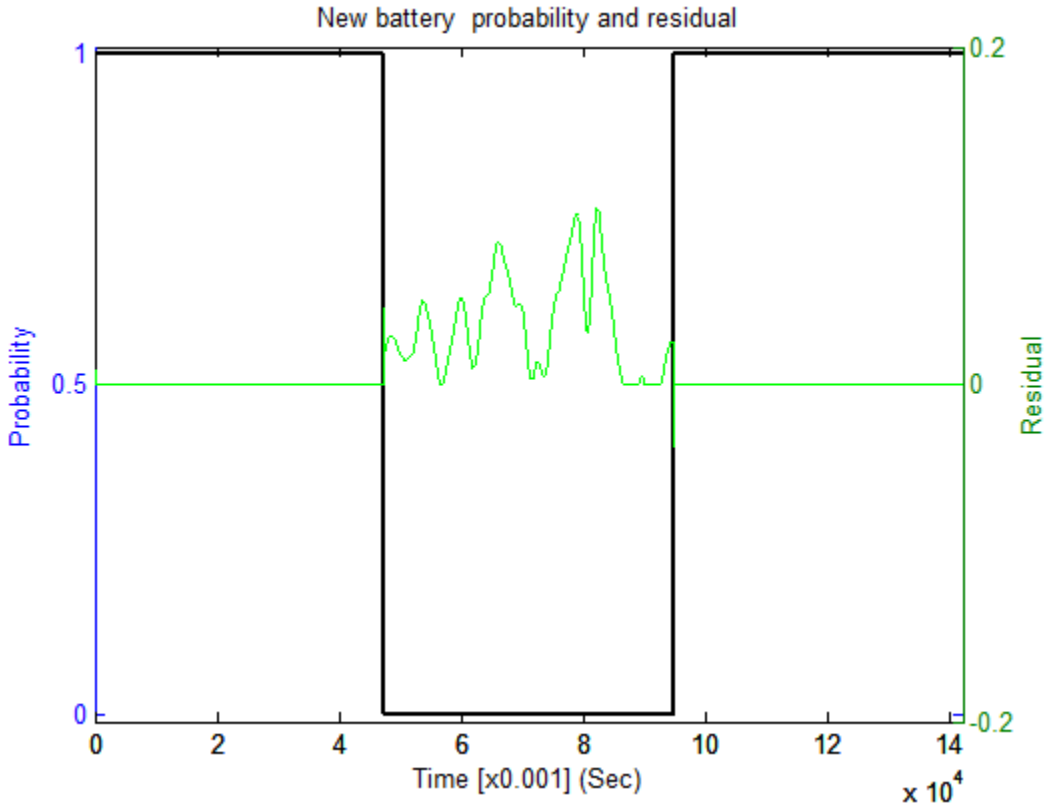

Figure C. 14 New battery probability and residuals (Navy over discharge)

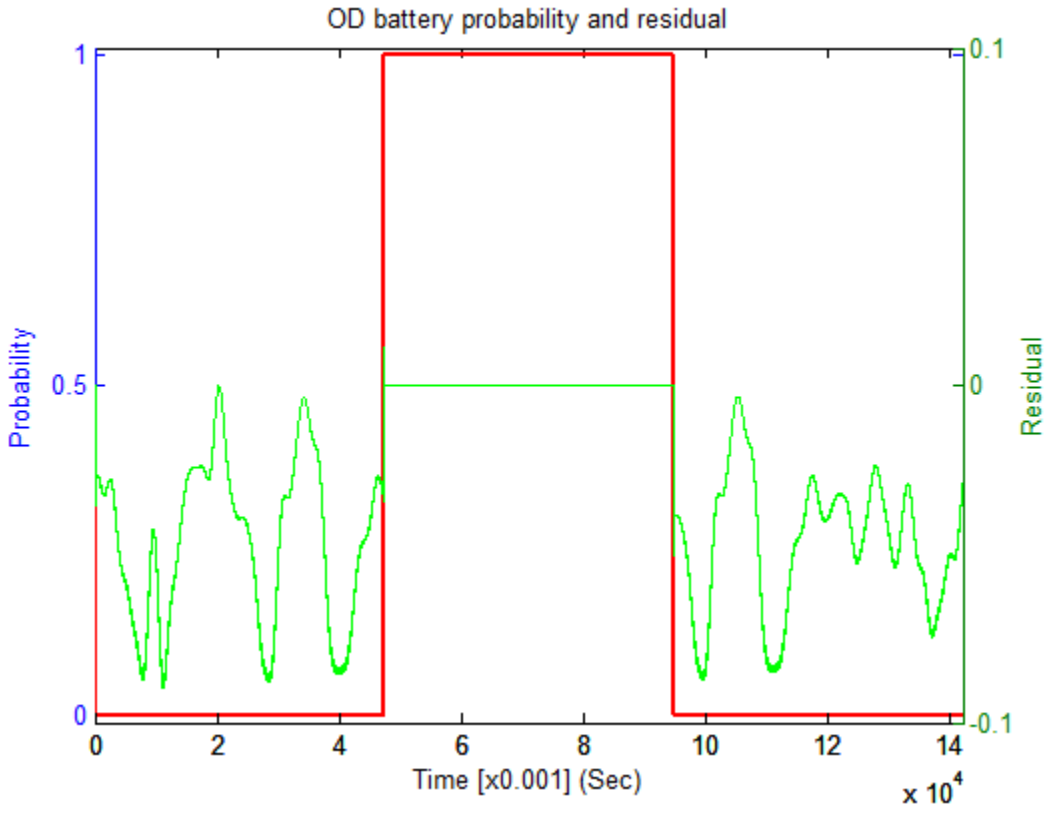

Figure C. 15 Over discharged battery probability and residuals (Navy over discharge)

C. 3. 24 Hour Overdischarge Cycle Based Models

The following figures show the variation in estimated terminal voltages, residuals and combined probability-residual change with system identification on 24 hour over discharge cycled battery.

The Figures C. 16, C. 17 and C. 18 show the variation of estimated terminal voltages with reference to the simulated measurement of terminal voltage $\hat{y}_m$. The system residuals are shown in Figure C. 19, and the conditional probabilities with associated residuals are as shown in Figures C. 20 and C. 21.

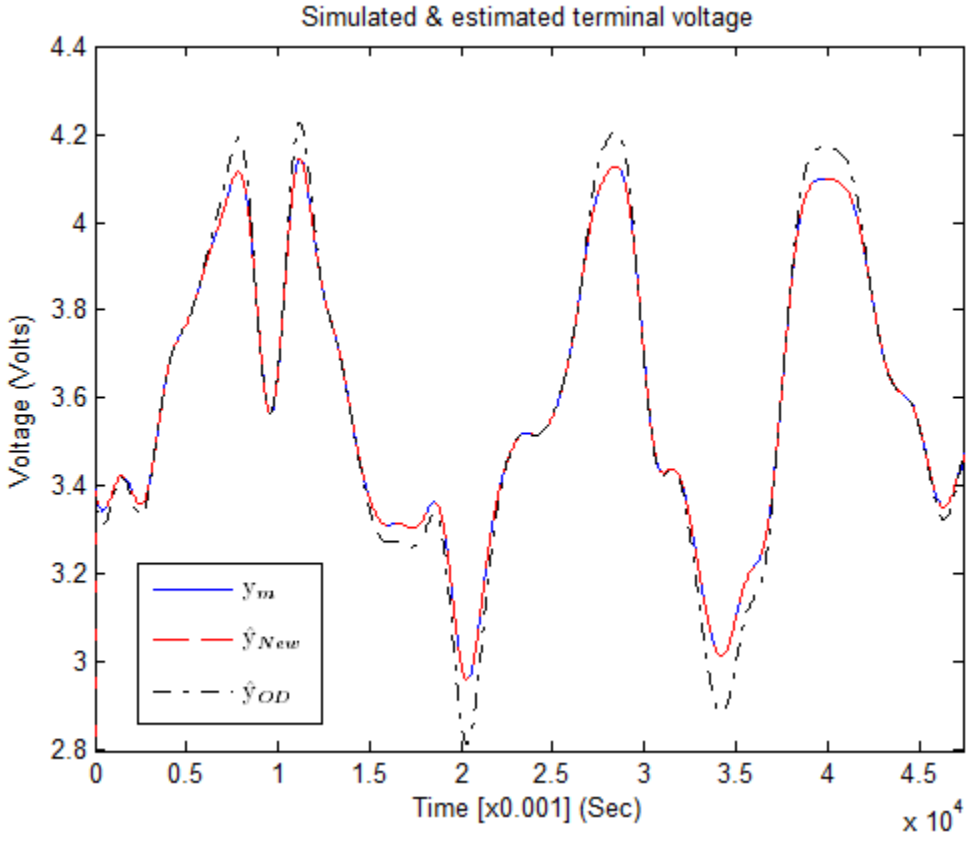

Figure C. 16 Simulated and estimated terminal voltages for 0 to 47.4 seconds (24 hour over discharge)

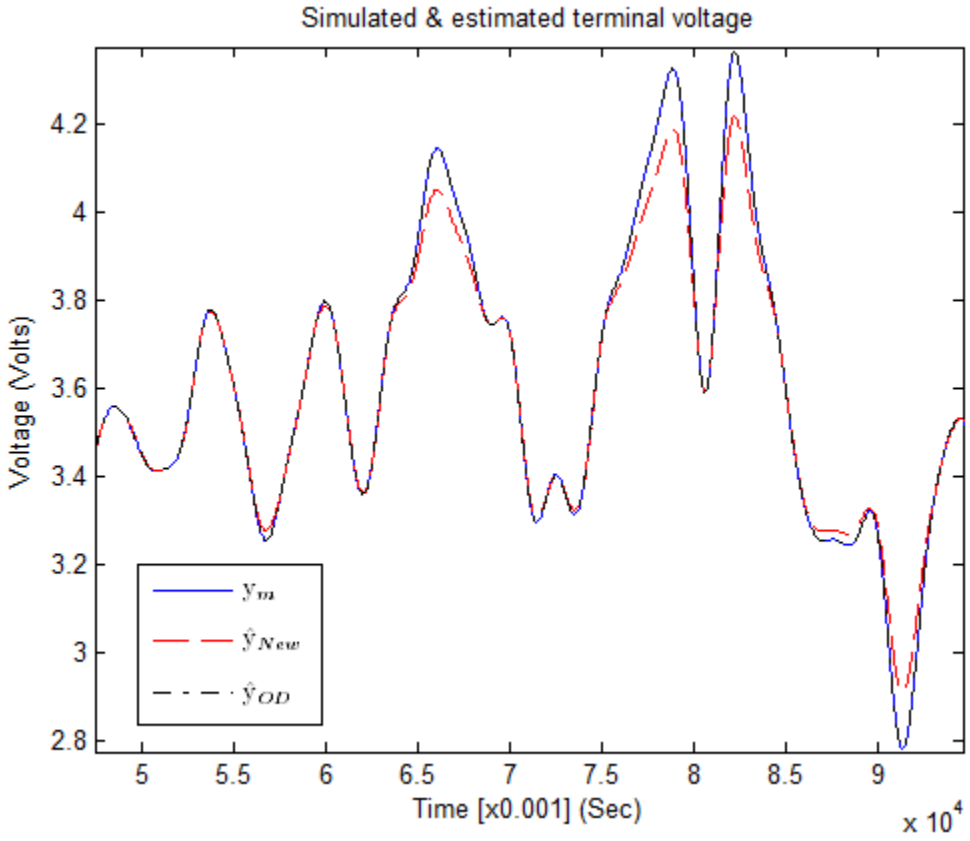

Figure C. 17 Simulated and estimated terminal voltages for 47.5 to 94.6 seconds (24 hour over discharge)

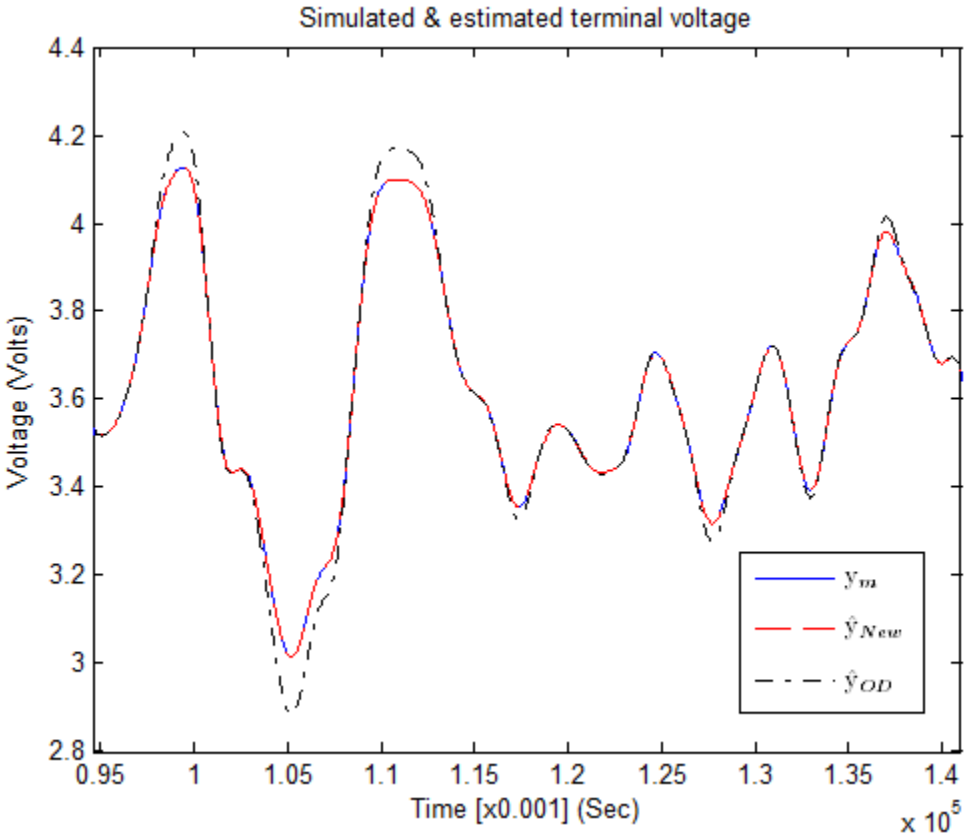

Figure C. 18 Simulated and estimated terminal voltages for 94.6 to 141 seconds (24 hour over discharge)

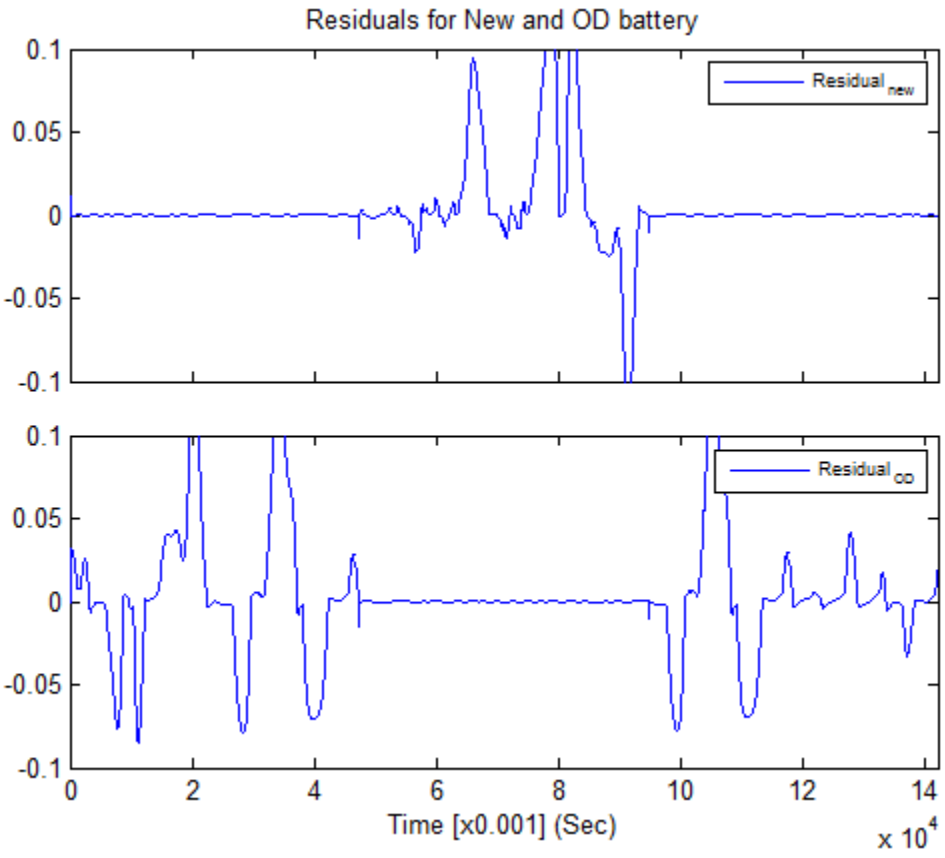

Figure C. 19 System residuals for new and over discharge battery (24 hour over discharge)

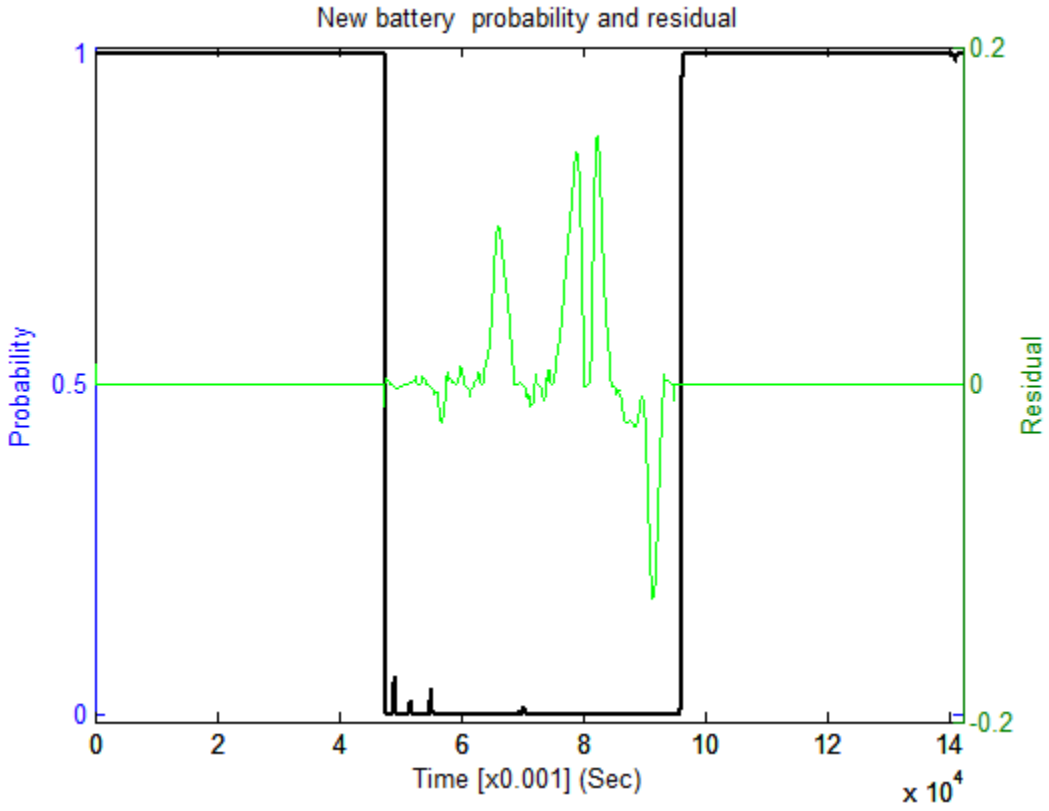

Figure C. 20 New battery probability and residuals (24 hour over discharge)

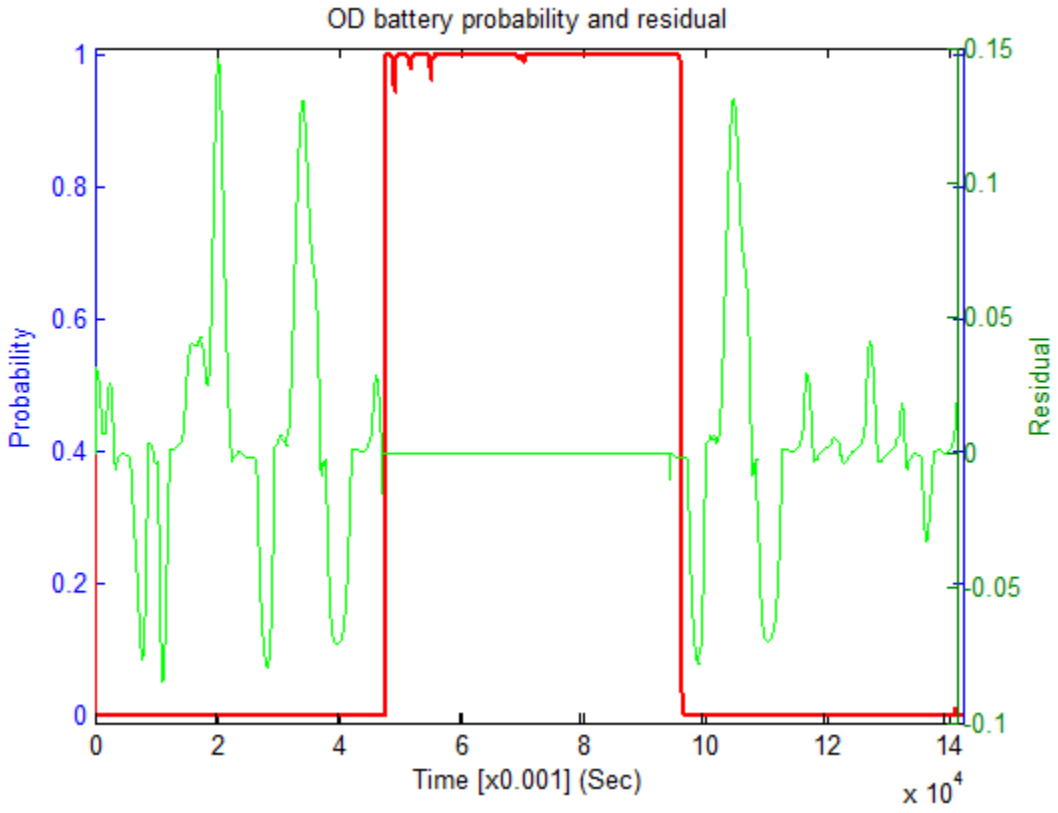

Figure C. 21 Over discharge battery probability and residuals (24 hour over discharge)